Investigating molecular mechanisms underlying Marfan syndrome, based on fibrillin-1 secretion and assembly



Ondine Atwa

Department of Biochemistry

Somerville College

University of Oxford

A thesis submitted for the degree of MSc (by research) at the University of Oxford, Hilary Term, 2020

Abstract

Fibrillin-1 is a major glycoprotein component of 10-12 nm microfibrils, consisting predominantly of calcium binding epidermal factor-like (cbEGF) and TGFß binding protein like (TB) domains. Mutations within the gene encoding fibrillin-1 cause Marfan Syndrome (MFS), an autosomal dominant disease of the connective tissue, characterized by a wide range of severity, with neonatal MFS (nMFS) lying at the most severe end of the spectrum. nMFS substitutions are clustered into domains TB3-cbEGF18, the 'neonatal' region of fibrillin-1. Thus far, the molecular pathology of MFS does not explain the severity associated with a dysfunctional neonatal region, especially since 'classical' MFS (cMFS) substitutions are also found in these domains.

This study aims to investigate the molecular and cellular factors that might contribute to disease severity in MFS. A set of cMFS and nMFS substitutions were investigated for their effect on the secretion of full-length GFP-Fbn expressed transiently in HEK293T cells, and of recombinant fragment NPro-TB3-cbEGF19 expressed stably in MSU1.1 fibroblasts and transiently in HEK293T cells. A microfibril assembly assay then tested the ability of the full-length GFP-Fbn variants to incorporate into FS2 assembled microfibrils.

Secretion results from the different systems were consistent, showing no effect of most of the cMFS and nMFS substitutions on the trafficking of fibrillin-1, with the exception of two cysteine variants that showed partial intracellular retention. Opposing secretion results of the same substitutions in different recombinant constructs provided insight into the role of domain TB3 in the folding of adjacent cbEGF domains. Microfibril assembly results distinguished, for the first time, the behavior of cMFS and nMFS variants. cMFS variants clearly assembled into FS2 microfibrils, suggesting that a dominant-negative effect involving mutant incorporation could contribute to the molecular pathology of MFS. nMFS variants, in contrast, did not incorporate into microfibrils, despite having the N- and C-termini implicated in early fibrillin multimerization, indicating that they may form non-productive complexes that are precluded from further assembly steps. These results indicate that phenotypic severity is correlated with the extent of microfibril assembly perturbation and suggest an important role for domains TB3-cbEGF19 in the lateral association of fibrillin-1 monomers during microfibril assembly.

Acknowledgments

I would like to start by expressing my deep gratitude for Professor Penny Handford and Dr Sacha Jensen's guidance, help and brilliant supervision. I want to thank Professor Handford for her direction not only on the project, but on how to create hypotheses, experimentally execute them, how to interpret and criticize data, and how to think as a scientist. A sincere thank you to Dr Sacha Jensen for his patience in the lab and for making time in the lab very enjoyable. I want to thank him for his constant help and support with experiments and thesis writing even when he was no longer my co-supervisor. I would like to extend my appreciation to all the other members of the Handford lab, Yao and Shruti, as well as other members of the biochemistry department, for fostering a helpful, cooperative and welcoming environment.

I also want to express my heartfelt appreciation for my parents' and brother's constant inspiration and motivation, without whom completing this degree wouldn't have been possible. A heartfelt thank you to them and my dearest friends from Egypt for their constant moral support and encouragement from across the lands.

My time in Oxford has been exceptional. To Somerville college, and to the closest friends I made here, I am forever grateful to you for that. Thank you for the special experiences, for the good times, for the constant support and for helping me grow. A sincere thank you to the various committees that made Somerville's MCR the inclusive, open and fun community that it is.

Thank you,

Ondine

List of abbreviations

AD: acromicric dysplasia

AGTR1: angiotensin II receptor type 1

BMPs: bone morphogenic proteins

bp: base pairs

Ca^{2+}: calcium

cbEGF: calcium binding epidermal growth factor-like

cDNA: complementary DNA

cMFS: classical Marfan syndrome

CMV: cytomegalovirus

DMEM: Dulbecco's Modified Eagle Medium

DMSO: dimethyl sulfoxide

DNA: deoxyribose nucleic acid

dNTPs: deoxyribonucleic acid

EB: elution buffer

ECL: enhanced chemiluminescence

ECM: extracellular matrix

EDTA: ethylenediaminetetraacetic acid

EGF: epidermal Growth Factor-like

ELISA: enzyme-linked immunosorbent assay

Endo H: endoglycosidase H

ER: endoplasmic reticulum

Fbn: fibrillin

Fbn1: fibrillin-1

FBN1: fibrillin-1 gene

FBN2: fibrillin-2 gene

FBN3: fibrillin-3 gene

FBS: fetal bovine serum

FNI: fibronectin type I

FS2s: Human dermal fibroblast lines from foreskin

FUN: Fibrillin Unique N-terminal

GD: geleophysic dysplasia

GDFs: growth and differentiation factors

GFP: green fluorescent protein

HEK293Ts: human embryonic 293Ts

HRP: horseradish peroxidase

HSPGs: heparan sulphate proteoglycans

HSVTK: Herpes Simplex Virus Thymidine Kinase

Hyb: hybrid domain

K_d: dissociation constant

kDa: kiloDaltons

LAP: latency-associated peptide

LTBPs: latent transforming growth factor-ß binding proteins

MAGP: microfibril-associated glycoproteins

MASS: mitral valve, aorta, skin and skeleton phenotype

MEM: minimum essential media

MFS: Marfan syndrome

MQ: milliQ

MSU 1.1: human skin fibroblast

nMFS: neonatal Marfan syndrome

NMR: nuclear magnetic resonance

PACE: paired basic amino acid cleaving enzyme

PAGE: polyacrylamide gel electrophoresis

PBS: phosphate buffer saline

PCOS: polycystic ovary syndrome pathogenesis

PCR: polymerase chain reaction

PFA: paraformaldehyde

PNGaseF: Peptide:N-glycosidase F

Pro-rich: proline-rich region

PTMs: post-translational modifications

RGD: Arg-Gly-Asp

RNA: ribose nucleic acid

RNAse: ribonuclease

RT: reverse transcription

SAXS: small-angle x-ray scattering

SDS: sodium dodecyl sulfate

SOC: Super Optimal Broth

SPR: surface plasmon resonance

STEM: scanning transmission electron microscopy

TAA: thoracic aortic aneurysm

TB: transforming growth factor β1-binding protein-like

TBE: Tris-borate-EDTA

TEM: transmission electron microscopy

TGFβ: transforming growth factor- ß

TGN: *trans*-Golgi network

UV: ultraviolet

WB: western blot

WMS: Weill-Marchesani syndrome

WT: wild type

Table of Contents

Abstract ii
Acknowledgments iii
List of abbreviations iv
Table of Contents vi

Chapter 1
1.1 10-12 nm microfibrils and the extracellular matrix....2
1.2 Fibrillin....3
1.2.1 Gene encoding fibrillin-1....4
1.2.2 Domain organization of fibrillin-1....4
1.2.2.1 cbEGF domain....6
1.2.2.2 TB domain....7
1.2.2.3 Hybrid domain....8
1.2.2.4 Proline-rich region....10
1.2.2.5 N- and C- terminal domains....10
1.2.3 Homotypic and heterotypic interdomain packing interactions....11
1.2.4 Fibrillin evolution....13
1.3 Fibrillin-1 organization into microfibrils....13
1.4 Fibrillin assembly....16
1.4.1 Post translational modifications of fibrillin-1....17
1.4.2 Furin-mediated cleavage of the fibrillin-1 N- and C- termini....17
1.4.3 N- and C- terminal interactions....18
1.4.4 Microfibril interactions....20
1.4.4.1 Fibronectin....20
1.4.4.2 Integrin....20
1.4.4.3 Heparin/heparan sulphate....21
1.4.4.4 LTBPs....21
1.5 FBN1 disease-causing mutations....23
1.5.1 Type-1 Fibrillinopathies....23
1.6 The Marfan syndrome....23
1.6.1 Marfan Syndrome-causing mutations....24
1.6.2 Marfan syndrome pathogenesis....25

1.6.2.1 TGFβ signaling in Marfan syndrome 26
1.6.3 Neonatal Marfan syndrome 26
1.6.4 Models of pathogenic mechanisms underlying Marfan syndrome 29
1.8 Thesis Aim 31

Chapter 2

2.1 DNA Cloning techniques 33
2.1.1 DNA amplification using polymerase chain reaction (PCR) 33
2.1.1.1 Oligonucleotide primers 34
2.1.1.2 Site directed mutagenesis 35
2.1.2 PCR product clean up 35
2.1.3 Agarose gel electrophoresis 35
2.1.4 Gel purification 36
2.1.5 Restriction enzyme digestion 36
2.1.6 Dephosphorylation 37
2.1.7 Ligation 37
2.1.8 Transformation of NEB-5α competent cells 37
2.1.9 PCR Based colony screening 38
2.1.10 Preparation and harvesting of plasmid DNA 39
2.1.11 Quantification of DNA and RNA 39
2.1.12 Sequencing DNA 40
2.2 Eukaryotic Protein expression 40
2.2.1 Maintenance of cell lines 40
2.2.2 Culturing and passaging of cells 40
2.2.3 Freezing and thawing of cells 41
2.2.4 Transient transfection of HEK293T cells and secretion assay set up 42
2.2.5 De-glycosylation assay 42
2.2.6 Secretion assay 43
2.2.6.1 Sample preparation for western blotting 43
2.2.6.2 Western blot 44
2.2.7 Microfibril assembly assay: 45
2.2.7.1 Co-culture set up 45
2.2.8 Stable transfection of MSU1.1 fibroblasts 46

2.2.9 Semi-quantitative gene expression analysis 47
2.2.9.1 RNA extraction.....47
2.2.9.2 Reverse transcription (RT) 47
2.2.9.3 Polymerase chain reaction.....48
2.3 Immunofluorescent imaging.....49
2.3.1 Preparing cells for immunostaining.....49
2.3.2 Immunostaining microfibrils 49
2.3.3 Immunofluorescent imaging.....50

Chapter 3

3.1 Introduction 52
3.2 Classical and neonatal MFS mutations.....53
3.3 Full length GFP-Fbn secretion and assembly assays.....56
3.3.1 Classical and neonatal MFS variants are secreted from HEK293T cells 56
3.3.2 Classical and neonatal MFS variants show differential microfibril incorporation.....58
3.7 Conserved residues in the neonatal region domains cbEGF11-14 are potential candidates for protein-protein binding 60
3.8 Discussion.....64

Chapter 4

4.1 Introduction 69
4.2 Constructing NPro-TB3-cb19 WT and mutant recombinant proteins.....70
4.3 Semi-quantitative gene expression analysis 73
4.4 Analysis of pools of MSU1.1 clones from stable transfection of NPro-TB3-cb19 recombinant fibrillin-1.....75
4.4.1 Classical and neonatal MFS variants are secreted from MSU1.1 fibroblasts 75
4.5 Analysis of pools of MSU1.1 clones from stable transfection of NPro-cb11-22 recombinant fibrillin-1.....77
4.5.1 Semi-quantitative gene expression analysis 77
4.5.2 Classical and neonatal MFS calcium binding variants in NPro-cbEGF11-22 are retained in cells 78
4.6 Recombinant protein (NPro-TB3-cb19) secretion from HEK293T cells.....79

4.6.1 Classical and neonatal MFS recombinant constructs are secreted from HEK293T cells 80
4.6.2 Fibrillin-1 domain cbEGF11 neonatal MFS variant (I1048T) introduces an extra N-linked glycosylation site 81
4.7 Discussion 82

Chapter 5

5. Discussion 87
5.1 Correlating molecular defects of cMFS and nMFS mutations to the trafficking of fibrillin-1 88
5.1.1 Calcium binding residues in domains TB3-cbEGF19 89
5.1.2 Cysteine residues in domains TB3-cbEGF19 90
5.1.3 Interdomain packing and cbEGF fold residues in domains TB3-cbEGF19 92
5.1.4 cbEGF deletions in domains TB3-cbEGF19 94
5.2 Molecular pathogenesis of Marfan syndrome 95
5.3 The neonatal region 99
5.4 Concluding remarks 102

References xi
Appendix xxii

Chapter 1

Introduction

1.1 10-12 nm microfibrils and the extracellular matrix

The extracellular matrix (ECM) is a highly dynamic, complex network of macromolecules that surrounds and supports cells within metazoan tissues. The ECM generates the mechanical properties and endows elasticity, extensibility, tensile and compressive strength to tissues. It maintains structural integrity of dynamic tissue by providing an architectural framework, anchoring the cells to substratum, providing structural signals, and imparting positional memory in cells. Specialized cells, predominantly fibroblasts, and smooth muscle cells produce, assemble and maintain components of the ECM. The ECM undergoes constant remodeling in response to cellular signals, enabling it to act as a regulator of cell adhesion, migration, proliferation, and differentiation. This interplay between cells and matrix plays an active role in physiological processes such as embryonic development, wound healing, immune response, as well pathological processes such as tumorigenesis (Frantz *et al.,* 2010; Engel and Chiquet, 2011).

The biochemical components of the ECM are heterogeneous and tissue specific. Five types of macromolecules form the ECM: elastin, collagens, glycoproteins (fibronectin, laminin, and fibrillin), hyaluronan and proteoglycans (aggrecan and versican). Many of the constituent proteins are modular, consisting of arrays of similar domains, and are subject to extensive post-translational modifications (PTMs) that assist their assembly into higher-order structures, required for their multifunctional roles within the ECM (Engel and Chiquet, 2011). The 10-12 nm diameter microfibrils are dynamic fibre-like components of the ECM that confer mechanical stability and maintain tissue integrity. In mammals, 10-12 nm microfibrils are composed mainly of fibrillins, a family of three ~350 kDa (kiloDaltons) glycoproteins. They provide a framework for the deposition of elastin and are essential for adult elastic tissue homeostasis. Fibrillin microfibrils occur in proximity to the basement

membrane, in association with elastin in elastic fibers, or in the form of microfibril bundles in elastin free tissue, such as the ciliary zonule or the kidney glomerulus, where they confer elasticity and extensibility. Microfibrils also play vital roles in regulating growth factor bioavailability, through their interaction with bone morphogenic proteins (BMPs), growth and differentiation factors (GDFs) and latent transforming growth factor-ß binding proteins (LTBPs; Isogai *et al.,* 2003; Gregory *et al.,* 2005), mediating matrix-matrix interactions (Cain *et al.,* 2005) and cell-matrix interactions and signaling, through their binding to cell surface integrin receptors (Pffaf *et al.,* 1996; Sakamoto *et al.,* 1996). Studies on mouse models have demonstrated that a threshold level of microfibrils is required to maintain normal connective tissue function and homeostasis (Pereira *et al.,* 1999; Judge *et al.,* 2004; Carta *et al.,* 2006).

1.2 Fibrillin

There are three human isoforms of fibrillin; fibrillin-1 (Maslen *et al.,* 1991), fibrillin-2 (Lee *et al.,* 1991) and fibrillin-3 (Corson *et al.,* 2004). Fibrillin isoforms consist of the same modular domain organization but are encoded by different genes, have different expression patterns and distributions within tissues. Fibrillin-1 is the major structural glycoprotein component of 10-12 nm microfibrils, it is expressed during embryonic development and remains active throughout adult life (Sakai *et al.,* 1986). Fibrillin-2 and -3 however, are only expressed during embryonic developmental stages (Corson *et al.,* 2004; Ramirez and Sakai, 2009). The isoforms also differ in a variable domain rich in proline (fibrillin-1), glycine (fibrillin-2), or both proline and glycine (fibrillin-3). Fibrillin-1 (*FBN1*) has been identified as the defective gene in Marfan Syndrome (MFS), and its responsibility for it was confirmed when *de-novo* mutations on the gene were characterized in two MFS patients (Section 1.6; Dietz *et al.,* 1991). Mutations in the fibrillin-2 gene (*FBN2*) are associated with

congenital contractual arachnodactyly or 'Beal's syndrome', and mutations in fibrillin-3 gene (*FBN3*) have been suggested to play a role in polycystic ovary syndrome (PCOS) pathogenesis (Robinson, 2000; Segars and Decherney, 2010). Homo- and heterotypic interactions between fibrillin-1 and -2 mediate the assembly of microfibrils. Several studies have demonstrated that fibrillin-2 oligomerization depends on the deposition of fibrillin-1, but not vice-versa (Lin *et al.,* 2002; Zhang *et al.,* 1994)

1.2.1 Gene encoding fibrillin-1

The gene encoding for fibrillin-1 is located on human chromosome 15q21.1, it contains 65 exons (Magenis *et al.,* 1991) and spans ~200 kb of genomic DNA (Biery *et al.,* 1999). The ATG codon is the start site of translation and is found within a Kozak consensus sequence, GGCATATGCGG, occurring in human exon 1 (Kozak 1991; Kettle *et al.,* 2000). The full-length human prefibrillin-1 mRNA consists of 9663 nucleotides with untranslated sequences on both 5' and 3' ends, and thus an open reading frame of 8613 nucleotides.

1.2.2 Domain organization of fibrillin-1

Profibrillin-1 consists of 2,871 amino acids with a calculated molecular mass of ~350 kDa. Profibrillin-1 is processed at the cell surface, with pro-peptide sequences at both the N- and C- terminal ends being cleaved, yielding a ~320 kDa polypeptide (Pereira *et al.,* 1993). The domain that constitutes the majority of fibrillin-1's primary structure (Figure 1.1) is the Epidermal Growth Factor-like (EGF) domain. 43 of the 47 EGF domains are calcium (Ca^{2+}) binding and known as calcium binding epidermal growth factor-like (cbEGF) domains. Interspersed between them are 7 transforming growth factor β1-binding protein-like (TB) domains, and 2 hybrid (hyb) domains, which possess features of both TB and cbEGF

domains. The fibrillin C-terminus consists of two cysteine residues clustered together that are known as the 2Cys domain. The flexible N-terminal domain contains four-cysteine residues and is referred to as the Fibrillin Unique N-terminal (FUN) domain, and a proline-rich region (Pro-rich) follows the first TB domain (Corson *et al.,* 1993; Pereira *et al.,* 1993; Handford *et al.,* 2000).

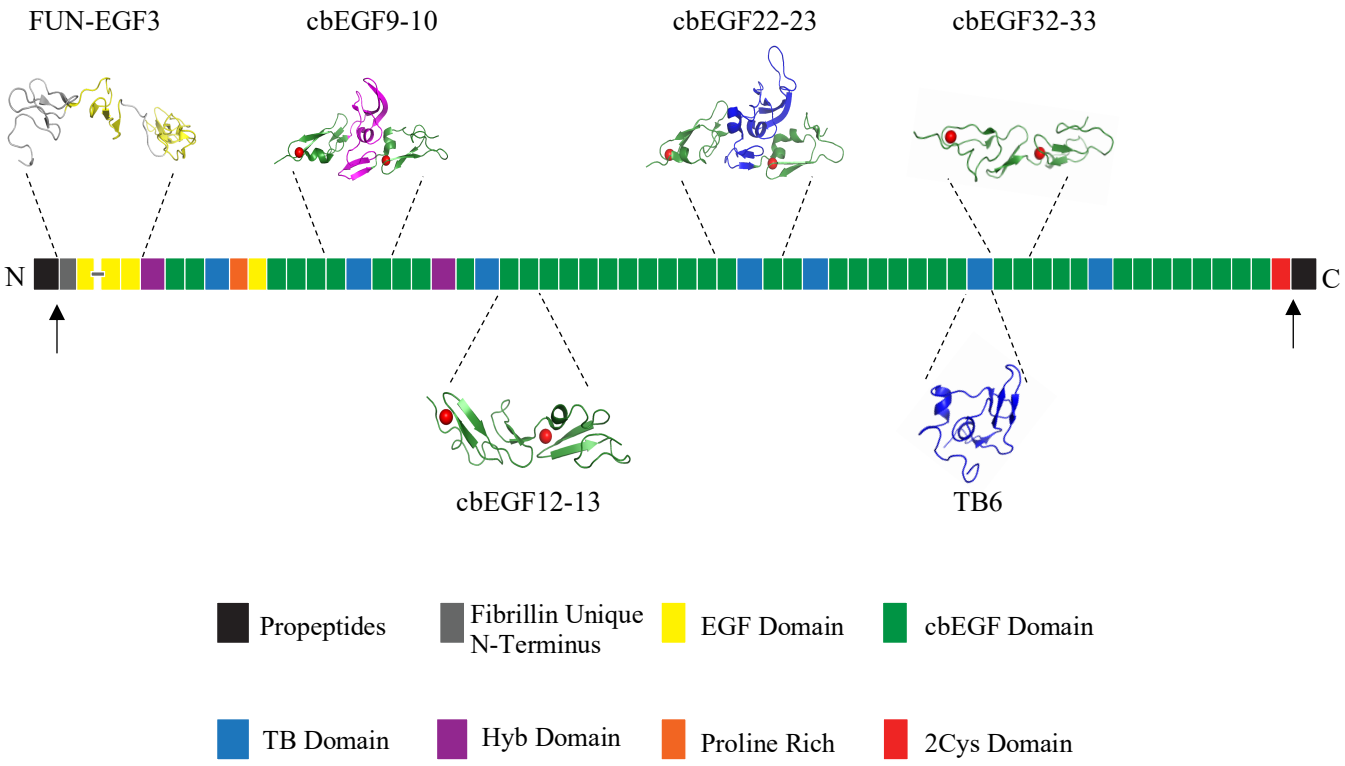


Figure 1.1 Schematic diagram of fibrillin-1 domain organization. Human fibrillin-1 is composed predominantly of EGF-like domains, 43 of the 47 are cbEGF domains, interspersed between them are 7 TB and 2 hyb domains. The Proline-rich region is glycine-rich and glycine/proline rich in fibrillin-2 and -3 respectively. Two cysteine residues clustered together near the C-terminal are known as the 2Cys domain. There are furin cleavage sites at the N- and C- terminal ends that allow for cleavage of the respective pro-peptides. High-resolution structures have been solved for the fibrillin-1 fragments FUN–EGF3 (PDB 2M74), cbEGF9–hyb2–cbEGF10 (PDB 2W86), cbEGF12–cbEGF13 (PDB 1LMJ), cbEGF22–TB4–cbEGF23 (PDB 1UZJ), isolated domain TB6 (PDB 1APJ) and cbEGF32–cbEGF33 (PDB 1EMN). Figures were rendered using pyMOL (Schrödinger, LLC).

1.2.2.1 cbEGF domain

EGF/cbEGF domains are common to membrane (Notch, Delta, Serrate, low-density lipoproteins), extracellular (Fibrillins, Fibulins, LTBPs, Nidogen) and plasma (Factor IX and X, proteins C and S, thrombomodulin) proteins. Their secondary structure consists of major and minor double stranded anti-parallel β-hairpins at the N- and C- termini respectively (Figure 1.2A). All EGF domains consist of 40–50 residues, including 6 cysteine residues that form 3 intramolecular disulfide bonds, paired up in a C1-C3, C2-C4, C5-C6 arrangement. CbEGFs contain a calcium binding consensus sequence –Asp/Asn-X-Asp/Asn-Gln/Glu-X_m-Asp/Asn*-X_n-Tyr/Phe, where m and n indicate variable numbers of amino acid residues, and * indicates potential β-hydroxylation of side chains of the aspartate/asparagine residue (Figure 1.2B). Calcium is usually held in a pentagonal bipyramidal arrangement and binds to ligands provided by oxygen atoms of backbone carbonyl groups, side chain residues, and H_2O (Figure 1.2B; Rees *et al.,* 1988; Rao *et al.,* 1995; Downing *et al.,* 1996). There is also a G-F/Y/W conserved sequence present in cbEGF domains, the hydrophobic residue of which is involved in interdomain packing interactions with the following domain in a cbEGF-cbEGF pair (Section 1.2.3; Downing *et al.,* 1996; Smallridge *et al.,* 2003).

Nuclear magnetic resonance (NMR) titrations, calcium chelation competition assays and equilibrium dialysis studies demonstrate that calcium has significantly varying (10-200 μm) affinities (K_d: dissociation constant) across cbEGF domains (Handford *et al.,* 1991; Mcgettrick *et al.,* 2000; Yuan *et al.,* 2002; Jensen *et al.,* 2005; Jensen *et al.,* 2009). Calcium binding plays a major role in maintaining the structure of fibrillin and stabilizes interdomain cbEGF-cbEGF interactions to produce an extended rod-like conformation. Together with the disulfide bonding and hydrophobic packing, calcium binding restricts the flexibility and

extensibility of cbEGF domains, and protects fibrillin from proteolytic cleavage (Reinhardt *et al.,* 1997). Calcium binding also mediates homo- and heterotypic interactions between fibrillin-1 and -2, and fibrillin-1 intermolecular interactions with other extracellular matrix proteins including microfibril-associated glycoproteins (MAGP)-2, fibulin-2, -4 and -5, aggrecan and versican (Jensen *et al .,* 2001; Rock *et al.,* 2004). More than 60% of Marfan syndrome associated mutations have been localized to cbEGFs, a large number of which were linked to decreased calcium binding, which emphasizes its importance for fibrillin functionality (Smallridge *et al.,* 2003)

1.2.2.2 TB domain

TB domains are found exclusively in the fibrillin and LTBP family of proteins (Robertson *et al.,* 2011). Along fibrillin-1 there are 7 TB domains, each of which is stabilized by four intramolecular disulfide bonds, formed between 8 cysteine residues, in a C1-C3, C2-C6, C4-C7, C5-C8 pattern (Figure 1.2B). TB domains have a small hydrophobic core, arranged around a conserved aromatic residue (usually tryptophan), as part of a G-X-X-W/F-G motif. NMR studies and crystal structures revealed that the secondary structure of TB modules consists of 4-stranded anti-parallel β-sheets, two small alpha-helices, and a final 2 strand β-hairpin at the C-terminus (Figure 1.2A). This secondary structure confers a relatively globular fold, in contrast to the more elongated fold of cbEGF domains (Yuan, 1997). A C-C-C triplet motif, uniquely conserved in TB domains, is found at the C-terminus of the first helix, such that it forms covalent bonds to three other regions in the domain. The final β-hairpin contains a G-F/Y motif that is involved in interdomain interactions with adjacent cbEGF domains (Yuan, 1997).

TB domains are responsible for specific protein-protein interactions that are essential for the functionality of the fibrillin/LTBP family. TB4 of fibrillin-1 mediates cell surface

interactions through binding to integrins using an RGD (Arg-Gly-Asp) sequence, while TB5 domain binds to heparan sulphate proteoglycans (HSPGs; Cain *et al.,* 2005). Together, these interactions contribute to fibroblast migration and the formation of focal adhesions. (Lee *et al.,* 2004; Sakamoto *et al.,* 1996). In LTBPs, the second TB domain forms disulfide linkages to the pro-peptide of transforming growth factor-ß (TGFβ). This interaction, is dependent on the presence of an amino acid pair (usually FP) on the β-sheet prior to the seventh cysteine residue and plays a role in sequestering TGFβ and regulating its activity (Section 1.6.2.1; Saharinen *et al.,* 2000; Chen *et al.,* 2005).

1.2.2.3 Hybrid domain

In addition to fibrillins, hyb domains are only present in the LTBP family of proteins. Hyb domains consist of an N-terminal sequence that resembles that of TB domains and a C-terminal sequence similar to that of cbEGF domains, which suggests that it evolved as a result of the fusion of a TB-EGF domain pair. X-ray crystallography studies have shown that the domain contains 8 cysteine residues disulfide bonded in a C1-C3, C2-C5 C4-C6, and C7-C8 arrangement. The first hybrid domain of all three fibrillins contains a ninth unpaired cysteine residue (Figure 1.2B; Corson *et al.,* 1993; Jensen *et al.,* 2009) which is likely involved in intermolecular interactions that take place during microfibril assembly (Reinhardt *et al.,* 2000). Similar to TB domains, hybrid domains have a globular fold consisting of a central α-helix and three β-sheets (Figure 1.2A), contain a G-X-X-W/F-G motif and a cysteine triplet motif at the end of the helix. Furthermore, a G-F/Y sequence, analogous to that of cbEGF domains, is present at the C-terminal end of the domain (Jensen *et al.,* 2009).

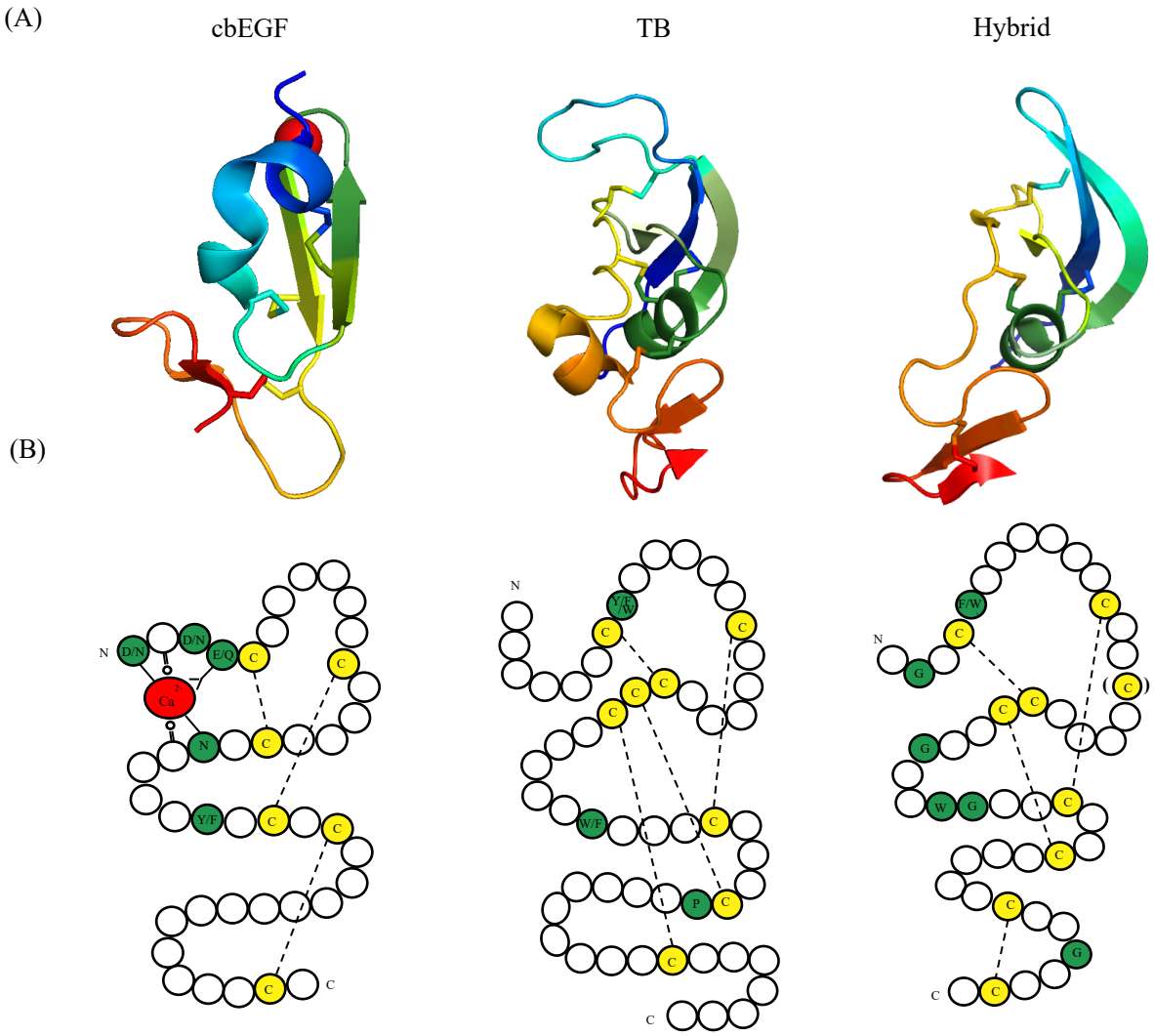


Figure 1.2 Structures of Fibrillin-1 Modular Domains (A) Three-dimensional structures of cbEGF, TB and hyb domains taken from high resolution fragment structures: cbEGF9–hyb2–cbEGF10 (PDB 2W86), cbEGF12-cbEGF13 (PDB 1LMJ) and domain TB6 (PDB 1APJ). Structures are represented in rainbow colors, with the N-terminal end in blue and the C-terminal end in red. The disulfide bonds are shown using stick representations and the Ca^{2+} bound to cbEGF domains is shown as a red sphere. (B) Schematic representation of cbEGF, TB and hyb domains. Cysteine residues are shown in yellow; the disulfide bonds are illustrated as dashed lines and the conserved residues in each domain type are shown in green. Calcium, held in a pentagonal bipyramidal arrangement in cbEGF domains is shown, with predicted amino acid side chain and carbonyl ligands indicated.

1.2.2.4 Proline-rich region

The Pro-rich region is unstructured and lacks any disulfide bonding (Ashworth *et al.,* 1999). For this reason, it is predicted to confer flexibility to the N-terminal region by enabling the molecule to fold over itself (Pereira *et al.,* 1993). Although the functional significance of the region remains unclear, it is predicted to interact with tropoelastin as part of the elastic fiber assembly process (Rock *et al.,* 2004).

1.2.2.5 N- and C- terminal domains

Fibrillin-1 is expressed as profibrillin-1 with a signal peptide at the N-terminus and pro-peptides of 17 residues and 140 residues at the N- and C-termini respectively. Each pro-peptide is adjacent a tribasic consensus sequence R-X-K/R-R (residues 42-45) that acts as a recognition signal for furin/paired basic amino acid cleaving enzyme (PACE). Those cleavage sites are conserved across all fibrillin isoforms (Robertson *et al.,* 2011; Piha-Gossack *et al.,* 2012). The FUN domain contains two loops stabilized by disulfide bonds arranged in a C1-C4 and C2-C5 pattern, and 4 flexible glycine residues at the N-terminal end of the domain (Yadin *et al.,* 2013). A GFP tag was inserted within this glycine stretch to genetically engineer a GFP-Fibrillin-1 (GFP-Fbn1) recombinant protein, to be used for secretion and microfibril assembly assays (Jensen *et al.,* 2014). The FUN domain forms a stable interface with EGF1 and the linker between EGF1 and -2 confers flexibility to this region. Most significantly, the FUN domain contains a recognition site for both the C-terminus and HSPGs required for early-stage microfibril assembly and localization at the cell surface (Cain *et al.,* 2005; Cain *et al.,* 2008; Yadin *et al.,* 2013).

The C-terminal propeptide, along with domains cbEGF41-43 are required for fibrillin-1 secretion, and cleavage of the propeptide is necessary for its assembly the cell surface

(Jensen *et al.,* 2014). Furthermore, the highly conserved 2Cys motif, present between cbEGF43 and the furin/PACE cleavage site, is predicted to play a role in C-terminal multimerization during microfibril assembly (Hubmacher *et al.,* 2008).

1.2.3 Homotypic and heterotypic interdomain packing interactions

X-ray crystallography and NMR data have furthered our understanding of interdomain packing interactions within fibrillin-1. Interdomain interactions are dependent on calcium binding, the G-F/Y/W motif present at the C-terminal end of cbEGF, TB and hyb domains, as well as TB-cbEGF linker regions. Fibrillin-1 contains 34 cbEGF-cbEGF, seven cbEGF-TB and six TB-cbEGF linkages. Linker regions are extensible, for example, the linker connecting TB4 to cbEGF23 forms a β-hairpin that is proposed to have a tension absorbing role by acting as an elastic spring in dynamic extracellular matrix environments. Jensen *et al.,* (2005) have later shown that calcium affinity provides a more representative measure of interdomain flexibility than the length of the linker region.

Calcium binding affinity of fibrillin-1 cbEGF domains is significantly modulated by the presence of an N-terminal domain. Higher calcium binding affinity values have been observed in cbEGF domain pairs (10-200 μM) in comparison to isolated domains, as seen by ~70× increase in calcium affinity of cbEGF13 associated with the addition of cbEGF12 (Figure 1.3A; Smallridge *et al.,* 1999). Even higher calcium binding affinity values (K_d in nm) have been attributed to TB-cbEGF and hyb-cbEGF domain pairs. Crystal structures and NMR measurements of cbEGF22-TB4-cbEGF23 (Figure 1.3B) and cbEGF9-hyb2-cbEGF10 (Figure 1.3C) domains propose that hydrophobic interactions, involving the aromatic residue of the G-F/W motif, and a hydrophobic residue from the conserved dipeptide 'XG', contribute to enhanced calcium binding by these domains. This suggestion

also explains the low calcium affinity observed in the heterologous TB6-cbEGF32 domain pair, given that it lacks this extensive hydrophobic interface (Lee *et al.,* 2004; Jensen *et al.,* 2009). The calcium concentration in extracellular environments is 1-2 mM, suggesting that high affinity calcium binding sites would be fully saturated in the ECM, while low affinity calcium binding sites would only be partially saturated. It is likely that the variability in calcium saturation is critical for the elasticity, flexibility and protein-protein interactions of fibrillin-1 (Hubmacher *et al.,* 2005).

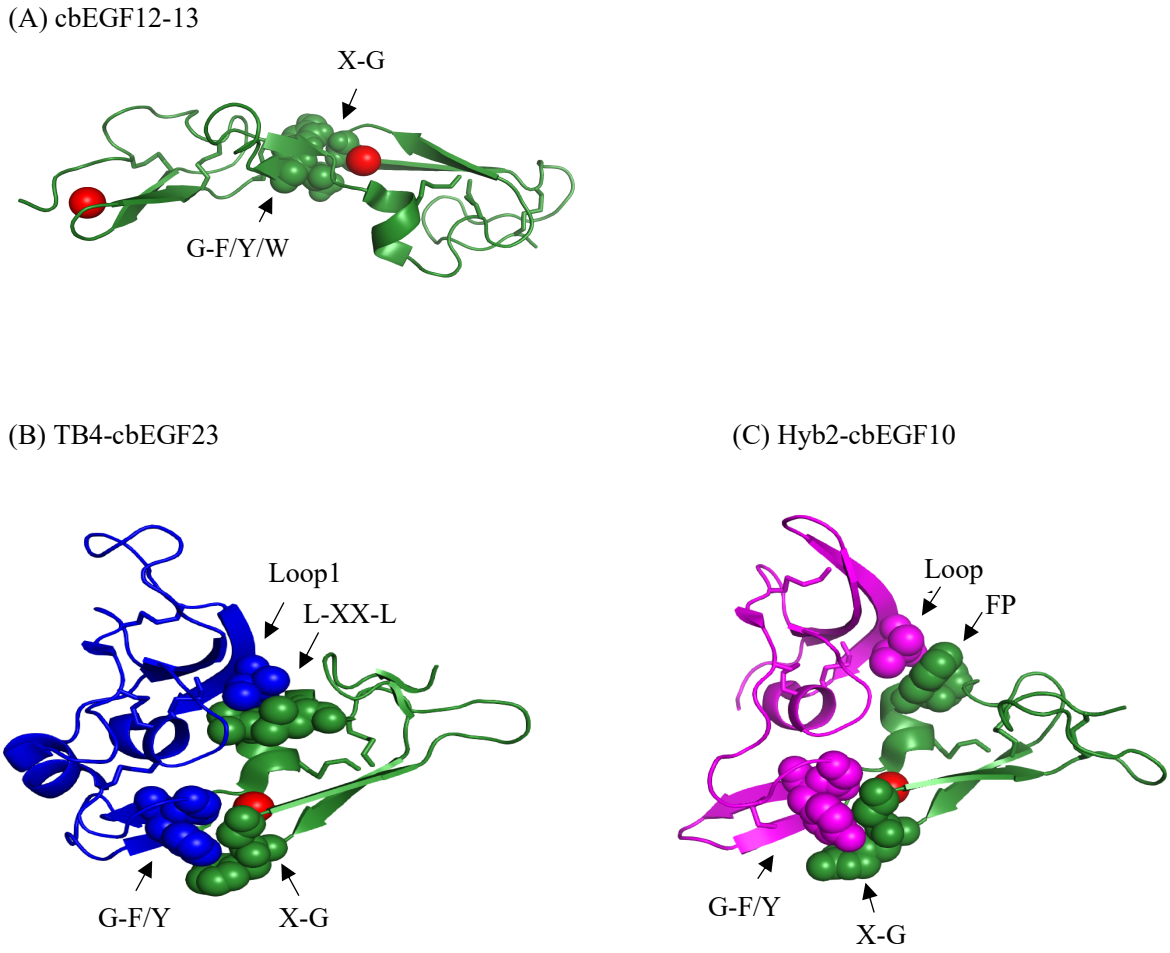


Figure 1.3 Interdomain packing interactions. Residues involved in interdomain packing in cbEGF-cbEGF, TB-cbEGF and hyb-cbEGF pairs are shown using sphere representations. Disulfide bonds are shown using stick representations and the Ca^{2+} bound to cbEGF domains is shown as a red sphere. (A) cbEGF12-13. G-F/Y/W motif in cbEGF12 packs against X-G motif in cbEGF13. (B) TB4-cbEGF23. G-F/Y motif in TB4 packs against X-G motif in cbEGF23. Also, loop 1 in TB4 packs with two leucine residues found in cbEGF23. (C) Hyb2-cbEGF10. G-F/Y in Hyb2 packs against X-G in cbEGF10 and loop 1 in hyb domains packs with tan FP motif sequence in cbEGF10.

1.2.4 Fibrillin evolution

The characteristic fibrillin domain organization emerged 600 million years ago. Fibrillin is widely distributed across species, from cnidarians to humans. All mammals, except rodents, armadillo and platypus contain fibrillin. Fibrillins are absent from the nematode *Caenorhabditis elegans* and the fruit fly *Drosophila melanogaster* although the gene sequence is present in other arthropods. Structures resembling microfibrils have been identified in tissues of several invertebrate species which lack elastin (Davison *et al.,* 1995; Reber-Muller *et al.,* 1995; Thurmond and Trotter, 1996), consistent with a conserved role of fibrillins in the formation of 10-12 nm microfibrils. The domain architecture is remarkably similar across the phylogenetic tree and is entirely conserved between all the three fibrillins in mammals, with the only exception being the alternatively spliced domain at the N-terminus of fibrillin-3 (Robertson *et al.,* 2011; Piha-Gossack *et al.*, 2012). This highlights the importance of register and indicates that spacing of the domains relative to each other maybe functionally relevant for microfibril assembly. Furthermore, the features of interdomain interactions remained similar throughout evolution (Jensen *et al.,* 2012), suggesting also conservation of the conformation of fibrillin.

1.3 Fibrillin-1 organization into microfibrils

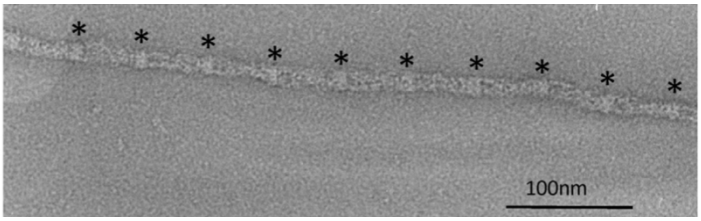
When viewed by electron microscopy after rotatory shadowing microfibrils appear to have a “bead on the string structure” (Figure 1.4A; Kielty *et al.,* 1995; Keene *et al.,* 1991). Scanning transmission electron microscopy (STEM) mass mapping studies demonstrated that microfibrils consist of eight fibrillin molecules in cross section, however, the process of fibrillin assembly into oligomeric microfibrils remains poorly understood (Baldock *et al.,* 2001). Two classes of models have been suggested to rationalize how ~150 nm fibrillin

monomers are arranged into microfibrils with an average inter-bead periodicity of 50-60 nm. Each model also proposes a corresponding mechanism for extensibility and recoil of microfibrils. Antibody epitope mapping, of fibrillin fragments within microfibrils, provided the basis of several studies of microfibril organization. Initially, Reinhardt *et al.,* (1996) showed that the N- and C- terminal regions overlap and reside at the 'bead' region but did not distinguish between the proposed models of either staggered or pleated microfibril assembly.

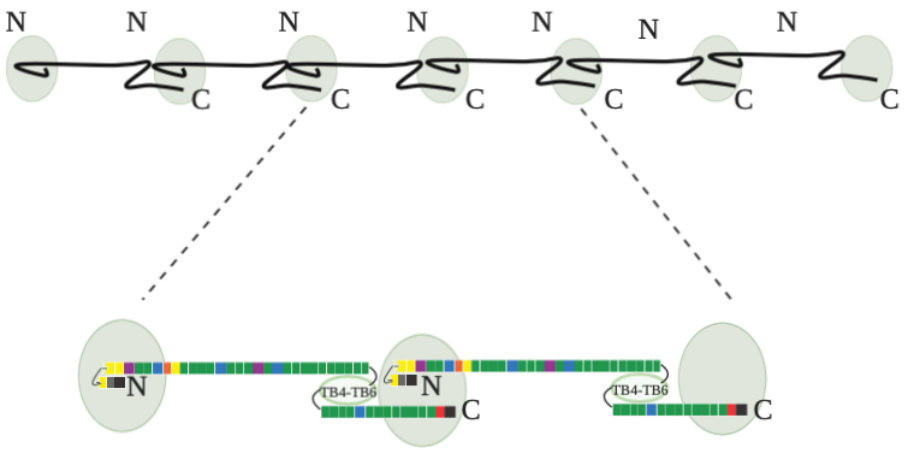
The pleated (unstaggered) model of microfibril organization proposes that individual fibrillin monomers are folded to fit within one bead-to-bead repeat distance but are extended at higher periodicities. This model is based on transmission electron microscopy mapping, antibody mapping and small-angle x-ray scattering (SAXS) data of overlapping multi-domain, recombinant, fibrillin fragments (Baldock *et al.,* 2006). The model predicts that the N-terminal region up to cbEGF2 is folded, and that the region spanning domains TB4 to TB6 is highly compacted, giving rise to the observed globular feature of microfibrils. The pleated model suggests that domain-domain conformational changes enable linearization and extensibility upon imposed force, but does not provide an explanation for how recoil could occur. Evidence for fibrillin extension was provided by studies that showed increase in inter-bead distance from ~50 nm to 150-160 nm upon microfibril extraction by applied force or increased ionic strength (Wang *et al.*, 2009). Furthermore, high-resolution structures of fibrillin domains in combination with calcium binding studies have identified two flexible domain interfaces; EGF1-EGF2 and TB6-cbEGF32, in addition to the hinge-like Pro-rich region that facilitates the folding mechanism (Jensen *et al.,* 2012; Yadin *et al.,* 2013). Nonetheless, the majority of the fibrillin molecule consists of tandem repeats of cbEGF domains that confer a near-linear rigid arrangement, which supports a more linear model of microfibril organization (Downing *et al.,* 1996).

The linear (staggered) model is based on high resolution structural information from NMR and X-ray crystallography, as well as antibody mapping of fibrillin microfibrils. The model proposes that fibrillin monomers have a largely linear conformation and form a ternary complex where the N- and C-terminal domains overlap at the bead structure, and that a central region of fibrillin, the 'neonatal' region is also positioned at the bead region (Lee *et al.,* 2004; Kuo *et al.,* 2007). Electron microscopy data of fibrillin-1 showing a 140-150 nm length of the extended molecule supports this model of microfibril assembly (Sakai *et al.,* 1991; Reinhardt *et al.,* 1997). This model postulates that extension and recoil are achieved by localized reversible folding and unfolding of domain interfaces which is assisted by the elasticity of the β-hairpin linker and heterologous TB-cbEGF and hyb-cbEGF domain interfaces (Lee *et al.,* 2004; Jensen *et al.,* 2009).

(A)



(B)



(C)

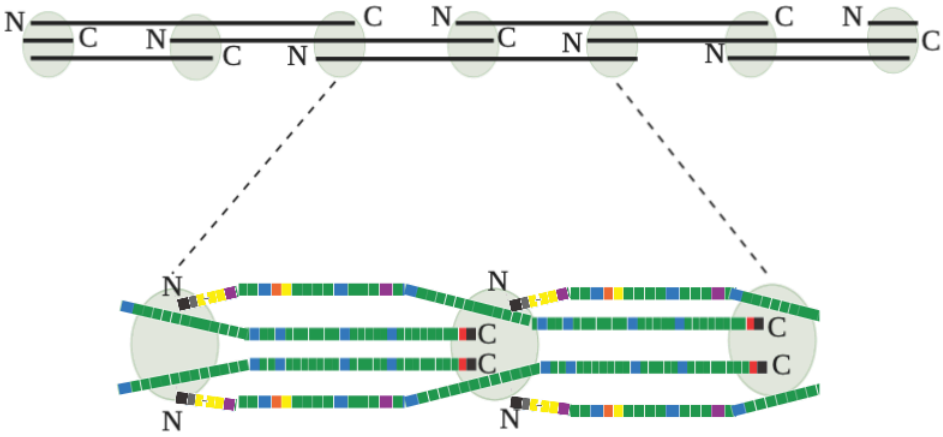


Figure 1.4 Proposed models of fibrillin organization into microfibrils. (A) Bead-on-the string structure of negatively stained TEM 10-12 nm microfibrils (Thomson *et al.,* 2019). (B) The pleated model suggests that folding of the FUN-EGF2 domain at the N-terminal end and folding of TB4-TB6 domains allow fibrillin monomers to fit within one bead-to-bead distance. Green ovals represent the 'bead' region. (C) The linear model predicts the formation of a ternary complex where the N- and C-terminal ends interact with the central region of another fibrillin monomer at the bead region. One fibrillin monomer spans two inter-bead distances.

1.4 Fibrillin assembly

Fibrillin assembly into microfibrils occurs in a highly regulated manner, however, the process is only partially understood. The multistep pathway involves post-translational modifications, furin-mediated processing of the N- and C- terminal propeptides, fibrillin localization at the cell surface through interaction with HSPGs, and multimerization of the fibrillin C-terminus which promotes intermolecular N- and C- terminal interaction of fibrillin molecules (Figure 1.5).

1.4.1 Post translational modifications of fibrillin-1

Profibrillin-1 undergoes extensive post-translational modifications within the cell. Some cbEGF domains contain potential sites for β-hydroxylation of specific aspartate or asparagine residues in the calcium binding site, but data verifying the use of this site is still lacking. O-linked glycosylation of a serine residue on fibrillin-1 has also been observed (Pereira *et al.,* 1993; Glanville *et al.,* 1994). Furthermore, sixteen potential sites for *N*-linked glycosylation of asparagine residues within an N-X-T/S sequence have been identified on fibrillin-1. It has been shown that only a number of these sites are utilized during normal physiological processing (Raghunath *et al.,* 1995; Reinhardt *et al.,* 1996). Although the functional roles of most of these PTMs remain elusive, the *N*-glycan site located near the C-terminal furin/PACE cleavage site is suggested to play a role in profibrillin cleavage (Raghunath *et al.,* 1995).

1.4.2 Furin-mediated cleavage of the fibrillin-1 N- and C- termini

Furin is a calcium-dependent serine endoprotease member of the subtilisin-like furin/PACE superfamily of proteases. It is a membrane protein that cycles between the cell surface and the *trans*-Golgi network (TGN), as well as in a truncated active form outside cells. Profibrillin is processed by furin into fibrillin at the cell surface (Wallis *et al.,* 2003). Cleavage occurs before and after the mature N- and C-termini respectively, producing full-length fibrillin starting with the N-terminal residue R45 after the cleavage site (Kettle *et al.,* 2000).

Cleavage of the C-terminal propeptide by furin is necessary for fibrillin assembly into the nascent microfibril. The presence of nonsense and missense mutations, associated with MFS

or related disorders, that alter the propeptide sequence and inhibit furin cleavage highlight the importance of C-terminal propeptide cleavage. Initially, data from a patient possessing skeletal features of MFS, as a result of a missense mutation two residues before the furin cleavage site, indicated that unprocessed fibrillin-1 does not incorporate into microfibrils, despite being secreted from cells (Milewicz *et al.,* 1995). Subsequently, recombinantly expressed mini-fibrillin constructs, full-length GFP-Fbn constructs, and protein engineering experiments designed to block furin activity, confirmed the necessity of furin processing for fibrillin-1 assembly at the cell surface (Lönnqvist *et al.,* 1998; Raghunath *et al.,* 1999; Jensen *et al.,* 2014). The role of N-terminal propeptide cleavage has not been directly investigated thus far.

1.4.3 N- and C- terminal interactions

Head-to-tail N- and C- terminal interactions are critical for fibrillin multimerisation. The first direct interaction of the N- and C- termini was provided by Lin *et al.,* (2002), using enzyme-linked immunosorbent assay (ELISA) and surface plasmon resonance (SPR) assays, demonstrating high-affinity binding of recombinant fragments of the respective domains. The interacting domains were then narrowed down to FUN-EGF3 at the N-terminus and cbEGF41-43 at the C-terminus in studies using pulldown experiments of purified N- and C- terminal fragments (Yadin *et al.,*2013).

Furthermore, a study by Hubmacher *et al.,* (2008) demonstrated that disulfide bond mediated multimerization of the C-terminus takes place at the cell surface and generates high affinity binding sites for the N-terminal region of fibrillin-1. Multimerization takes place as an intermediate step before bead-like structures interact with the N-terminus. The interaction mediating the multimerization was fine-mapped to the last 3 cbEGF domains cbEGF41-43.

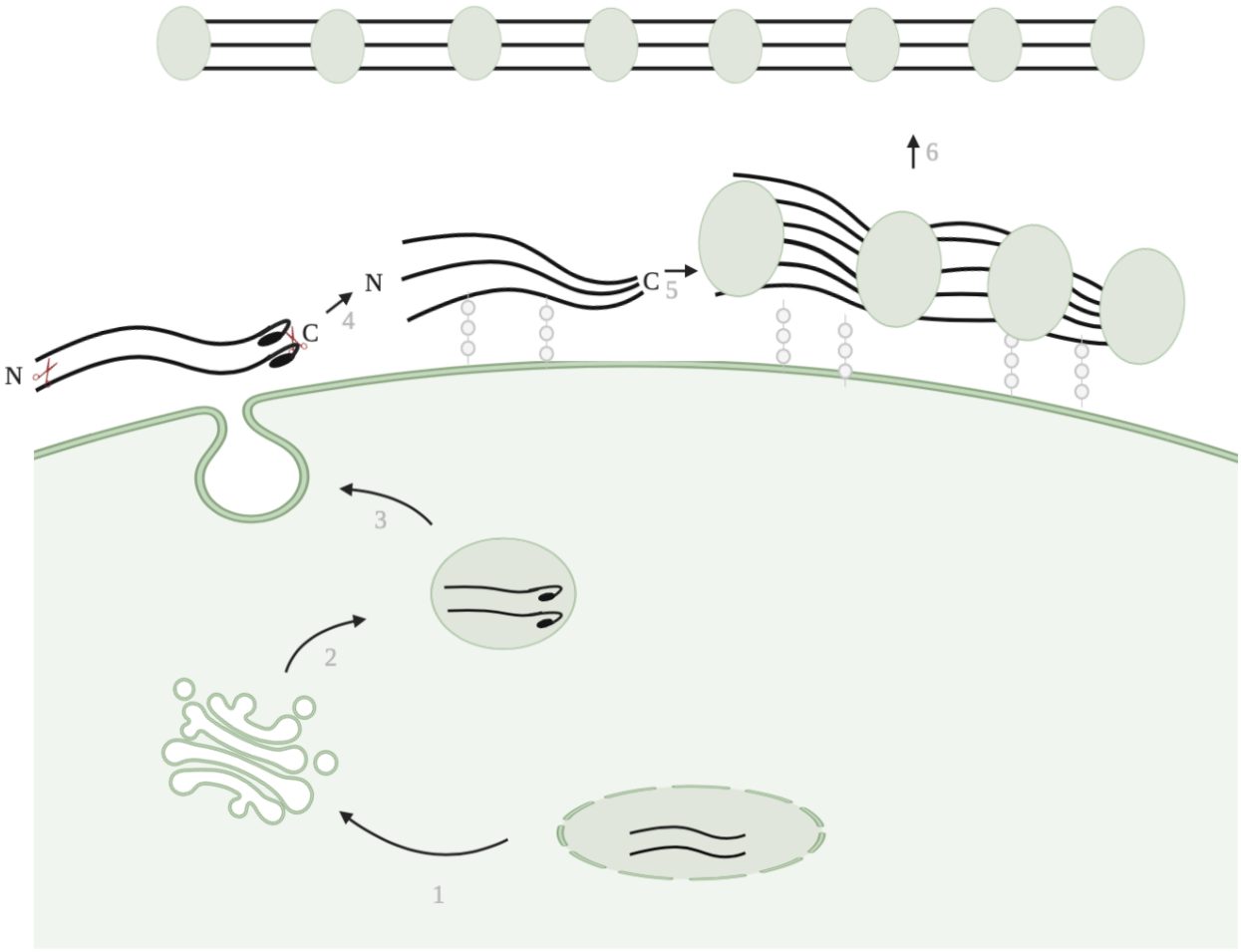


Figure 1.5 Fibrillin Assembly into Microfibrils. Fibrillin is translated (1) and passes through the secretory pathway where it is folded, forms disulfide bonds, undergoes O- and N-linked glycosylation, and potentially β-hydroxylation (2). Fibrillin is secreted from cells (3), and its pro-peptides are cleaved by furin at the cell surface (4), which allows for multimerization of the C-terminal ends of fibrillin monomers (4). The C-terminal oligomers interact with N-terminal ends of fibrillin with high affinity at the 'bead' region (5). Fibrillin is then arranged into mature microfibrils to form the bead-on-the string structure (6).

1.4.4 Microfibril interactions

Fibrillin microfibrils are also involved in heterotypic interactions with a variety of ECM, elastic fiber and cell-surface components (Figure 1.6). The extended architecture, domain modularity, and the flexible regions of fibrillin assist the binding of diverse proteins and proteoglycans to the assembled molecules. While the functional roles of some of these interactions remain unclear, they are what allow fibrillin microfibrils to have both structural and regulatory roles in the ECM. The physiological relevance of some of these interactions has been highlighted through their association with human and mouse pathologies.

1.4.4.1 Fibronectin

An intact fibronectin network is an essential prerequisite for the assembly of fibrillin-1 into microfibrils by mesenchymal cells in higher metozaons. Sabatier *et al.,* (2009) demonstrated the colocalization of fibrillin-1 and fibronectin in early-stages of ECM formation, and verified a direct interaction using fibrillin and fibronectin recombinant fragments. Moreover, ELISA and mapping studies demonstrated that the C-terminal regions of fibrillin-1, -2, and -3 as well as the N-terminal region of fibrillin-1interact with the collagen/gelatin-binding region between domains 6 to 9 of fibronectin type I (FNI_6 -FNI_9; Sabatier *et al.,* 2013).

1.4.4.2 Integrin

Integrins mediate cell adhesion to the ECM through an RGD tripeptide motif found on domain TB4 in fibrillin molecules (Pereira *et al.,* 1993; Pfaff *et al.,* 1996; Sakamoto *et al.,* 1996). A number of integrins ($\alpha_5\beta_1$, $\alpha_8\beta_1$, $\alpha_{IIb}\beta_3$, $\alpha_v\beta_3$, $\alpha_v\beta_1$, $\alpha_v\beta_6$, and $\alpha_v\beta_5$) have been shown to interact with fibrillin-1 recombinant fragments with varying affinities (Bax *et al.,* 2003; Lee *et al.,* 2004; Jovanovic *et al.,* 2007; Del Cid *et al.,* 2019). Integrin mediated cell-matrix interactions are involved in the regulation of cell adhesion and migration, reorganization of

the actin cytoskeleton, growth, proliferation, and differentiation. Maintenance of a specific level of fibrillin-integrin interaction is necessary for the regulation of ECM production in the skin, and its interruption results in ECM component overproduction and a fibrosis response in a tissue-specific manner (Bona *et al.,* 1997; Siracusa *et al.,* 1996). A subset of *FBN1* mutations that give rise to stiff skin syndrome (SSS) have been localized to the RGD-containing domain TB4 of fibrillin-1, highlighting the physiological importance of integrin binding to fibrillin-1 (Loeys *et al.,* 2010).

1.4.4.3 Heparin/heparan sulphate

Heparan sulfate proteoglycans are involved in fibrillin assembly at the cell surface. Seven heparin-binding sites of varying affinities have been mapped to fibrillin-1 including: two at the FUN domain, cbEGF1-2, cbEGF12-cbEGF14, TB5-cbEGF25, cbEGF38, and the C-terminal furin cleavage site. Initial evidence of the interaction is based on studies that demonstrated inhibition of microfibril assembly upon exogenous addition of heparin or heparin sulfate analogues in mesenchymal cell culture (Tiedemann *et al.,* 2001; Cain *et al.,* 2008). Studies have illustrated that heparin binding at the N-terminus influences fibrillin-cell interactions, while its binding at the C-terminal end is involved in the regulation of elastin deposition (Cain *et al.,* 2008). Further data confirmed the need for heparin for fibrillin sequestration at the cell surface and regulation of microfibril formation at the point of bead interaction via its binding at the FUN-EGF3 domain (Yadin *et al.,* 2013; Sabatier *et al.,* 2014).

1.4.4.4 LTBPs

Fibrillin interaction with LTBPs is critical for regulating the activity of the growth factor TGFβ in the ECM. LTBPs play a role in the secretion of TGFβ from cells as well as its

activation by integrins. LTBP-1, -2 and -4 bind to fibrillin-1. Recent studies have shown that domain TB2 located at the C-terminal region of LTPB-1 binds to the domains EGF2-cbEGF1 of fibrillin-1 via a bipartite interaction (Figure 1.6; Hirani *et al.,* 2007; Isogai *et al.,* 2003; Robertson *et al.,* 2017). LTBPs maintain TGFβ in a latent state through a covalent interaction with a latency-associated peptide (LAP) which in turn binds TGFβ through a non-covalent linkage. Integrin binding to the RGD motif is required to generate force to pull the latency complex apart and enable the release and activation of TGFβ. (Miyazono *et al.,* 1988; Miyazono *et al.,* 1991).

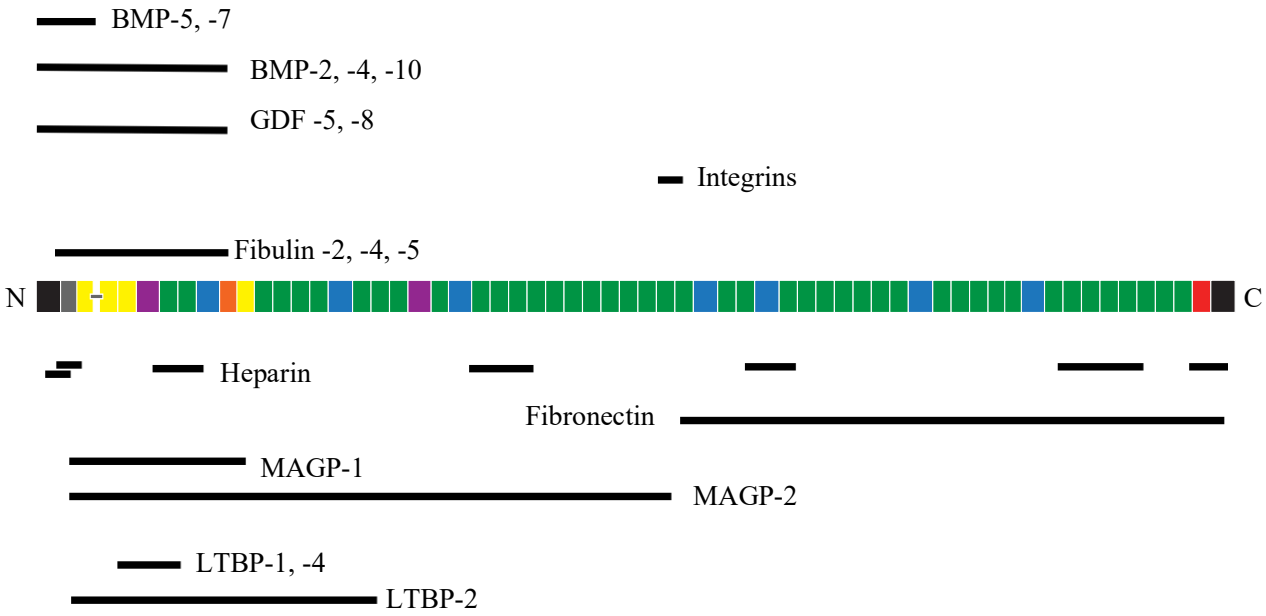


Figure 1.6 Fibrillin-1 proteoglycan/glycosaminoglycan interactions. Binding sites of accessory factors that interact with fibrilin-1 in the extracellular matrix are represented as black bars. Interaction sites were obtained from: Heparin (Tiedemann *et al.,* 2001; Cain *et al.,* 2008), Fibronectin (Sabatier et al., 2009) MAGP-1(Jensen *et al .,* 2001) MAGP-2 (Hanssen et al., 2004), LTBP-1 -4 (Isogai et al., 2003; Ono *et al.,* 2009) , LTBP-2 (Hirani et al., 2007), BMPs (Gregory et al., 2005; Sengle *et al.,* 2008), GDF -5 -8 (Sengle *et al.,* 2008), Integrins (Pffaf *et al., 1996*; Sakamoto *et al.,* 1996) and fibulin (Ono *et al.,* 2009)

1.5 *FBN1* disease-causing mutations

1.5.1 Type-1 fibrillinopathies

The importance of fibrillin-1 as a major structural protein is emphasized by the implication of its associated substitutions on connective tissue dysregulation and dysfunction. Substitutions affecting domains across the whole of fibrillin-1 give rise to Marfan Syndrome (MFS; MIM #154700) while others, localized to specific domains, have been linked to other connective tissue disorders collectively known as type-1 fibrillinopathies. Substitutions altering the RGD integrin binding motif on TB4 cause SSS (MIM #184900; Loeys *et al.,* 2010), substitusions affecting domain TB5 result in acromicric dysplasia (AD; MIM #102370; Takeshima *et al.,* 2013) and geleophysic dysplasia (GD; Le Goff *et al.,* 2011; Lee *et al.,* 2013), and mutations in domains TB1-EGF4 and domain TB5 give rise dominant Weill-Marchesani syndrome (WMS; MIM #277600; Backer *et al.,* 2007; Stheneur *et al.,* 2009). Several characteristic phenotypes associated with these disorders, including short stature, skin thickening, joint stiffness, and short extremities, contrast strongly to those present in MFS (Section 1.6), which highlights the pleiotropic role of fibrillin microfibrils. Despite the phenotypic variability, dysregulation of TGFβ is a common prominent feature observed in all fibrillin-1 associated disorders (Section 1.6.3).

1.6 The Marfan syndrome

Marfan Syndrome is an autosomal dominant hereditary disease of the connective tissue with an average prevalence of 2-3 in every 10,000 individuals, with no gender, ethnic, or geographical bias (Dietz and Pyeritz, 1995). MFS is associated with variable clinical manifestations occurring in the cardiovascular, skeletal and ocular systems. Skeletal

deformities include tall stature, bone overgrowth (dolichostenomelia), long fingers (arachnodactyly) and chest deformities (pectus carinatum and pectus excavactum), ocular defects include displacement of the lens (ectopia lentis), caused by weakness of the ciliary zonule, and cardiovascular phenotypes include myopia, aortic dilation and dissection, the latter of which is the main cause of morbidity and mortality in MFS (Sakai *et al.,* 1986; Gray and Davies, 1996). MFS is characterized by inter- and intrafamilial phenotypic variability and a wide spectrum of severity. Mildly affected patients possess isolated features of MFS, such as ascending aortic aneurysm but lack ocular or skeletal defects (Francke *et al.* 1995). Patients with mitral valve, aorta, skin and skeleton phenotype (MASS; MIM #604308) are affected with less progressive cardiovascular phenotypes and no ocular defects (Milewicz *et al.* 1996). The most severe end of the spectrum is neonatal Marfan Syndrome (nMFS) which is associated with perinatal mortality and death <2 years after birth (Godfrey *et al.* 1995).

1.6.1 Marfan syndrome-causing mutations

Dietz *et al.,* (1991) were the first to show that MFS arises as a result of mutations in the gene encoding fibrillin-1 when they identified a *de novo* R→P substitution in a patient with sporadic disease. Currently, >3000 different mutations have been found on *FBN*1 (http://www.umd.be/FBN1/ - last updated 8/29/2014). Point mutations are the most common type, followed by deletions, splice site mutations and to a lesser extent, insertions and duplications. The larger percentage of point mutations are missense mutations, rather than nonsense mutations, the highest number of which affect cbEGF domains.

Several studies using MFS patient fibroblasts or engineered fibrillin mutations elucidate the structural and functional effects of amino acid substitutions on fibrillin domains. Most

mutations perturb the fold of cbEGF domains either by substituting cysteine residues and disrupting the disulfide bonding pattern or by substituting residues involved in calcium binding (Downing *et al.,* 1996). A set of calcium binding residue substitutions (N548I) have localized structural effects, increasing proteolytic susceptibility of adjacent domains only, while others (D1113G, D1115G, N1131Y, E1073K) have both short- and long-range structural consequences, leading to increased susceptibility to proteolytic cleavage of N-terminally adjacent domains (Whiteman *et al.,* 2007). Furthermore, a number of cysteine substitutions, associated with classical MFS (C1129Y, C1117Y, C1564Y, C1719Y, C1720Y), result in complete retention of fibrillin-1 in the endoplasmic reticulum (ER) when expressed as recombinant fibrillin fragments, which is indicative of a folding defect (Whiteman and Handford 2003, Jensen *et al.,* 2015), while others (C219Y, C1409S, C351S, C765R, C1323S) result in delayed secretion and reduced deposition of fibrillin-1 in the matrix surrounding patient cells (Aoyama *et al.,* 1993; Halliday *et al.,* 1999). Mutations affecting other residues (G1127S) result in minor structural alterations that does not inhibit fibrillin-1 secretion from cells, shown both in patient (Francke *et al.,* 1995) and recombinant fragment studies (Whiteman and Handford 2003).

1.6.2 Marfan syndrome pathogenesis

Disease progression in MFS is associated with perturbed TGFβ signalling and loss of connective tissue integrity. Changes in the mechanical properties of tissues result from reduction in the quality and quantity of fibrillin microfibrils due to deficiencies in the biogenesis of the microfibril/elastic fibre system and/or increased degradation of this system. The ultrastructural and biomechanical properties of microfibrils are often

compromised in MFS. However, the precise mechanism by which this leads to disease is still unclear.

1.6.2.1 TGFβ signaling in Marfan syndrome

TGFβ is a multipotent extracellular matrix cytokine involved in mesenchymal cell growth, proliferation and differentiation, embryonic development, ECM remodeling, apoptosis induction, migration, adhesion and cell survival, as well as upregulating synthesis of other extracellular matrix components. Dysregulation of TGFβ has been implicated in fibrotic and non-fibrotic diseases and is correlated with aortic aneurysm development and all other fibrillin associated disorders (Ng *et al.,* 2004; Loeys *et al.,* 2005; Loeys *et al.,* 2010). The direct mechanism by which fibrillin microfibrils attenuate TGFβ levels in the ECM is unclear, however it has been hypothesized that fibrillin-1 deficiency in hypomorphic mouse models resulted in insufficient latency of TGFβ, which leads to its overactivation (Neptune *et al.,* 2003). Together, these results indicated that upregulation of TGFβ signaling as well as loss of structural and mechanical properties of microfibrils are major drivers of connective tissue dysregulation observed in MFS **(**Doyle *et al.,* 2012; Sakai *et al.,* 2016). Furthermore, treatment with Losartan, an angiotensin II receptor type 1 blocker (AGTR1), which both lowers blood pressure and attenuates TGFβ signaling, ameliorated the thoracic aortic aneurysm (TAA) phenotype in MFS mice (Habashi *et al.,* 2006). This further highlights the controversy of TGFβ signaling to the development of MFS.

1.6.3 Neonatal Marfan syndrome

Because of the challenging nature of the ECM and difficulties associated with studying ECM proteins, clear genotype-phenotype correlations in MFS have only recently started

emerging. Most strikingly, a clustering of mutations, associated with the more severe form, neonatal MFS, has been mapped to the central region of the protein spanning domains TB3-cbEGF18 (exons 24-32), known as the 'neonatal' region (Figure 1.7). The majority of nMFS mutations are missense mutations, however splice donor and deletions have also been identified in nMFS patients. Mutations associated with the milder form, 'classical' Marfan syndrome (cMFS) are found in this region as well. The neonatal region is found within the longest stretch of cbEGF domains, which makes significant contributions to the extended rod-like conformation of fibrillin-1 and provides a surface area for the binding of other ECM components including versican and heparin (Isogai *et al.,* 2002; Cain *et al.,* 2005). This central region is also hypothesized to interact with fibrillin N- and C- termini according to the staggered model of microfibril assembly (Kuo *et al.,* 2007).

Neonatal MFS patients share typical clinical features with cMFS patients along with additional severe skeletal and cardiovascular phenotypes. In addition to the pectus deformities, neonatal MFS patients have congenital flexion contractures and loose redundant skin. They are also affected with more progressive cardiovascular phenotypes including cardiac valve regurgitation and dilation of the proximal aorta, which leads to death before two years of age due to congestive heart failure.

While several studies have demonstrated that mutations associated with nMFS result in increased susceptibly of recombinant fibrillin-1 to proteolysis and reduce its ability to bind heparin, the pathogenic mechanisms that give rise to the severity of nMFS remain elusive. Therefore, correlation between domain defects and their cellular consequences on fibrillin-1 secretion and assembly is key to understanding the threshold loss of microfibril functionality observed in MFS.

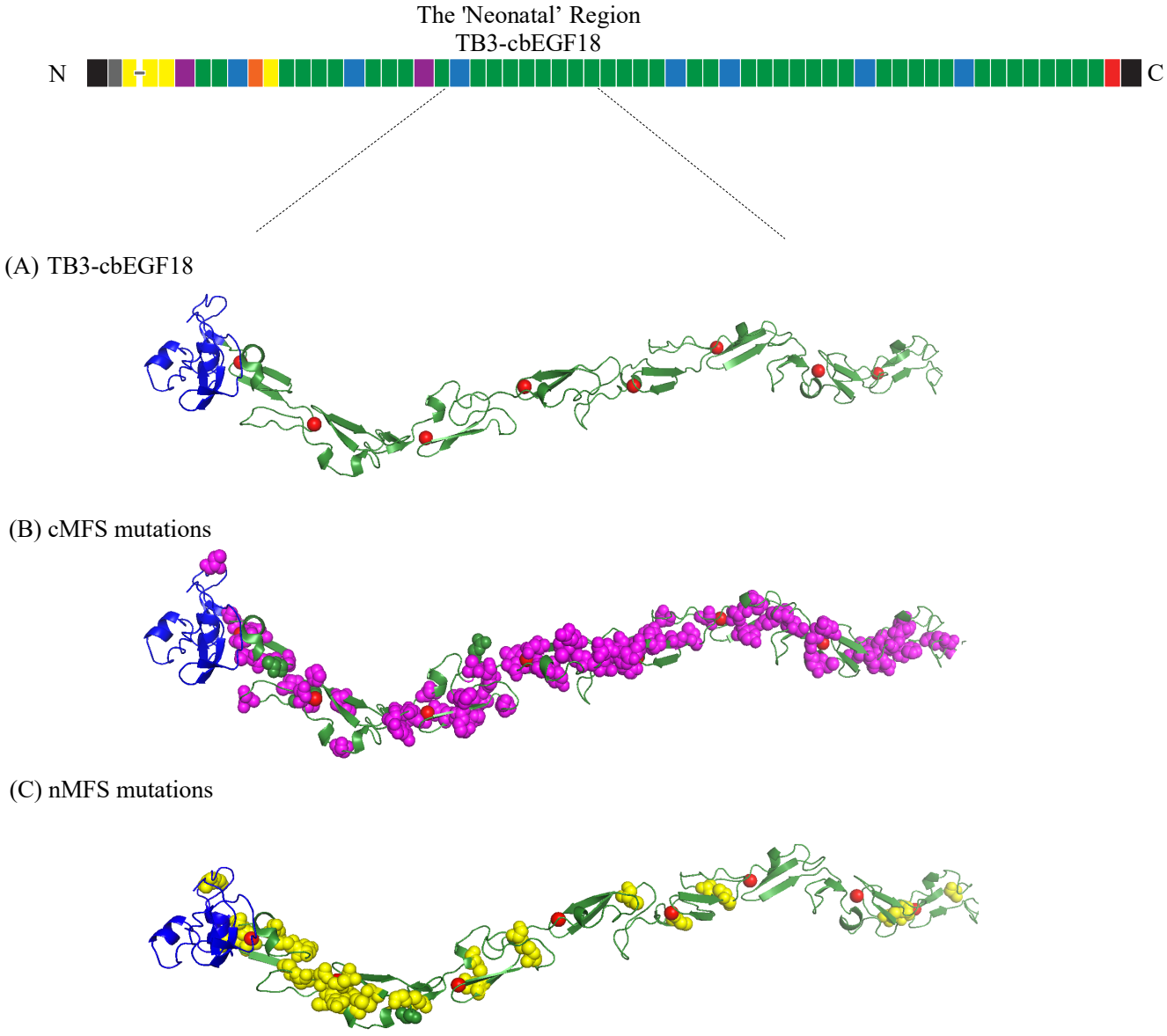


Figure 1.7 Clustering of the neonatal MFS and 'classical' MFS mutations in the Fibrillin-1 'neonatal' region. (A) Three-dimensional homology model (Jensen *et al.,* 2016) of fibrillin-1 domains TB3-cbEGF18 known as the 'neonatal' region. (B) Mapping of mutations associated with 'classical' MFS found in domains TB3-cbEGF18. Point mutations are represented as magenta spheres. (B) Mapping of mutations associated with neonatal MFS that are localized to this region. Point mutations are shown as yellow spheres. All mutations were obtained from http://www.umd.be/FBN1/. Figures were rendered using pyMOL (Schrödinger, LLC).

1.6.4 Models of pathogenic mechanisms underlying Marfan syndrome

Two major underlying mechanisms of MFS pathogenesis have been proposed. The haploinsufficiency model indicates that reduced amount of fibrillin microfibrils results in MFS, while the dominant negative mechanism suggests that defective microfibril function caused by incorporation of mutant fibrillin underlies MFS pathology.

Evidence from clinical characterization of patients with nonsense alleles, where premature termination codon mutations result in rapid degradation of the mutant transcript via the nonsense-mediated mRNA decay pathway, indicate that haploinsufficiency underlies pathogenesis in MFS (Hewett *et al.,* 1994; Frischmeyer and Dietz, 1999). Findings of a *FBN1* deletion in a patient showing marfanoid characteristics (Hutchinson *et al.,* 2003) and evidence of reduced fibrillin microfibrils in mouse models (Judge *et al.,* 2004), also suggest that reduction in amounts of fibrillin-1, rather than incorporation of mutant protein, accounts for the threshold loss of fibrillin in the matrix, consistent with the haploinsufficiency model of MFS pathogenesis. Furthermore, studies showing ER retention of fibrillin-1 mutant constructs in fibroblasts, suggested that disease associated with these misfolding mutations arises as a result of an intracellular dominant negative effect or haploinsufficiency (Whiteman and Handford, 2003; Jensen *et al.,* 2015).

A dominant negative mechanism of MFS pathogenesis involves the mutant protein either interacting with wild type (WT) fibrillin, precluding its efficient assembly into microfibrils, or being mis-incorporated into microfibrils. The dominant negative model of microfibril

biogenesis is based on observations in molecular mechanisms associated with collagen substitutions, where interacting molecules participate in initial stages of assembly, but subsequent assembly steps are impaired (Hoda *et al.,* 2015). In fibrillin-1 associated diseases, evidence for this model is based on studies that reported a dramatic reduction in matrix-assembled microfibrils in cell cultures of MFS patients, significantly less than the 50% level predicted from simple loss of expression of the mutant allele (Aoyama *et al.,* 1993; Kielty *et al.,* 1995). These results were recapitulated using pulse-chase metabolic labelling and immunohistochemical analysis showing that expression of mutant allele interferes with normal microfibrillar assembly, causing a substantial decrease in assembled fibrillin microfibrils (<50%) despite normal protein synthesis and secretion (Eldadah *et al.,* 1995). Together, these results suggest that dominant negative interference could take place at the level of microfibril assembly, although molecular/cellular assays proving such a mechanism have been difficult to establish.

1.8 Thesis Aim

This study aims to investigate the molecular pathology underlying nMFS and cMFS, based on fibrillin-1 secretion and assembly. Thus far, the molecular pathology of MFS does not explain the wide range of severity associated with substitutions in domains TB3-cbEGF18. Therefore, a set of substitutions associated with cMFS (Y1101C, D1113G, D1115G, N1382S and N2144S), nMFS (I1048T, E1078K, C1086Y, C1111R, N1131Y and splice site mutation Δcb16) and isolated aortic aneurysm (G1127S), in TB3-cbEGF19, were investigated for their effect on fibrillin-1 trafficking. The aims of this thesis are as follows:

- To determine the effect of these variants on the secretion of GFP-Fbn1 from transiently transfected HEK293T cells.
- To determine the ability of these variants to incorporate into FS2 assembled microfibrils.
- To determine residue and/or residue sequence conservation in cbEGF11-14 vs cbEGF25-28 using bioinformatics analysis.
- To determine the effect of these variants on the secretion of recombinant fibrillin-1 proteins from pools of MSU1.1 clones.
- To verify the effect of these variants on the secretion of recombinant fibrillin-1 proteins from transiently transfected HEK293T cells.

Chapter 2

Materials and Methods

2.1 DNA Cloning Techniques

2.1.1 DNA amplification using polymerase chain reaction (PCR)

The required region of fibrillin-1 was amplified from the pcDNA-GFP-Fbn vector, encoding full-length fibrillin-1 with an N-terminal GFP tag (Jensen *et al.,* 2014). Amplified regions were used for mutagenesis and cloned back into the GFP-Fbn vector or into the pKG52(polyA) vector, encoding the N-terminal region of fibrillin-1 up to the Pro rich region (residues 1–446) under the control of a thymidine kinase promoter (Appendix 1). Mutant constructs were created using site-directed mutagenesis (Section 2.1.1.2). All PCR reactions were run on Biometra T3 Thermocycler. The enzyme KOD Hot Start Polymerase (Novagen) was used for insert amplification. The PCR cycle steps are summarized in Table 2.1. Reactions were carried out in a total volume of 50 µl with components summarized in Table 2.2, in 600 µl thin walled PCR tubes (Axygen).

Table 2.1 PCR thermocycler times and temperatures.

PCR Step	Temperature (°C)	Time (s)	
Initial Denaturation	95	180	
Denaturation	95	20	×30
Annealing	55	10	
Extension	70	20/1kb	
Keep	4	-	

Table 2.2 KOD Polymerase master-mix component mixture.

PCR master-mix component	Volume (µl)
10 ng/µl Template DNA (FBN1 cDNA)	2

10× KOD Buffer	5
2 mM dNTPs	5
25 mM $MgSO_4$	3
10 µM Forward Primer	1.5
10 µM Reverse Primer	1.5
KOD Hotstart Polymerase	1
MilliQ (MQ)	31
Total	50

2.1.1.1 Oligonucleotide primers

The hybridization temperatures were based on a lowest primer melting temperature (T_m) of 62°C and calculated using the equation: $T_m = 4 \times (G + C) + 2 \times (A + T)$, where A, T, G, and C are the numbers of each nucleotide present in the DNA molecule. All primers were synthesized and supplied by Thermofisher UK. The oligonucleotides, of varying concentrations, were diluted in 500 µl of MQ H_2O for storing stocks and kept at -20°C. Working stocks of 10 µM or 15 µM were made for the PCR amplification reaction using KOD or Taq Polymerase. The extension time corresponded to the length of the DNA construct (20s/1kb). The sizes of the PCR products were confirmed using agarose gel electrophoresis (section 2.1.3).

For cloning of the construct encoding domains TB3-cbEGF19 into the pKG52(polyA) expression vector, the forward and reverse primers were designed to contain *SalI* restriction sites. These sites were used for inserting the amplified DNA into the *XhoI* restriction sites in the expression vector (Appendix 1 and 2).

2.1.1.2 Site directed mutagenesis

Base substitutions were introduced into the amplified region using overlapping extension PCR with oligonucleotide primers containing the required mutation. Two separate PCRs were run simultaneously; the first using a forward primer and a reverse mutagenic primer creating the 5' product, and the other using a reverse primer and the forward mutagenic primer creating the 3' product. The first set of PCR products were purified using the PCR product clean up method (Section 2.1.2). The second PCR was run using the forward and reverse primers along with 2 µl of each of the 3' and 5' PCR products to create the final mutant product.

2.1.2 PCR product clean up

After each PCR, the DNA was purified using Qiagen PCR Product Clean Up Kit according to manufacturer's instructions, yielding 30 µl of purified DNA.

2.1.3 Agarose gel electrophoresis

1 – 2 % (w/v) agarose gels, depending on the expected size of the DNA molecules, containing a final concentration of ~2 µg/ml ethidium bromide were prepared by addition of Agarose Powder (MP Biomedicals) in 1× Tris-borate-EDTA (TBE) buffer (Appendix 3). The agarose was dissolved by heating the solution until boiling temperature and left to set into gel form, in a small or wide Mini-Sub Cell (Biorad) at room temperature. DNA samples were supplemented with 1× DNA loading dye (New England Biolabs) and loaded onto the agarose gel alongside 100 bp or 1 kb standard size markers (New England Biolabs). Electrophoresis was carried out in 1× TBE buffer at 80V for 60 minutes. DNA bands were

identified by exposing the gel to a hand-held long wave ultraviolet (UV)-transilluminator (UVItech) to avoid DNA damage, and excised using razor blades. The gel was photographed using a UVP imager (AnalytikJena).

2.1.4 Gel purification

DNA was purified from the excised gel slices using Qiagen Gel Purification Kit according to manufacturer's instructions, yielding 30 µl of the insert DNA product with the desired mutation.

2.1.5 Restriction enzyme digestion

For the preparation of vectors for cloning restriction digests typically contained 2-3 µg of DNA or the entire 30 µl insert DNA. Digestion mixtures containing components summarized in Table 2.3 were set up. Mixtures were incubated at 37°C for 1 hour using a thermomixer (Eppendorf).

Table 2.3 Vector backbone and insert digestion mixture components.

Digestion mixture component	**PCR Product (**µl)	**Vector** µl
DNA	30	4 (782 ng/µl stock)
10× Cut Smart Buffer	5	5
10 or 20U/µl Restriction Digest	1	1
MQ H_2O	14	40
Total	50	50

2.1.6 Dephosphorylation

For dephosphorylation of the 5' end of digested DNA, both insert and vector DNA were incubated with 1U/100 µl calf intestine alkaline phosphatase (CIP) enzyme (Roche) for a further 30 minutes at 37°C. Dephosphorylation was stopped by the addition of DNA loading dye to a 1× concentration and the DNA products run on a 1% agarose gel (Section 2.1.3) alongside a 1 kb ladder, followed by excision and purification of the bands (Section 2.1.4).

2.1.7 Ligation

Ligation was performed using a Rapid DNA Ligation kit (Roche). Approximately 100 ng of insert DNA was used in ratios of vector to insert of 1:1 – 1:6. DNA was incubated at 25°C for 10 minutes with 1× ligation buffer, 1× DNA dilution buffer and 5 U of 5 U/µl T4 DNA ligase in a total reaction volume of 21 µl.

2.1.8 Transformation of NEB-5α competent cells

Plasmids were transformed into NEB-5α chemically competent *E.coli* (New England Biolabs) for cloning. The cells were thawed on ice for 10 minutes. 1-5 µl of the DNA mixture was pipetted into 100 µl of the *E.coli*, mixed gently and incubated on ice for 30 minutes. The cells were heat shocked at 42°C for 30 seconds followed by incubation with 950 µl Super Optimal Broth (SOC) medium (New England Biolabs) at 37°C for 60 minutes. The transformed cells were then plated on pre-heated agar plates containing 100 µg/ml ampicillin and incubated at 37°C overnight. A negative control transformation, where the ligation

mixture did not contain insert DNA was carried out to confirm complete digestion of the vector.

2.1.9 PCR based colony screening

To examine the presence of DNA fragments at the expected size and correct orientation PCR based colony screen was performed. 8 individual colonies were picked using a sterile metal loop, resuspended in 50 µl of MQ H_2O and vortexed briefly. 6 µl of the colony suspension was added to 30 µl of a PCR screen master mix with components summarized in Table 2.4. A forward primer spanning a sequence in the vector and a reverse primer spanning a DNA sequence in the insert were used (Appendix 2). The thermal profile composed of an initial denaturation step for 3 minutes at 95°C, followed by 30 cycles of denaturation, annealing and extension and a final extension step at 72°C as detailed in Table 2.5. 6 µl of a 6× DNA loading dye was added to the 30 µl PCR product. 12 µl of the mixture was run on a 1% agarose gel alongside a 1kb ladder (Section 2.1.3). The positive clones were prepared for plasmid DNA harvesting.

Table 2.4 PCR based colony screen Taq Polymerase PCR component mixture.

PCR master-mix component	**Volume (µl)**
Bacterial colony	6
10× Taq Polymerase Buffer (New England Biolabs)	3
10 µM dNTPs (Roche)	0.6
15 µM Forward Primer	0.3
15 µM Reverse Primer	0.3
5U/µl Taq Polymerase Enzyme	0.2
MQ H_2O	19.6
Total	30

Table 2.5 PCR thermocycler times and temperatures.

PCR Step	Temperature (°C)	Time (Minutes)
Initial Denaturation	95	3
Denaturation	95	1
Annealing	55	0.5
Extension	72	2
Final Extension	72	10
Keep	4	-



2.1.10 Preparation and harvesting of plasmid DNA

Single bacterial colonies were used to inoculate 100 ml of autoclaved 2× YT medium (MP Biochemicals) containing 100 μg/ml ampicillin. The cultures were incubated at 37°C and shaken at 280 rpm overnight. The cells were harvested by centrifugation in 50 ml falcon tubes (Greiner Bio-one) and plasmid DNA isolated using Qiagen Plasmid Midi Kit. The DNA pellet was diluted in 400 μl MQ H_2O.

2.1.11 Quantification of DNA and RNA

Samples of plasmid DNA were diluted 1:20 in elution buffer (EB; Qiagen) in a total volume of 100 μl. A Shimadzu UV-mini 1240 spectrophotometer was used to measure the absorbance of the dsDNA at 260 nm (A_{260}) in a 100 μl quartz cuvette (Hellma). The concentration of DNA was calculated on the basis that A_{260} for 50 μg/ml is 1.0 and therefore ($A_{260} \times 50 \times 20$) was used to provide the concentration of DNA in μg/ml. The concentration of RNA was calculated on the basis that A_{260} for 40 μg/ml is 1.0.

2.1.12 Sequencing DNA

To confirm the correct DNA sequence and presence of point mutations, 100 μg/ml of plasmid DNA and 3.2 μM custom primers were each diluted in MQ H_2O in 1.5 ml Eppendorf tubes. Samples were sent to and processed by Source Bioscience Oxford.

2.2 Eukaryotic protein expression

2.2.1 Maintenance of cell lines

Human dermal fibroblast lines from foreskin (FS2s), human embryonic kidney 293T cells (HEK293Ts) and human skin fibroblast (MSU 1.1) lines were used for protein expression, secretion and microfibril assembly experiments. Cells were maintained in pre-warmed Dulbecco's Modified Eagle Medium (DMEM; Invitrogen), supplemented with 10% (v/v) fetal bovine serum (FBS; Invitrogen), 50 U/ml penicillin, 50 μg/ml streptomycin and 2 mM L-glutamine (Sigma-Aldrich), to make complete DMEM. All cell lines were cultured in 175 cm^2 tissue culture flasks (T175; Greiner Bio-one) and incubated in a humidified CO_2 incubator at 37^oC and 5% CO_2. Cells were passaged every 3 – 4 days, or when ~90% confluent. Subcultures of cells for the respective experiments were made from the original maintenance flasks.

2.2.2 Culturing and passaging of cells

Typically, confluent monolayers of cells in T175 flasks were washed with 10 ml phosphate buffer saline (PBS; Sigma Aldrich) containing 0.02% (w/v) ethylenediaminetetraacetic acid (EDTA; MP Biochemicals), detached using 5 ml 1:10 Trypsin-EDTA(Sigma

Aldrich)/PBSE and the flask incubated at 37ºC for 1-5 minutes. Trypsinization was terminated by addition of 15 ml complete DMEM and the cells pelleted by centrifugation at 1000 rpm for 3-6 minutes (ALC centrifuge PK120, T534 rotor). The cell pellet was resuspended gently in 25, 15 or 5 ml of fresh complete DMEM. Typically, cells were split 1:2 (FS2s), 1:10 (HEK293Ts) and 1:6 (MSU 1.1).

2.2.3 Freezing and thawing of cells

Cells were washed with 10 ml PBSE, detached using of 5 ml 1:10 trypsin-EDTA in PBSE, and centrifuged at 1000 rpm for 3 minutes. Cells at a concentration of ~$3x10^6$ cells/ml or a ~90% confluent T25 were resuspended in 1 ml 10% dimethyl sulfoxide (DMSO, Sigma Aldrich) in 90% FBS. The cells were frozen slowly to -80°C in 2 ml cyrotubes (Nunc) using a Stratacooler cryofreezer (Stratagene) before being transferred for long term storage in liquid nitrogen.

For rapid thawing of cells, cryotubes containing frozen cells were thawed in a 37 ºC water bath for 10-30 seconds. The cells were then pipetted into 6 ml of complete DMEM in a 15 ml falcon tube (Greiner Bio-one) and centrifuged at 1000 rpm for 5 minutes. The cell pellet was resuspended in 5 ml complete DMEM and placed in a fresh 25 cm^2 tissue culture flask (T25; Greiner Bio-one). The cells were transferred to 75 cm^2 tissue culture flasks (T75; Greiner Bio-one) and then to T175 flasks when they reached ~90% confluency and maintained as outlined in section 2.2.1.

2.2.4 Transient transfection of HEK293T cells and secretion assay set up

24 h prior to transfection, HEK293T cells, from a ~90% confluent T175 flask, were trypsinized, centrifuged and resuspended in 20 ml fresh complete DMEM (section 2.2.2). 600 µl of cells (1:2 ratio) were sub-cultured into 6 well tissue culture plates (Greiner Bio-one), completed to 3 ml with fresh complete DMEM and left to grow overnight. For transient transfection, 0.5 µg of plasmid DNA were added to 3 µl TransIT-X2 Transfection Reagent (Mirus) and 100 µl opti-MEM reduced serum medium (Life Technologies) and incubated for 20 minutes at room temperature. Cells were refreshed with 3 ml complete DMEM followed by gentle pipetting of the complete optiMEM-DNA-X2 complex into each well and incubation overnight. 24 hours post transfection, cells from each well were washed with 2 ml PBSE, trypsinized using 500 µl 1:10 trypsin-EDTA/PBSE and incubated at 37 ºC for 60 seconds. Trypsinization was terminated by addition of 4.5 ml of complete DMEM and transfer of the cells from each well into 15 ml falcon tubes for centrifugation at 1000 rpm for 3 minutes at room temperature. Cells were re-suspended in 5 ml of fresh complete DMEM and left to grow in T25 tissue culture flasks for 3 days before harvesting media and cell lysate samples for western blot (WB) analysis (Section 2.2.6.1).

2.2.5 De-glycosylation assay

1 ml of conditioned media from a confluent monolayer of transfected HEK293T cells from a T25 flask was collected into 1.5 ml Eppendorf tubes and centrifuged at 3000 rpm for 5 minutes (Thermo scientific Pico17 Centrifuge). 450 µl of media were aliquoted into new eppendorf tubes. Cells from each flask were detached and resuspended using 5 ml PBSE, and 450 µl of the cells were aliquoted into Eppendorf tubes. Cell and media samples were boiled at 100 ºC for 10 minutes with 50 µl of 10× denaturing buffer (New England Biolabs).

Denatured samples were treated with endoglycosidase H (Endo H; New England Biolabs) or Peptide:N-glycosidase F (PNGaseF; New England Biolabs) in their respective digestion mixtures (Table 2.6) and incubated at 37 ºC for 60 minutes. 15 µl of reducing sodium dodecyl sulfate (SDS) -loading dye was added to digested samples and boiled at 100 ºC for 10 minutes, before loading the samples on a 6% SDS-polyacrylamide gel electrophoresis (PAGE; Appendix 3) for WB analysis (section 2.2.6.2)

Table 2.6 Endoglycosidase enzyme digestion mixtures.

Endo H Digestion Mix		**Control**	**PNGaseF Digestion Mix**	
Component	**Volume (µl)**	**Volume (µl)**	**Component**	**Volume (µl)**
Media/lysate sample	22	22	Media/lysate sample	22
Buffer (G3)	3	3	Buffer (G2)	3
MQ H_2O	3	5	10% NP40	3
Endo H	2	-	PNGase F	2
Total	30		Total	30

2.2.6 Secretion assay

2.2.6.1 Sample preparation for western blotting

Cell lysate and media samples were harvested for analysis by western blotting. 1 ml of conditioned media from a T25 flask was transferred into 1.5 ml Eppendorf tubes and centrifuged at 3000 rpm for 5 minutes, 450 µl of each media sample was added to another labelled 1.5 ml Eppendorf tube. Cells were detached and fully suspended in 5 ml PBSE, 250 µl of which were added to labelled 1.5 ml Eppendorf tubes. Media and cell samples were supplemented with 180 µl and 250 µl of 4× reducing SDS-PAGE loading dye (Appendix 2) respectively, before boiling at 100ºC for 5 minutes. Medium and cell samples were stored

at -20 ºC until required for analysis. Samples were not stored for more than 30 days to avoid protein degradation. 40 µl of cells and medium samples were loaded onto 6% SDS-PAGE gels alongside a color prestained protein standard, broad range (10–250 kDa) ladder (New England Biolabs).

2.2.6.2 Western blot

Samples were separated using 6% SDS-PAGE at 150V for 70 minutes in 1× running buffer (Appendix 2). Proteins were transferred onto a nitrocellulose membrane in 1× transfer buffer (Appendix 2) by electrophoresis at 100V for 90 minutes using a mini Trans-Blot apparatus (Biorad). Subsequently, the nitrocellulose membrane was placed in a blocking solution of 5% (w/v) skim milk powder (Sigma Aldrich) in PBST (PBS containing 0.1% (v/v) triton X-100; Sigma Aldrich) with gentle shaking for 1 hour at room temperature or overnight at 4ºC. The membrane was then incubated in a 50 ml falcon tube containing primary rabbit anti fibrillin-1 polyclonal antibody (anti-Pro; Kettle *et al.,* 2000) or chicken anti-GFP (Abcam; ab13970) antibody diluted 1:1000 – 1:10000 in fresh blocking solution, on a digital tube roller (Stuart) for 1-2 hours at room temperature or overnight at 4ºC. The membrane was washed 5 × 3 minutes in PBST with gentle shaking followed by incubation with the secondary anti-rabbit IgG whole molecule peroxidase conjugate (Sigma) or goat anti-chicken HRP conjugate (Abcam; ab97135) respectively, diluted 1:1000 – 1:5000 for 1 hour at room temperature on a digital tube roller. The membrane was washed again 5 × 3 minutes in PBST with gentle shaking and rinsed with MQ H_2O. The blot was developed using 4 ml Amersham ECL western blotting plus detection reagents (GE Healthcare) according to manufacturer's instructions. Excess reagent was drained off, and the nitrocellulose membrane was covered in cling film before being placed in a film cassette. The blot was

exposed to Amersham hyperfilm ECL (GE Healthcare) in a dark room for 5-180 seconds and films were developed by a Compact-X4 developer (Xograph Imaging systems).

2.2.7 Microfibril assembly assay:

2.2.7.1 Co-culture set up

HEK293T cells were sub-cultured into 6 well plates in a 1:2 ratio and transfected as previously described (section 2.2.4). 24 hours post transfection HEK293T cells were trypsinized, centrifuged and resuspended in 3 ml of fresh complete DMEM. 20 µl of cells was diluted 1:5 in a total volume of 100 µl containing 30 µl DMEM and 50 µl trypan blue (Sigma Aldrich), 10 µl of which were applied to a hemocytometer for counting under a light microscope.

FS2 fibroblasts were washed with 10 ml PBSE and harvested from their T175 maintenance flask by trypsinization followed by centrifugation at 1000 rpm for 6 minutes at room temperature and subsequent resuspension of the cells in 4 ml fresh complete DMEM. A 50 µl aliquot of cells was supplemented with 50 µl trypan blue in a total volume of 100 µl. 10 µl of the cell suspension was applied to a haemocytometer for counting.

An equivalent volume of 2×10^5 HEK293T cells and 2×10^5 FS2 fibroblasts were added to 1.5 ml Eppendorf tubes. The co-culture was gently mixed by pipetting and plated into 24 well plates on 13 mm diameter glass coverslips (VWR), and completed with DMEM to 1000 µl per well. The co-culture was left for 5 days and refreshed with 1 ml of complete DMEM every day, before being processed for immunofluorescence imaging (section 2.3).

2.2.8 Stable transfection of MSU1.1 fibroblasts

MSU1.1 fibroblasts were maintained in T175 flasks and sub-cultured into 6 well plates in a 1:2 ratio 24 hours prior to transfection as described for HEK293T cells (section 2.2.2). For stable transfection, 2.5 µg of plasmid DNA were added to 5 µl X2 Transfection reagent and 250 µl Opti-MEM and incubated for 20 minutes at room temperature. Cells were refreshed with 3 ml complete DMEM followed by gentle pipetting of the complete OptiMEM-DNA-X2 transfection mixture into each well and incubation of the plates overnight. 24 hours post transfection, cells from each well of the 6 well plate were washed with PBSE, trypsinized, centrifuged, resuspended in 15 ml fresh complete DMEM and transferred into T75 flasks (section 2.2.4). 72 hours later media was replaced with complete DMEM containing 2.5 µg/ml puromycin (Sigma). Selection was carried out by replacement of puromycin containing DMEM every 2-3 days for 21 days or until ~100 clones appeared. Subsequently, all clones were pooled together by trypsinization to average out the effects of clonal variability in expression levels. Cells were centrifuged and resuspended in 20 ml fresh complete DMEM containing puromycin in 50 ml falcon tubes. 1,000,000 cells, counted as described in section 2.2.7, were sub-cultured into T25 flasks, in 5 ml puromycin containing complete DMEM, and grown for 4 days before being harvested for western blot analysis. The remainder of cells in the 50 ml falcon tubes were split 1:4 (≈90% confluent T25) to freeze down (section 2.2.3) or sub-cultured into T25 flasks with 5 ml complete DMEM containing 2.5 µg/ml puromycin to process for RNA analysis (section 2.2.9).

2.2.9 Semi-quantitative gene expression analysis

2.2.9.1 RNA extraction

MSU1.1 cells were grown in a T25 flask until 80-90% confluent (≈1× 10^8 cells). The cells were trypsinzed and centrifuged as described previously. The supernatant was aspirated off and the cell pellet was kept on ice. RNA extraction and purification were carried out using Qiagen RNeasy Kit according to manufacturer's instructions, including homogenization using Qiagen QIAShredder kit and on-column DNA digestion using the Qiagen RNase-free DNase set. RNA was eluted using 30 µl RNase/DNase free H_2O, and a 5 µl aliquot was diluted 1:20 in a total volume of 100 µl of EB buffer for quantification of RNA (Section 2.1.11).

2.2.9.2 Reverse transcription (RT)

cDNA was produced using Qiagen RNA Omniscript Reverse Transcriptase. Primer working stocks of 10 µM in H_2O were prepared for the reverse transcription reaction. A single reverse primer complimentary to a DNA sequence at the 3' end of the recombinant construct was used for reverse transcription (cb14_rev; Appendix 3). For denaturation of secondary RNA structures, 2 µg of purified RNA were initially heated for 10 minutes at 70 °C, in 600 µl PCR Eppendorf tubes, using a Biometra T3 Thermocycler. The RNA was reverse-transcribed in a mixture containing components summarized in Table 2.7, in a total reaction volume of 20 µl. The reaction was set up in 600 µl PCR tubes kept on ice. A negative control sample was set up by addition of 1 µl of RNase free water instead of the reverse transcriptase. The mixtures were incubated at 37 °C for 60 minutes in the thermocycler.

Table 2.7 Reverse transcription reaction mixtures.

Reverse transcription reaction component	**Volume (µl)**	**Control(µl)**
Template RNA	to 2µg	to 2µg
10× Buffer RT	2	2
10× dNTP Mix (5µM each dNTP)	2	2
10µM Oligo-dT primer	1	1
10 units/µl RNase inhibitor	1	1
Omnicsript Reverse Transcriptase	1	-
RNase free water	variable	variable
Total	20	20

2.2.9.3 Polymerase chain reaction

1 µl of cDNA was added to a 25 µl Taq Polymerase reaction mixture with components detailed in Table 2.8. The same reverse primer (cb14_rev) was used with the forward primers (cb10_For and TB1_For) to amplify endogenous and recombinant RT products respectively. Primer working stocks of 10 µM, diluted in H_2O, were prepared for the PCR amplification reaction. PCR reactions of 20, 25 and 30 cycles of denaturation, annealing and extension were run as detailed in Table 2.9. 5 µl of 6× DNA loading dye were added to the 25 µl PCR product, 12 µl of which was run on a 1% agarose gel alongside a 1 kb ladder at 80V for 30 minutes (Section 2.1.3).

Table 2.8 Taq Polymerase PCR component mixture.

PCR MasterMix component	**Volume (µl)**
cDNA	1
10× Taq Polymerase Buffer	2.5
10 µM dNTPs	0.5
10 µM Forward Primer	0.5
10 µM Reverse Primer	0.5

5U/µl Taq Polymerase Enzyme	0.5
MQ H_2O	19.5
Total	25

Table 2.9 PCR thermocycler times and temperatures.

PCR Step	**Temperature (°C)**	**Time (Minutes)**
Initial Denaturation	95	1
Denaturation	95	1
Annealing	65	1
Extension	72	1
Final Extension	72	10
Keep	4	-



× 20, ×25, ×30

2.3 Immunofluorescent imaging

2.3.1 Preparing cells for immunostaining

After 5 days of co-culture on the 13mm coverslips, the cells were washed twice with 500 µl PBS and fixed by incubation with 500 µl 4% (w/v) paraformaldehyde (PFA) in PBS for 20 minutes at room temperature. Samples were quenched using 500 µl 50 mM NH_4Cl in PBS for a further 2 minutes. Cells were washed twice with 500 µl PBS and incubated in 500 µl blocking buffer (10% FBS/PBS) for 30 minutes at room temperature.

2.3.2 Immunostaining microfibrils

Cells were stained with 300 µl of 10% FBS/PBS containing primary anti-Pro (1:200) and anti-GFP (1:1000; Abcam; ab13970) antibodies for 1 hour at room temperature without prior permeabilization. Cells were washed carefully 5× with PBS before incubation with 300 µl

of 10% FBS/PBS containing secondary antibodies; goat anti-chicken Alexa488 (1:200), goat anti-rabbit Alexa568 (1:200; Invitrogen) and 0.2 μg/ml DAPI for 1 hour at room temperature. The coverslips were washed again 5× with PBS and the cell containing surface of the coverslip was mounted onto glass slides with 9 μl of Mowial mounting medium (Appendix 2). The Mowial solution was left to set for 1 hour at room temperature or 15 minutes at 37°C.

2.3.3 Immunofluorescent imaging

Images were collected using a Zeiss Axioplan 2 microscope with AxioVision Rel. 4.8 software. Contrast was adjusted with ImageJ software.

Chapter 3

The effect of cMFS and nMFS variants on full-length GFP-fibrillin-1 secretion and assembly

3.1 Introduction

Previous studies have demonstrated the effects of disease-causing mutations on fibrillin-1 transcription, intracellular processing and post-translational modifications, susceptibility to proteolytic degradation, as well as trafficking (Introduction Section 1.6.1). Therefore, all steps in the fibrillin-1 biosynthetic pathway need to be investigated to fully understand the pathogenic mechanism of a given mutation. Pulse-chase analysis provided the basis for studying fibrillin secretion and assembly using MFS patient fibroblasts, which provided initial evidence of the reduction or delayed secretion of fibrillin. Nonetheless, radioactive labeling cannot differentiate between WT and mutant fibrillin molecules, making it difficult to determine any intracellular dominant negative effects (Introduction section 1.6.4). Recently, methods have been developed that enable tracking of fibrillin molecules and determining their ability to assemble into microfibrils (Jensen *et al.,* 2014; Hubmacher *et al.,* 2014). These methods can be used to further our understanding of the effects of disease-associated mutations or the contribution of specific domains to the functionality and/or polymerisation of fibrillin-1 into microfibrils.

An engineered full-length GFP-fibrillin construct, created by Jensen *et al.,* (2014), provided an epitope with which engineered fibrillin mutants could be distinguished from the endogenous fibrillin molecules. The GFP tag was positioned within a flexible 4-glycine residue sequence found at the N-terminus of the FUN domain (Introduction section 1.2.2.5). The fusion protein undergoes normal secretion from HEK293T cells and cleavage of pro-peptide sequences occurs. Therefore, this system enabled the study of the behavior of full-length GFP-Fbn variants in HEK293T cells. HEK293T cells produce very little endogenous fibrillin-1 but are readily transfectable. Although they do not provide a native environment for fibrillin-1 trafficking as a mesenchymal cell line would, they can, as a protein production

"factory", give an indication if the full-length construct is retained in cells or secreted into the ECM. Furthermore, the GFP-tagged version of the protein enables the study of how WT and mutant fibrillin-1 proteins are incorporated into microfibrils, using an established microfibril assembly assay. This system was previously used by Jensen *et al.,* (2015) to distinguish between the microfibril assembly profiles of fibrillin-1 variants associated with MFS, showing lack of incorporation, and SSS, AD, and GD showing normal incorporation.

3.2 Classical and neonatal MFS mutations

Marfan syndrome is characterized by a wide spectrum of severities, that extend beyond the 'classical' MFS phenotypes, with neonatal MFS being at the most severe end of the spectrum (Introduction Section 1.6). So far, there is no mechanism of pathogenesis that explains why mutations in the neonatal region can give rise to more severe phenotypes, especially as mutations associated with classical MFS are also found in these domains. To investigate the molecular mechanisms that determine disease severity in MFS, we examined the secretion and microfibril assembly of cMFS and nMFS variants. The study focused on disease-causing mutations in domains TB3-cbEGF19 in order to examine the contribution of the neonatal region to the functionality of fibrillin-1 and its ability to assemble into microfibrils. The mutations investigated in this study were predicted to impart structural changes to their respective domains in a variety of ways (Table 3.1), either by disrupting calcium binding (E1073K, D1113G, D1115G, N1131Y and N1382S), disulfide bonding (C1086Y, C1111R), interdomain packing (I1048T, Y1101C, G1127S), altering glycosylation patterns (I1048T), or by deletion of an entire cbEGF domain (Δcb16; Figure 3.1)

Table 3.1 MFS variants investigated in this study.

	AA Substitution	Domain	Affected Function	Reference
Classical MFS	Y1101C	cbEGF12	Intradomain packing residue	Loeys *et al.,* 2001 Biggin *et al.,* 2004
	D1113G	cbEGF13	Ca^{2+}-binding residue	Liu *et al.,* 1997 Tjeldhorn *et al.,* 2006
	D1115G	cbEGF13	Involved in stabilization of the Ca^{2+}-binding site	Tiecke *et al.,* 2001 Chandra *et al.,* 2012
	G1127S* (isolated aortic aneurysm)	cbEGF13	Substitutes a flexible glycine residue at the start of a β-hairpin	Francke *et al.,* 1995
	N1382S	cbEGF19	Ca^{2+}-binding residue	Nijbroek *et al.,* 1995
Neonatal MFS	I1048T	cbEGF11	Introduces additional N-linked glycosylation site	Lonnqvist *et al.,* 1996 Bresters *et al.,* 1999 Jacobs *et al.,* 2002
	E1073K	cbEGF12	Ca^{2+}-binding residue	Nijbroek *et al.,*1995
	C1086Y	cbEGF12	Cysteine residue involved in C1-C3 disulfide bonding	Schrijver *et al.,* 1999 Tekin *et al.,* 2007
	C1111R	cbEGF12	Cysteine residue involved in C5-C6 disulfide bonding	Peng *et al.,* 2016
	N1131Y	cbEGF13	Ca^{2+}-binding residue	Wang *et al.,* 1997
	Δcb16	-	Domain Deletion	Stheneur *et al.,* 2009 Barnett *et al.,* 2010

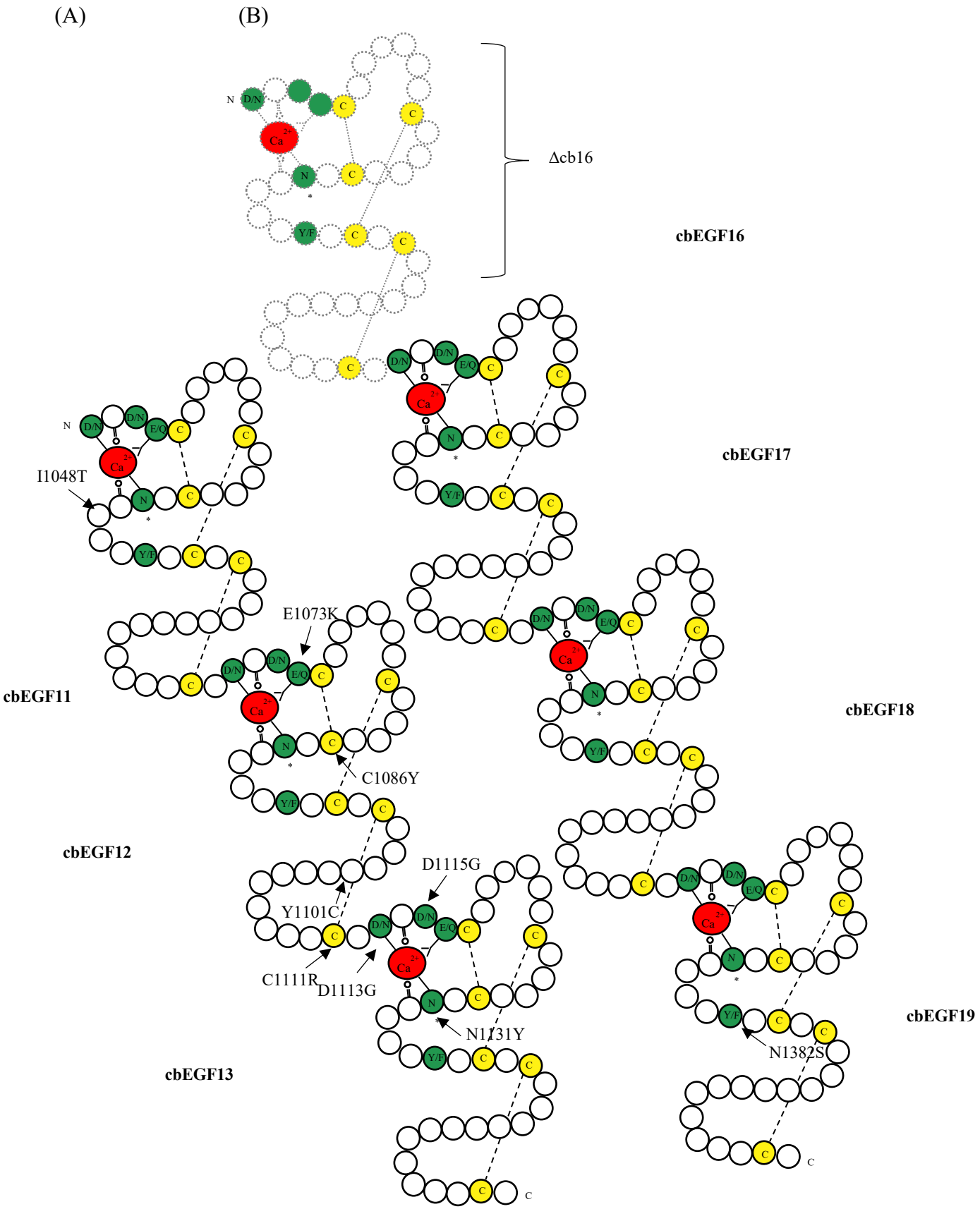


Figure 3.1 Schematic representation of domains (A) cbEGF11-13 and (B) cbEGF17-19, containing residue substitutions associated with c- and nMFS. Cysteine residues are shown in yellow; the disulfide bonds are illustrated as dashed lines and the conserved residues are shown in green. Calcium ions are shown in red with predicted amino acid side chain and carbonyl ligands indicated. The positions of the substitutions involved in this study are indicated using black arrows.

3.3 Full length GFP-Fbn secretion and assembly assays

To determine the effect of nMFS and cMFS associated substitutions on the secretion and trafficking of full-length fibrillin-1, the GFP-Fbn plasmid previously engineering by Jensen *et al.,* (2014) was used. The aforementioned pathogenic substitutions (Table 3.1) were introduced into the GFP-Fbn vector (Appendix 1) using overlapping extension PCR by Dr. Sacha Jensen. The cMFS and I1048T (nMFS) plasmids were sequenced and used to transiently transfect HEK293T cells for the respective assays. Secretion and assembly profiles of the cMFS variants were compared with those of nMFS variants tested by Dr. Sacha Jensen (unpublished data; Appendix 5). To confirm consistency in how assays were performed, results for the I1048T variant were recapitulated, as a representative of nMFS mutations.

3.3.1 Classical and neonatal MFS variants are secreted from HEK293T cells

Analysis of GFP-Fbn secretion from HEK293T cells was carried out by electrophoresis of cell lysate and conditioned media samples followed by immunoblotting (Materials and methods Section 2.6.2). WT GFP-Fbn was used as a positive control and an empty vector (pcDNA) as well as domain TB4 MFS-associated substitution C1564Y, previously shown to result in intracellular retention of GFP-Fbn *(*Jensen *et al.,* 2015*)*, were used as negative controls. The assay was performed three times to confirm the results.

In the case of cMFS associated variants and the G1127S isolated aortic aneurysm variant, all GFP-Fbn recombinant proteins were detected in culture medium at levels comparable to WT (Figure 3.2). Contrastingly, nMFS associated substitutions showed variability in absolute secretion levels from HEK293T cells. The nMFS-associated substitutions I1048T, E1073K, N1131Y, and splice site mutation (Δcb16) were secreted into conditioned media

at similar levels to WT, whereas the C1111R and C1086Y variants were found at lower but detectable levels in culture media (Appendix 5). All the variants were readily detectable in the cell lysate samples, indicating that reduction of recombinant material in conditioned media in the case of cysteine substitutions is not due to reduced protein expression levels. This result suggests that the degree of disruption is significant enough to result in partial retention of the nMFS associated cysteine substitutions in the neonatal region, but not as severe as MFS associated cysteine substitutions in domains TB4 (C1564Y) and TB5 (C1917Y and C1720Y) that result in complete intracellular retention (Jensen *et al.,* 2015).

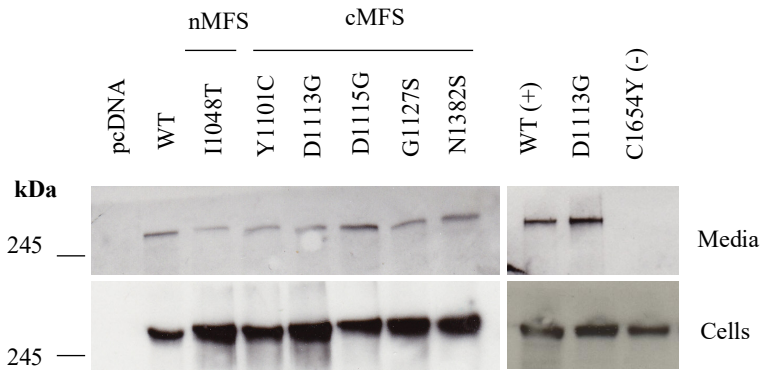


Figure 3.2 Secretion profile of GFP-Fbn variants associated with neonatal and classical Marfan Syndrome mutations. Mutations associated with nMFS and cMFS were introduced into a GFP-Fbn expression plasmid. Cell lysate and conditioned media samples of transiently transfected HEK293Ts cells were analyzed by electrophoresis using 6% SDS-PAGE under reducing conditions followed by western blotting using an anti-GFP antibody. The ~350 kDa wild-type GFP-Fbn construct (WT; Jensen *et al.,* 2014) was used as a positive control. Empty vector (pcDNA) and a TB4 MFS GFP-Fbn variant (C1654Y) previously shown to retain in cells, were used as negative controls. Molecular masses (kDa) of marker proteins are indicated. Cell lysate sampes provide evidence of comparable protein expression of the control, WT and mutant variants.

3.3.2 Classical and neonatal MFS variants show differential microfibril incorporation

To assess the incorporation of mutant fibrillin-1 molecules into microfibrils, a co-culture system, which exploits the ability of recombinant GFP-Fbn produced by HEK293T cells to assemble into an FS2 derived microfibril network, was used (Figure 3.3). WT GFP-Fbn1 was used as a positive control and empty vector (pcDNA) was used as a negative control (data not shown). The experiments were carried out three times to ensure the reproducibility of the results.

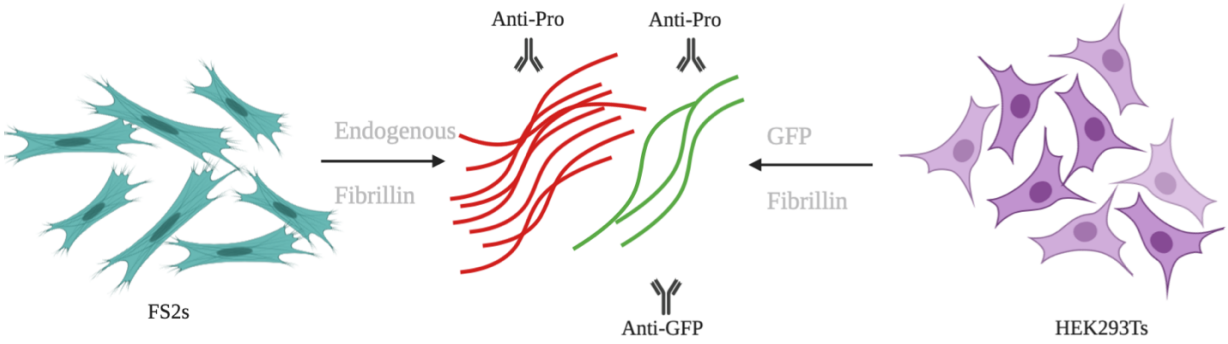


Figure 3.3 Schematic representation of the GFP-Fbn assembly assay set up. Recombinant GFP-Fbn (green) produced by transiently transfected HEK293T calls, can incorporate into FS2 assembled microfibrils (red). Anti-Pro antibody raised against the proline rich region of fibrillin-1, detects total fibrillin (endogenous fibrillin and GFP fibrillin), while the anti-GFP antibody only identifies recombinant GFP fibrillin-1.

As the cells were not permeabilized, the green spheres show intracellular fluorescence as a result of GFP fibrillin overexpressed in HEK293T cells. They are used as an indication of transfection efficiency in different experiments. The anti-Pro antibody, raised against the proline-rich region in fibrillin-1, was used to label the microfibril network formed from total fibrillin-1 (GFP-Fbn and endogenous fibrillin produced by FS2s). The merged image displays the overlap of GFP-Fbn with total fibrillin within the microfibril network. Yellow fluorescence observed in the merged images indicates that GFP-Fbn is incorporated into the network assembled by FS2s (Figure 3.4).

The microfibril assembly assay was used to examine the ability of nMFS and cMFS recombinant fibrillin-1 to incorporate into microfibrils assembled by FS2s fibroblasts (Figure 3.4). Results demonstrated a clear distinction in the capacity of cMFS and nMFS recombinant proteins to assemble into microfibrils. Although the mutant GFP fibrillin-1 network detected was weaker than that of WT GFP fibrillin-1, all cMFS variants, as well as the G1127S isolated aortic aneurysm variant showed clear incorporation into fibroblast-derived microfibrils. Overlap between recombinant and total fibrillin observed in the merged immunofluorescence images also indicates that cMFS substitutions do not hinder interaction or colocalization of mutant and endogenous fibrillin within microfibrils.

Assessment of the nMFS variants indicates the GFP-Fbn constructs harboring substitutions associated with nMFS are defective in their ability to incorporate into fibroblast assembled microfibrils (Appendix 5). Despite the secretion of the I1048T, E1073K, N1131Y and Δcb16 variants into medium of HEK293T cultures at a comparable level to WT, no GFP-Fbn protein was detected in the network produced by FS2s fibroblasts in the co-culture.

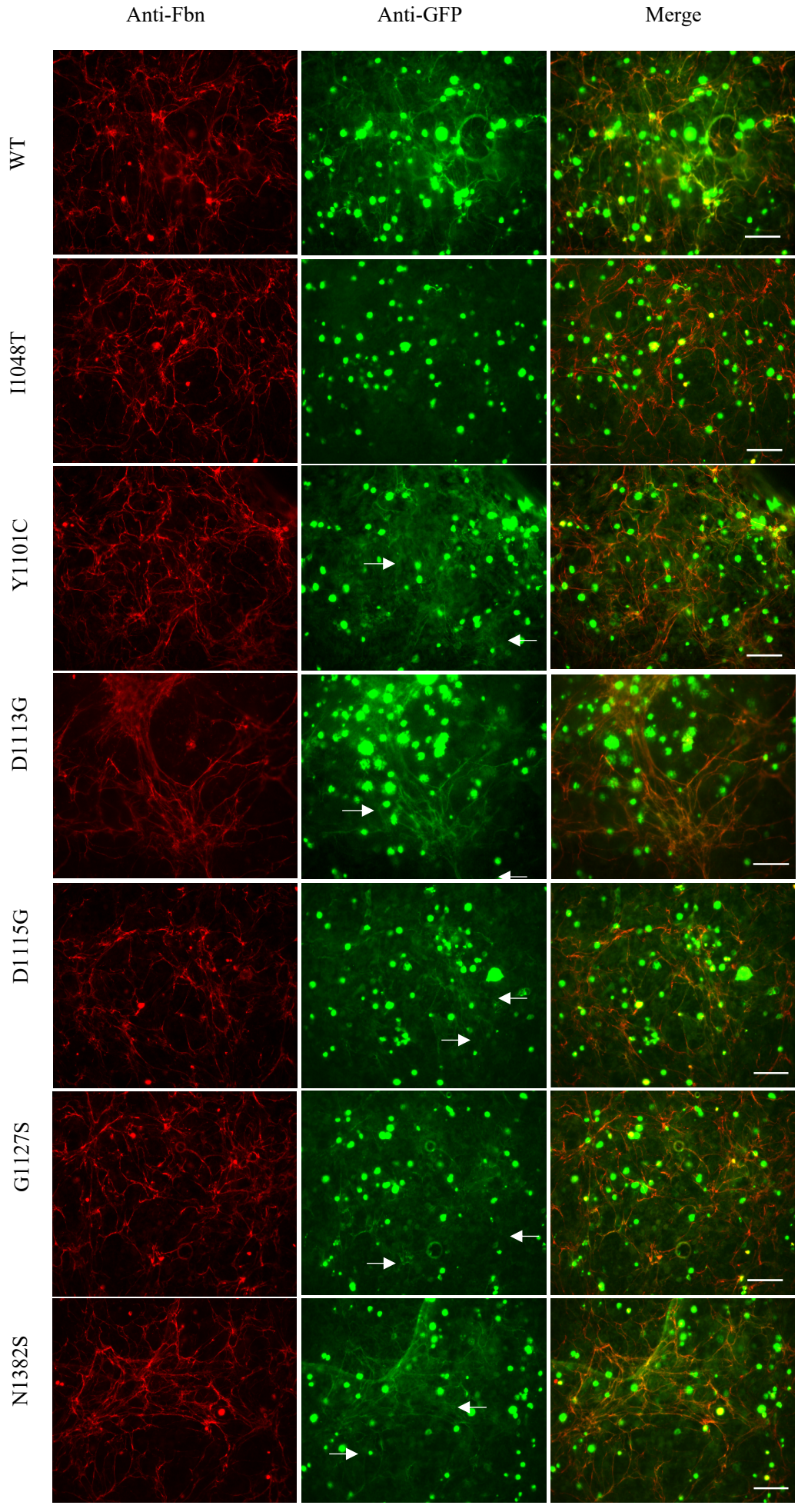

Anti-Fbn
Anti-GFP
Merge
WT
I1048T
Y1101C
D1113G
D1115G
G1127S
N1382S

Figure 3.4 Microfibril assembly of GFP-Fbn cMFS and nMFS variants. Transiently transfected HEK293T cells were co-cultured with FS2 fibroblasts for 5 days. The co-cultured cells were then fixed and stained using anti-Pro (total fibrillin-1) and anti-GFP (GFP-fibrillin-1) antibodies for viewing under immunofluorescence microscopy. All cMFS variants show near normal microfibril incorporation of GFP-Fbn (white arrows). The I1048T nMFS variant showed no incorporation into FS2 assembled microfibrils. A representative image from a single experiment is shown above. Similar results were obtained in each of the three independent transfections (Appendix 4). Bar = 100 µm.

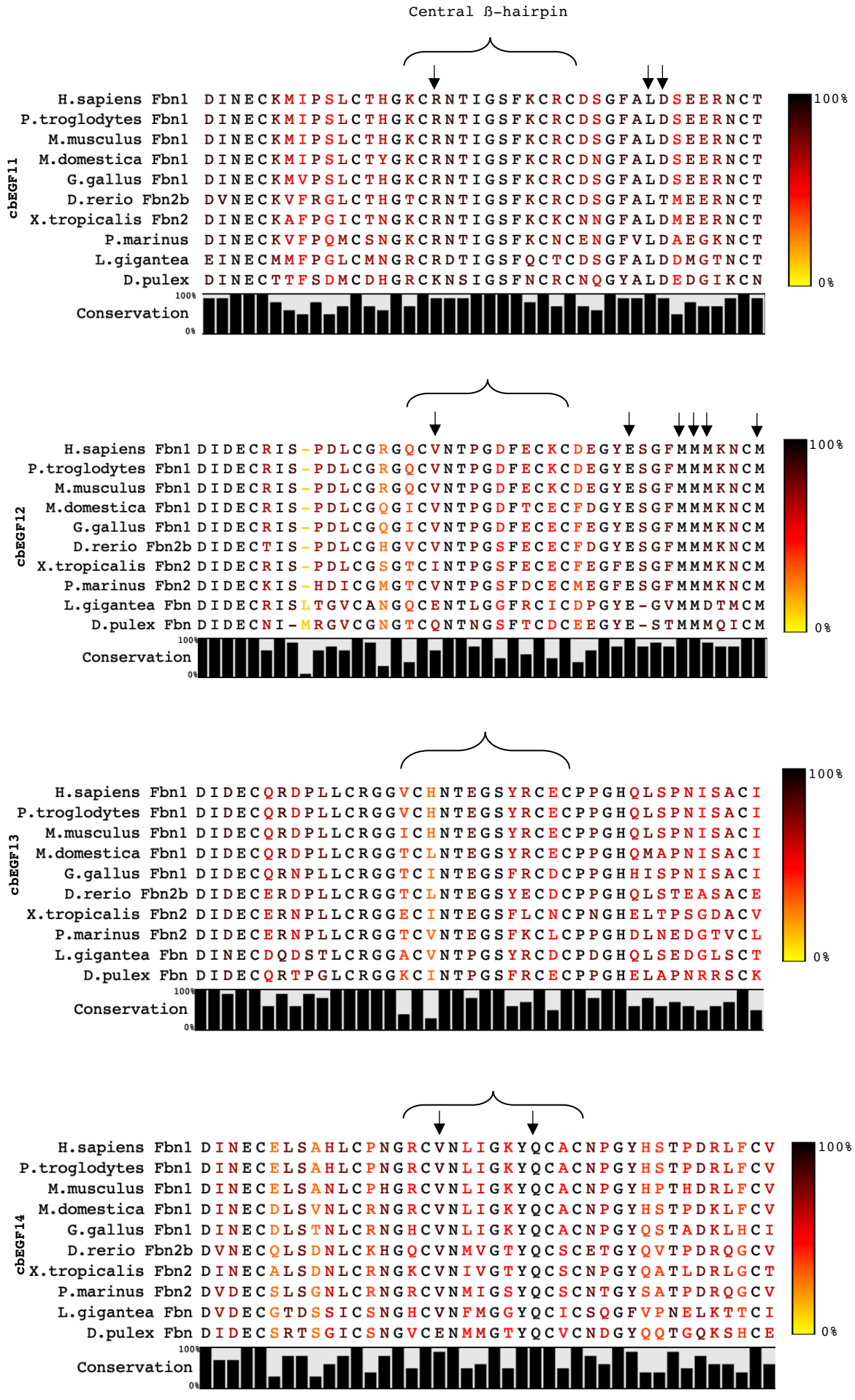
3.7 Conserved residues in the neonatal region domains cbEGF11-14 are potential candidates for protein-protein binding

The inability of nMFS variants to incorporate into microfibrils despite being secreted from cells with the intact N- and C-termini implicated in assembly, indicates that they may form complexes that hinder further assembly steps involving the neonatal region (Section 3.8). This suggests the presence of an undefined surface in domains TB3-cbEGF18 that plays a role in the lateral association of fibrillin molecules during microfibril assembly. In an effort to identify residues that could be candidates for binding, bioinformatics analysis, examining the evolutionary sequence conservation in cbEGF domains in the neonatal region, was performed. Conservation in neonatal region domains (cbEGF11-14) was compared to that in a stretch of cbEGF domains outside the neonatal region (cbEGF25-28), by aligning the cbEGF sequences in a range of higher and lower metazoan species. All structurally conserved residues including the calcium binding consensus sequence, cysteine residues, residues of the G-F/Y motif, and interdomain packing residues were excluded. Specifically, residues starting from the central ß-hairpin (C-X^1-N-X^2-G-S/T-F/Y- X^3-C) were examined for their evolutionary conservation (Figure 3.5).

Residues that show 90% evolutionary conservation in the selected species identified in cbEGF11 included an Arg (R), which corresponds to X^1 in the central ß-hairpin sequence (C-X^1-N-X^2-G-S/T-F/Y- X^3-C), and a Leu-Gly (LG) sequence at the C-terminal end of the domain. Furthermore, a Glu (E) residue, that is 100% conserved, as well as a group of four Met (M) residues in the sequence MMMKNCM at the end of cbEGF12, three of which are

100% and one 90% conserved, appear as unique features. In cbEGF14, a Val (V) and Gln (Q) that correspond to X^1 and X^3 in the central ß-hairpin sequence were also 90% conserved across these species. In cbEGF25 an Arg (R) which corresponds to X^1 in the central ß-hairpin sequence as well as a YNDKLLVCE sequence at the end of the domain, where the initial Tyr (Y) shows 100% conservation and the Asn (N) and final E are 90% conserved, were identified. Two Asn residues clustered together followed by an Asp (NND) at the C-terminal end of cbEGF28 show 100% conservation.

Overall, highly conserved residues were identified both in cbEGF11-14 and cbEGF25-28. However, the higher number of conserved residues or residue sequences in the neonatal region cbEGF domains that are potential candidates for binding could support the hypothesis that this region of fibrillin-1 is involved in homotypic intermolecular interactions. Substituting these residues and examining the effect of the variants on fibrillin-1 assembly would test their functional significance. Evolutionary sequence variation does not rule out the presence of a conserved binding region, as seen by the high level of sequence diversity between the β-hairpin sequence of domain EGF_{12} in human and evolutionarily distant *Drosophila* Notch proteins, despite their role in ligand binding. Caffrey *et al.,* (2004) have also found that interfaces are rarely more conserved than other surfaces when using different alignment types.


Central ß-hairpin
cbEGF11
H.sapiens Fbn1 DINECKMIPSLCTHGKCRNTIGSFKCRCDSGFALDSEERNCT
P.troglodytes Fbn1 DINECKMIPSLCTHGKCRNTIGSFKCRCDSGFALDSEERNCT
M.musculus Fbn1 DINECKMIPSLCTHGKCRNTIGSFKCRCDSGFALDSEERNCT
M.domestica Fbn1 DINECKMIPSLCTYGKCRNTIGSFKCRCDNGFALDSEERNCT
G.gallus Fbn1 DINECKMVPSLCTHGKCRNTIGSFKCRCDSGFALDSEERNCT
D.rerio Fbn2b DVNECKVFRGLCTHGTCRNTIGSFKCRCDSGFALTMEERNCT
X.tropicalis Fbn2 DINECKAFPGICTNGKCRNTIGSFKCKCNNGFALDMEERNCT
P.marinus DINECKVFPQMCSNGKCRNTIGSFKCNCENGFVLDAEGKNCT
L.gigantea EINECMMFPGLCMNGRCRDTIGSFQCTCDSGFALDDMGTNCT
D.pulex DINECTTFSDMCDHGRCKNSIGSFNCRCNQGYALDEDGIKCN
100%
Conservation
0%
100%
0%
cbEGF12
H.sapiens Fbn1 DIDECRIS-PDLCGRGQCVNTPGDFECKCDEGYESGFMMMKNCM
P.troglodytes Fbn1 DIDECRIS-PDLCGRGQCVNTPGDFECKCDEGYESGFMMMKNCM
M.musculus Fbn1 DIDECRIS-PDLCGRGQCVNTPGDFECKCDEGYESGFMMMKNCM
M.domestica Fbn1 DIDECRIS-PDLCGQGICVNTPGDFTCECFDGYESGFMMMKNCM
G.gallus Fbn1 DIDECRIS-PDLCGQGICVNTPGDFECECFEGYESGFMMMKNCM
D.rerio Fbn2b DIDECTIS-PDLCGHGVCVNTPGSFECECFDGYESGFMMMKNCM
X.tropicalis Fbn2 DIDECRIS-PDLCGSGTCINTPGSFECECFEGFESGFMMMKNCM
P.marinus Fbn2 DIDECKIS-HDICGMGTCVNTPGSFDCECMEGFESGFMMMKNCM
L.gigantea Fbn DIDECRISLTGVCANGQCENTLGGFRCICDPGYE-GVMMDTMCM
D.pulex Fbn DIDECNI-MRGVCGNGTCQNTNGSFTCDCEEGYE-STMMMQICM
100%
Conservation
0%
100%
0%
cbEGF13
H.sapiens Fbn1 DIDECQRDPLLCRGGVCHNTEGSYRCECPPGHQLSPNISACI
P.troglodytes Fbn1 DIDECQRDPLLCRGGVCHNTEGSYRCECPPGHQLSPNISACI
M.musculus Fbn1 DIDECQRDPLLCRGGICHNTEGSYRCECPPGHQLSPNISACI
M.domestica Fbn1 DIDECQRDPLLCRGGTCLNTEGSYRCECPPGHQMAPNISACI
G.gallus Fbn1 DIDECQRNPLLCRGGTCINTEGSFRCDCPPGHHISPNISACI
D.rerio Fbn2b DIDECERDPLLCRGGTCLNTEGSYECDCPPGHQLSTEASACE
X.tropicalis Fbn2 DIDECERNPLLCRGGECINTEGSFLCNCPNGHELTPSGDACV
P.marinus Fbn2 DIDECERNPLLCRGGTCVNTEGSFKCLCPPGHDLNEDGTVCL
L.gigantea Fbn DINECDQDSTLCRGGACVNTPGSYRCDCPDGHQLSEDGLSCT
D.pulex Fbn DIDECQRTPGLCRGGKCINTPGSFRCECPPGHELAPNRRSCK
100%
Conservation
0%
100%
0%
cbEGF14
H.sapiens Fbn1 DINECELSAHLCPNGRCVNLIGKYQCACNPGYHSTPDRLFCV
P.troglodytes Fbn1 DINECELSAHLCPNGRCVNLIGKYQCACNPGYHSTPDRLFCV
M.musculus Fbn1 DINECELSANLCPHGRCVNLIGKYQCACNPGYHPTHDRLFCV
M.domestica Fbn1 DINECDLSVNLCRNGRCVNLIGKYQCACNPGYHSTPDKLFCV
G.gallus Fbn1 DINECDLSTNLCRNGHCVNLIGKYQCACNPGYQSTADKLHCI
D.rerio Fbn2b DVNECQLSDNLCKHGQCVNMVGTYQCSCETGYQVTPDRQGCV
X.tropicalis Fbn2 DINECALSDNLCRNGKCVNIVGTYQCSCNPGYQATLDRLGCT
P.marinus Fbn2 DVDECSLSGNLCRNGRCVNMIGSYQCSCNTGYSATPDRQGCV
L.gigantea Fbn DVDECGTDSSICSNGHCVNFMGGYQCICSQGFVPNELKTTCI
D.pulex Fbn DIDECSRTSGICSNGVCENMMGTYQCVCNDGYQQTGQKSHCE
100%
Conservation
0%
100%
0%

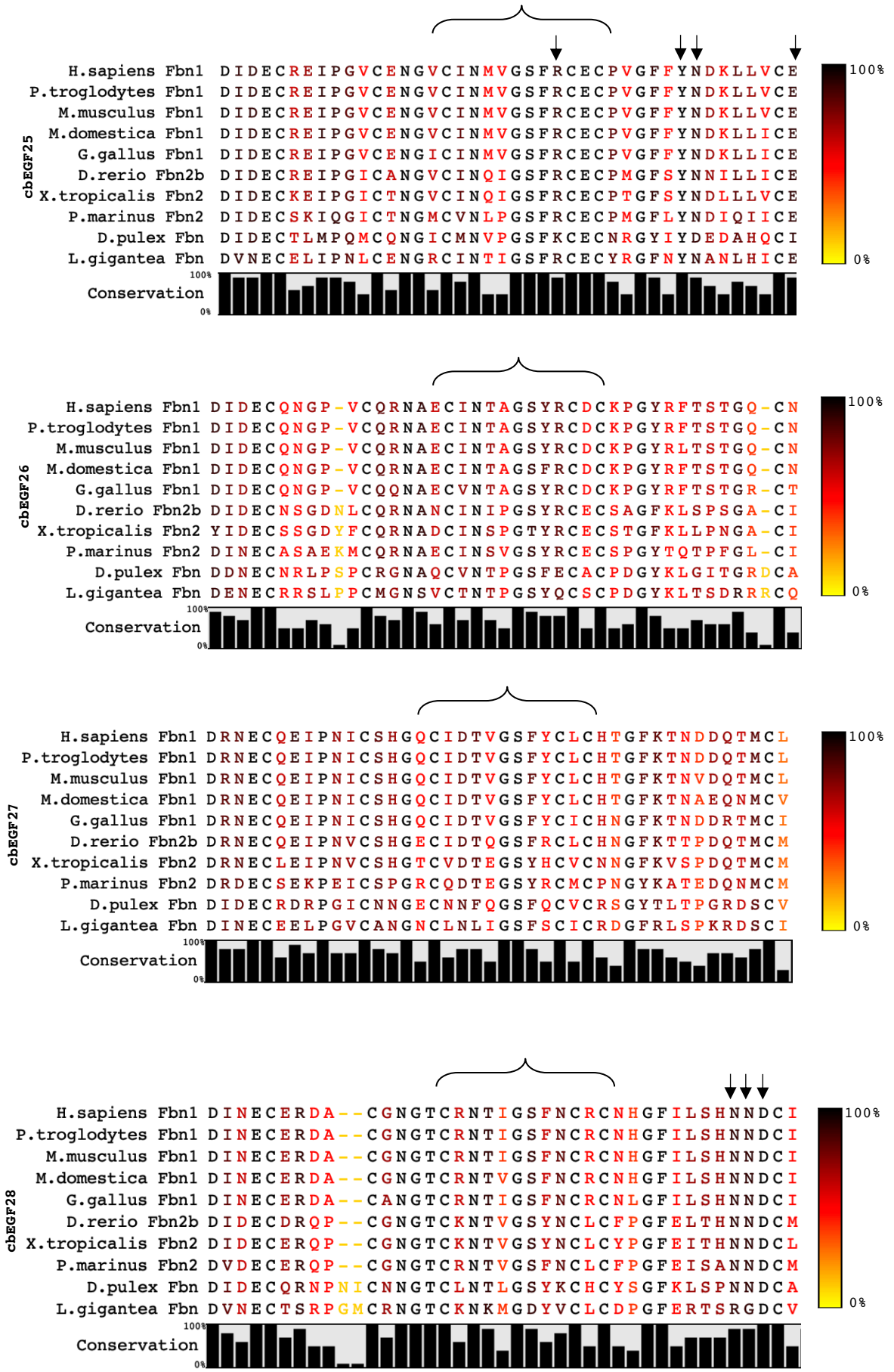


Figure 3.5 Sequence alignment of domains cbEGF11-14 and cbEGF25-28. The cbEGF domain sequences were derived from Uniprot and the evolutionary alignment was produced via the CLC sequence viewer 7 program. Residue conservation is shown using bar graphs and a color scheme where yellow represents the lowest conservation (0%) and black represents the highest conservation (100%). Residues forming the central ß-hairpin are indicated. Conserved residues that are potential candidates for protein binding are identified using arrows. Species listed: human (*Homo sapiens*), mouse (*Mus musculus*), opossum (*Mono-delphis domestica*), chicken (*Gallus gallus*), zebra-fish (*Danio rerio*), frog (*Xenopus tropicalis*), lamprey (*Petromyzon marinus*), limpet (*Lottia gigantea*) and water flea (*Daphnia pulex*).

3.8 Discussion

Full-length GFP-Fbn secretion and assembly assays were used to compare the fates of cMFS and nMFS fibrillin-1 variants. Testing the secretion of the variants from HEK293T cells provides insight into the extent of structural perturbation caused by a given mutation. Misfolded proteins may be recognized and retained in the ER and/or targeted to the protein degradation machinery within the cell, and therefore would not reach their target location in the extracellular matrix. Nonetheless, as only the steady-state levels of the protein were analyzed, detection of the mutant protein outside the cells does not rule out any minor structural defect of the substitutions.

The data presented show normal GFP-Fbn secretion of all cMFS variants and most nMFS variants, with the exception of two cysteine substitutions in cbEGF12 (C1086Y, C1111R), that were detected in reduced amount in the media. Partial intracellular retention of these mutants suggests that they cause more severe misfolding in comparison to the rest of the mutants. A proportion of the synthesized proteins escape the quality control system in the ER and are secreted from cells. Although mechanisms that govern protein surveillance in are not clearly understood, this could suggest that the mutations do not completely disrupt the fold of fibrillin-1. Also, the possibility of increased proteolytic degradation of these fibrillin variants within microfibrils, could not be ruled out. Normal secretion of cMFS and most nMFS variants from HEK293T cells indicate that the majority of the chosen mutations enable the protein to evade the cellular misfold detection machinery. Their presence in conditioned media, provides clear evidence of protein production and lack of protein degradation, suggesting that the cMFS and most nMFS fibrillin-1 variants are stable in culture media.

The microfibril assembly assay allowed us to examine the cellular consequences of these mutations and to discriminate between cMFS and nMFS substitutions based on their ability to incorporate into microfibrils. All the cMFS variants showed microfibril incorporation similar to WT GFP-Fbn, indicating that they result in minor perturbation of fibrillin assembly. nMFS variants on the other hand showed greatly diminished GFP-Fbn incorporation in the co-culture, despite their secretion from cells at levels comparable to WT. Lack of incorporation of the nMFS variants is unlikely to be associated with a defect in initial multimerization stages given that the N- and C-terminal domains, required for initial stages of fibrillin-1 assembly are present and functional. This indicates that nMFS variants interact with WT fibrillin-1 forming non-productive complexes that are unable to assemble further into microfibrils. These results, supported by the presence of conserved residues in domains cbEGF11-14, identified using bioinformatics analysis, suggest but do not prove, the presence of surface for binding within the neonatal region.

The endogenous fibrillin-1 produced and assembled by fibroblasts, demonstrated a pronounced array of microfibrils in the co-cultures, suggesting that the microfibril network was not affected by the production of disease-causing mutants. However, this does not rule out the possibility of mutant fibrillin affecting the assembly of WT fibrillin for a number of reasons. Firstly, the relative concentration of mutant fibrillin-1 produced by the HEK293T cells to endogenous fibrillin-1 could be insufficient to result in disruption of microfibril formation. Secondly, the GFP-Fbn is not being produced or secreted from the fibroblasts, therefore, protein-protein interactions that take place at the cell surface or during initial stages of fibrillin polymerization would remain unaffected by an exogenously introduced mutant protein.

These findings highlight the complexity in the molecular pathology associated with MFS and show that the local context of the substitution within the extended monomer, as well as the amino acid change are likely to play a role in the mechanism of pathogenesis. Collectively, these results show for the first time that microfibril incorporation profiles for cMFS and nMFS variants can be distinguished, suggesting that the differences in severity of clinical phenotypes arises as a consequence of different perturbations to the microfibrils.

Chapter 4

The effect of cMFS and nMFS variants on recombinant fibrillin-1 (NPro-TB3-cb19) secretion

4.1 Introduction

Pulse-chase studies measuring the synthesis and secretion of fibrillin-1 from MFS patient fibroblasts have demonstrated different cellular phenotypes which contributes to the complexity of MFS genotype-phenotype correlations. Normal, delayed secretion or intracellular retention of fibrillin-1 were previously observed in MFS (Introduction 1.6.4). These cellular phenotypes were correlated to pathogenic mechanisms of either a dominant negative effect or functional haploinsufficiency (Aoyma *et al.,*1994; Suk *et al.,* 2004; Whiteman and Handford 2003). Nonetheless, during pulse-chase radioactive labeling, the WT protein cannot be distinguished from mutant fibrillin-1. Therefore, it was not possible to determine if the reduction in fibrillin secretion occurs as a result of mutant retention or if mutant proteins interact and affect the production of WT proteins from cells through an intracellular dominant negative effect. Furthermore, previous studies have reported intracellular retention of fibrillin-1 recombinant proteins with disease causing mutations, which indicated that MFS was a result of haploinsufficiency in these cases (Whiteman and Handford 2003; Jensen *et al.,* 2015). Determining whether proteins harboring cMFS and nMFS substitutions in the neonatal region are secreted from fibroblasts, would provide insight into the pathogenic mechanism by which they give rise to MFS.

In the previous chapter the respective variants were assessed for their secretion from HEK293T cells in the form of full-length GFP-Fbn constructs. Nonetheless, a cell line that does not assemble microfibrils may lack the native cell surface and accessory molecules required for the biosynthetic pathway of fibrillin-1. Consistent with the understanding that microfibril assembly depends on the correct folding and post-translational modifications of fibrillin molecules, and that defects in these processing steps could be part of the pathogenic mechanism associated with some mutations, an appropriate microfibril assembling cell line

was chosen to investigate the trafficking of the variants for comparison with HEK293T cells. MSU1.1 cells are a human fibroblast line derived from foreskin transformed by a viral v-myc oncogene, that assemble fibrillin microfibrils in a manner similar to human primary dermal fibroblasts. They contain all the cellular machinery required for fibrillin folding, processing (including *N*-linked glycosylation), secretion and assembly (Cardy and Handford 1998). Pulse chase studies showed that the expression profile of fibrillin-1 from MSU1.1 fibroblasts is identical to that of human dermal fibroblasts (Kettle *et al.,* 2000). Additionally, by expressing the recombinant construct in this cell line, any potential intracellular dominant negative effects on the expression and/or trafficking of endogenous fibrillin-1 could be identified. The large size of the fibrillin gene and cDNA generates difficulties in producing a full-length transgene form in MSU1.1 fibroblasts. Therefore, we investigated the effect of fibrillin-1 nMFS and cMFS substitutions on the secretion of chimeric protein constructs from an MSU1.1 fibroblast cell line. A well-established system using a recombinant protein consisting of the N-terminal region of fibrillin-1, fused with an array of cbEGF domains from the central region of the protein has previously been used to determine the effect of folding mutations on fibrillin-1 delivery into the ECM (Whiteman and Handford 2003; Suk *et al.,* 2004).

4.2 Constructing NPro-TB3-cb19 WT and mutant recombinant proteins

A recombinant minigene consisting of the region endocing fibrillin-1 domains TB3-cbEGF19 was cloned into the mammalian expression vector pKG52polyA, which encodes the N-terminal region of fibrillin-1 up to the Pro-rich region (NPro, previously referred to as NterPro in Whiteman *et al.,* 2007). The pKG52polyA expression vector uses a natural leader sequence of fibrillin-1, under the control of the Herpes Simplex Virus Thymidine Kinase (HSVTK) promoter, which has been used in previous studies to examine the effect

of cbEGF mutations on recombinant protein secretion (Whiteman and Handford 2003; Whiteman *et al.,* 2007). The vector also contains a puromycin resistance gene that allows for selection of successfully transfected clones. Furthermore, the Pro-rich region provides an epitope that can be used for the detection of both the endogenous and recombinant protein constructs during immunoblotting, and the smaller size of the construct enables its clear distinction from the endogenous fibrillin-1 band. The respective substitutions associated with nMFS (I1048T, E1073K, C1086Y, C1111R, N1131Y and Δcb16), cMFS (Y1101C, D1113G, D1115G, and N1382S) and isolated aortic aneurysm (G1127S) within domains TB3-cbEGF19 were cloned into the pKG52polyA vector to create the recombinant mutant products (Figure 4.1). The restriction enzyme *Xho*1 was used to cleave the expression vector, creating stick ends that were compatible with the sticky ends created by the digestion of the insert DNA with *Sal*I (Appendix 1 and 2). The insert could be positioned in either direction, therefore, a PCR based colony screen was performed on individual bacterial colonies to identify correctly positioned inserts. Correct clones with the respective mutations were confirmed by DNA sequencing carried out in both 5' and 3' directions. Transfection of MSU1.1 fibroblasts with NPro-TB3-cb19 recombinant constructs, followed by puromycin selection for ~21 days, yielded >100 clones stably expressing the fibrillin mini-gene. To eliminate effects associated with random integration of the transfected DNA into genomic DNA, and clonal variability in expression levels, pools of clones were assessed for their expression of the recombinant construct. Transfection of each recombinant minigene was carried out twice and the assay was performed three independent times.

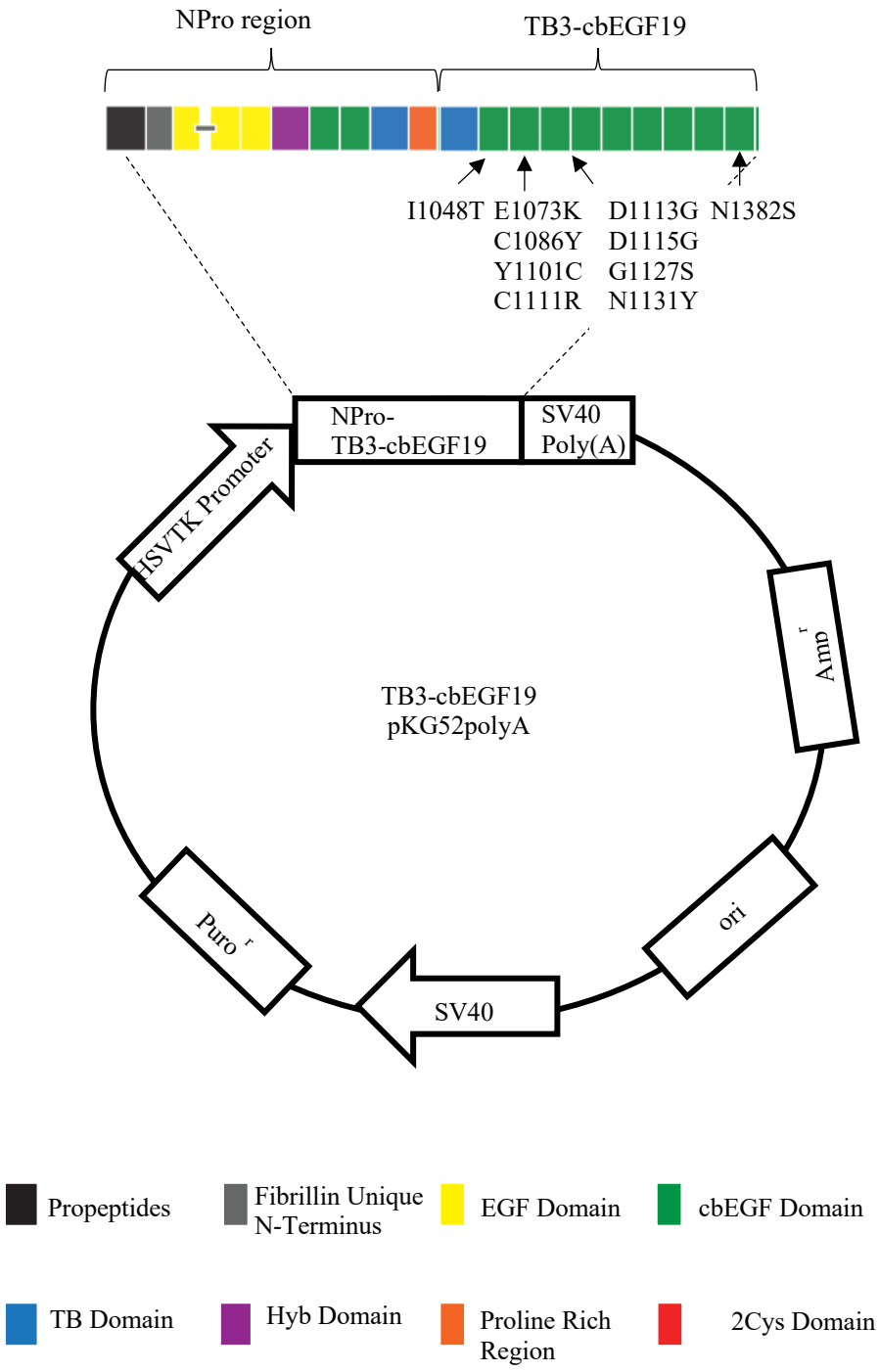


Figure 4.1 Cloning cDNA encoding NPro-TB3-cbEGF19 into the pKG52polyA expression vector. The HSVTK promoter, puromycin and ampicillin resistance genes, SV40 promoter , origin of replication and polyA sequence are indicated. Locations of the amino acid substitutions within the recombinant construct are indicated using black arrows.

4.3 Semi-quantitative Gene Expression Analysis

RNA levels of pools of MSU1.1 clones were analyzed using semi-quantitative RT-PCR to determine whether the different pools of clones expressed the mini-gene constructs at comparable levels (Jensen *et al.,* 2014, Jensen *et al.,* 2015). Endogenous fibrillin-1 mRNA levels were used as an internal control to ensure there were no variations in the cDNA quantities used in each of the reactions. A negative control with no reverse transcription was run to detect any level of contaminant DNA.

A reverse primer that binds to part of the sequence encoding domain cbEGF14 (cb14_rev) was used for the reverse transcription of DNA free RNA to cDNA. The same reverse primer was used with the forward primers that bind to parts of the sequence encoding domains cbEGF10 (cb10_for) and TB1 (TB1_for) for selective amplification of endogenous and recombinant Fbn1 cDNA respectively (Figure 4.2). The primer pair used to amplify endogenous fibrillin cDNA produced a fragment of ~750 bp as opposed to the ~1050 bp fragment expected from PCR amplification of recombinant cDNA. The expression levels of endogenous and recombinant DNA were determined by a gradual increase in PCR cycle number (20, 25 and 30). Absence of the ~1050 bp fragment in the un-transfected sample (MSU1.1) confirmed that the band was an amplification product of the recombinant cDNA. Overall, the results demonstrate successful amplification of bands at the expected size and indicate that there are comparable levels of recombinant transcripts within the WT and most mutant pools of clones (Figure 4.3). The G1127S and Δcb16 recombinant mini genes demonstrate marginally lower RNA expression levels compared to the WT transcript, which is likely due to pooling of low expressing clones in this experimental replicate.

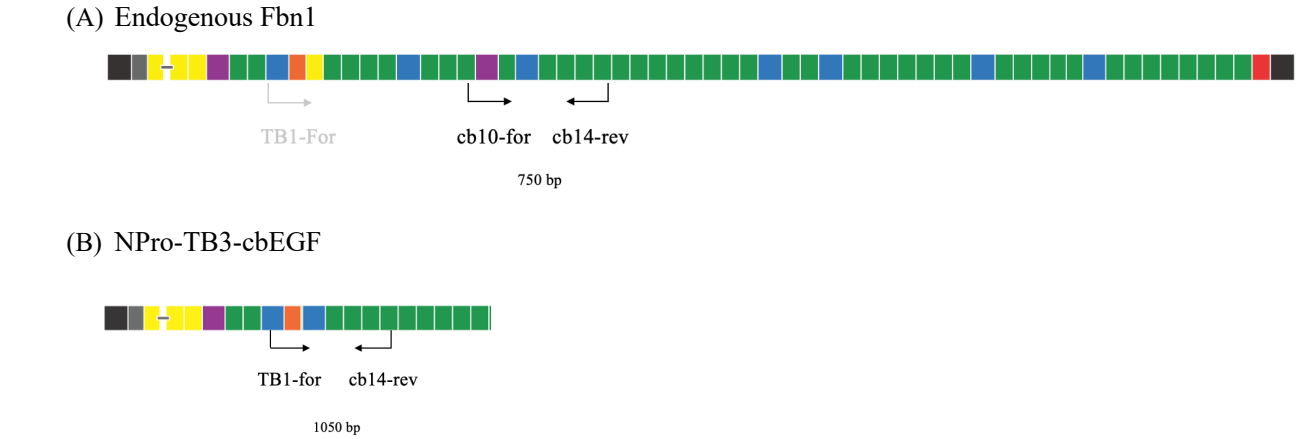


Figure 4.2 Semiquantitative RNA Analysis. Primers used for gene expression analysis by RT-PCR. Schematic diagrams of endogenous and recombinant fibrillin-1 proteins. Total RNA was extracted from pools of MSU1.1 clones grown to ~80-90% confluent in a T25 flask. Reverse transcription was carried out using a reverse primer that binds to part of the sequence encoding cbEGF14 (cbEGF14_rev). (A) PCR amplification of the endogenous Fbn1 sequence was carried out using the same reverse primer in combination with a forward primer that binds to part of the sequence encoding cbEGF 10 (cb10_For) yielding a 750 bp product. (B) A forward primer that binds to a part of the sequence encoding TB1 (TB1_for) was used to amplify the recombinant construct sequence yielding a 1050 bp product.

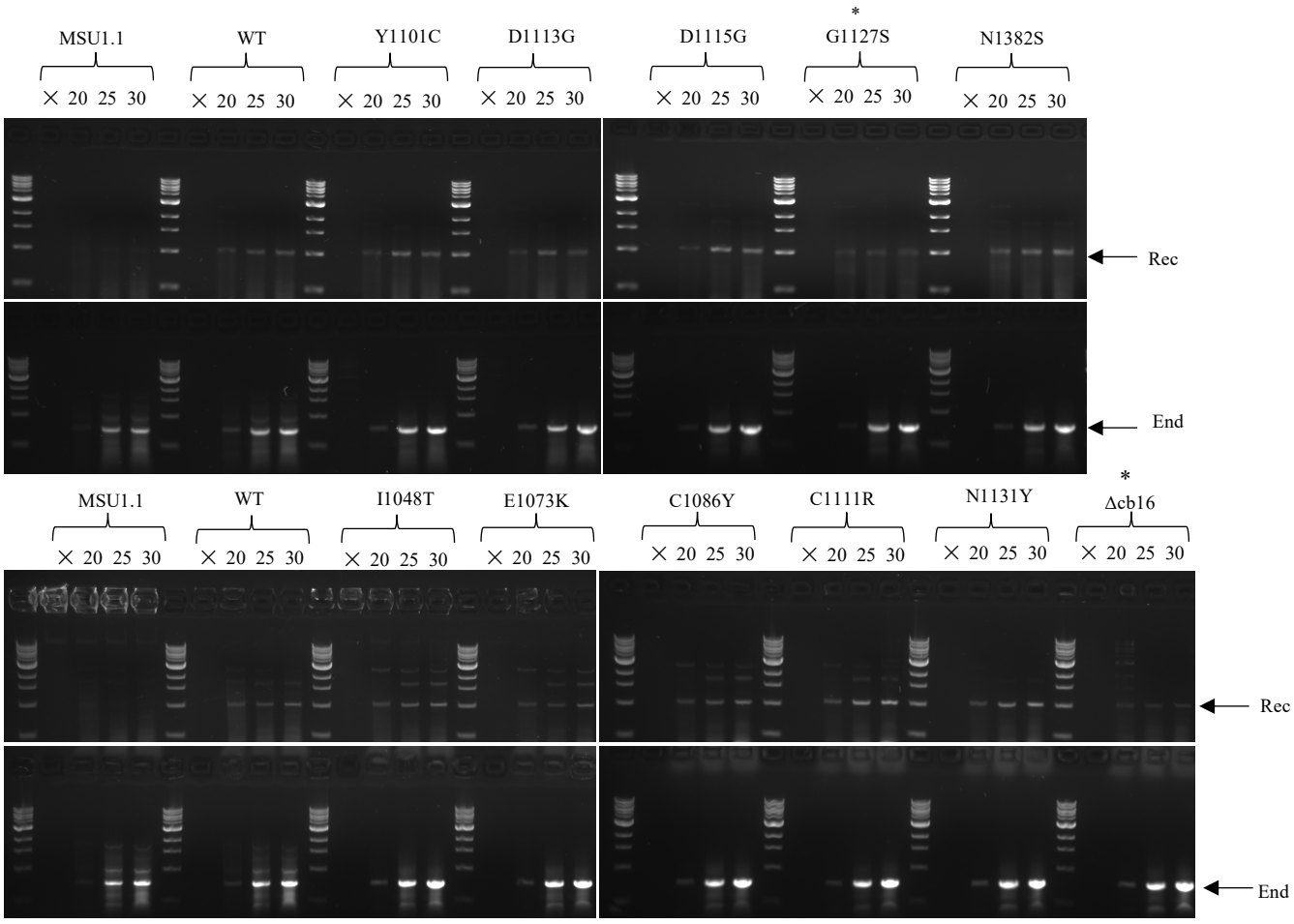


Figure 4.3 Semi-quantitative Gene Expression Analysis of pools of stably transfected MSU1.1 fibroblasts. Different primer pairs were used for selective amplification of the recombinant (Rec; top) and endogenous (End; bottom) RNA. Gradual increase in cycle number (20, 25, 30) was used to assess variation in expression levels of the recombinant genes. Endogenous Fbn1 was used as an internal control to compare amount of starting material used in all the reactions. A no-RT sample (×) was used to test for the presence of any contaminant DNA. Results indicate similar expression levels of recombinant mutant mini genes to the WT, with noted lower RNA expression of G1127S and Δcb16 (*).

4.4 Analysis of pools of MSU1.1 clones from stable transfection of NPro-TB3-cb19 recombinant fibrillin-1

Conditioned medium samples of pools of clones stably expressing NPro-TB3-cb19 were analyzed by reducing SDS-PAGE, followed by western blot analysis with the anti-Pro antibody. Full length endogenous fibrillin-1 acted as an internal loading control and the recombinant constructs were readily detectable by immunoblotting due to their lower molecular weight (~130 kDa) relative to endogenous fibrillin-1 (~350 kDa). Fibroblasts transfected with the WT construct and un-transfected fibroblasts (MSU1.1) were used as positive and negative controls. The WT NPro-TB3-cb19 was detected as a monomer as expected. The band position on the gel corresponded to ~130 kDa, which is slightly higher than the expected molecular weight of the recombinant construct of ~100 kDa, suggesting that the fragment is glycosylated.

4.4.1 Classical and neonatal MFS variants are secreted from MSU1.1 fibroblasts

Western blot analysis from conditioned media of pools of clones expressing mutant recombinant constructs showed that both cMFS and nMFS fragments were secreted from fibroblasts at levels comparable to WT (Figure 4.4). Absence of the immunoreactive ~130 kDa band in the medium from untransfected MSU1.1 cells confirms that this protein is a product of the stable transfection. The western blot images demonstrate reduced secretion of the G1127S and Δcb16 fragments. Nonetheless, as indicated by the RNA analysis, low transgene expression levels within the respective pools of clones, rather than reduced protein secretion, most likely accounts for their reduced levels in the media.

Noticeably, the I1048T variant band migrated slower in comparison to the WT fragment, consistent with the previous observation that the amino-acid substitution creates an

additional site for *N*-linked glycosylation, resulting in an increase in the molecular weight of the fragment (Lonnqvist *et al.,* 1996). On the other hand, the ΔcbEGF16 deletion mutation migrates faster in the gel and appears to have a lower molecular weight than the WT fragment, as a result of the exon skip mutation eliminating domain cbEGF16.

Some differences to the HEK293T cell expression system were observed (Results section 3.3.1). Secretion of the C1068Y and C1111R nMFS variants was comparable to WT and the partial retention indicated by the full-length GFP-Fbn analysis was not observed when testing recombinant construct secretion from MSU1.1 fibroblasts. Moreover, results for the N1131Y, D1113G and D1115G substitutions were inconsistent with data from previous studies showing that these variants, within the recombinant construct NPro-cbEGF11-22, were retained in the ER (Whiteman *et al.,* 2007).

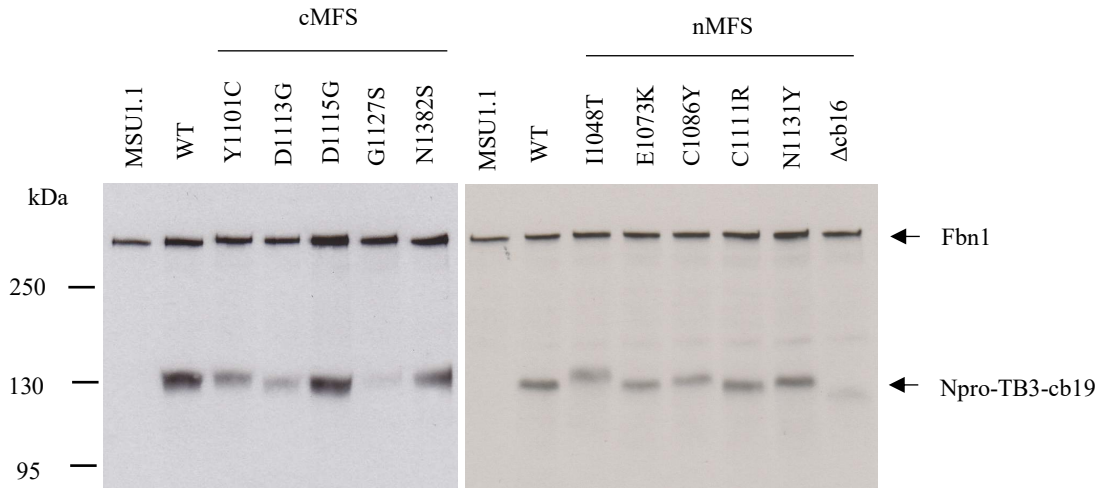


Figure 4.4 MSU1.1 expression of TB3-cbEGF19 WT and mutant constructs associated with cMFS and nMFS. Conditioned media samples of pools of MSU clones were analyzed on 6% reducing SDS-PAGE followed by western blotting using the anti-Pro antibody. Endogenous fibrillin-1 (~350 kDa) was used as an internal loading control. The lower molecular weight of recombinant proteins (~130 kDa) allowed for their identification on the blot. The wild-type (WT) recombinant construct and untransfected MSUs (MSU1.1) were used as positive and negative controls. Molecular masses (kDa) of marker proteins are indicated.

4.5 Analysis of pools of MSU1.1 clones from stable transfection of NPro-cb11-22 recombinant fibrillin-1

As results showing the secretion of the N1131Y, D1113G and D1115G variants from MSU fibroblasts within the context of NPro-TB3-cb19 contrasted with previous published data showing complete intracellular retention of these variants within the context of the NPro-cb11-22 fragment (Whiteman *et al.,* 2007), the secretion of these variants in NPro-cb11-22 fragments was reexamined. The recombinant constructs, provided by Dr. Pat Whiteman, contained the N-terminal region up to the proline rich region, fused with domains cbEGF11-cbEGF22, cloned in the pKG52polyA mammalian expression vector. The plasmids were sequenced confirming the positions of the respective substitutions, and the absence of additional variations in the gene sequence. The plasmids were transfected into MSU1.1 cells as described previously, creating pools of clones stably expressing the mini gene.

4.5.1 Semi-quantitative gene expression analysis

Transcript expression levels were determined using semi-quantitative RT-PCR, with gradual increase in PCR cycle number, as previously described (Figure 4.5; Section 4.3). The results demonstrate comparable gene expression levels of all variants to WT mRNA (Figure 4.6).

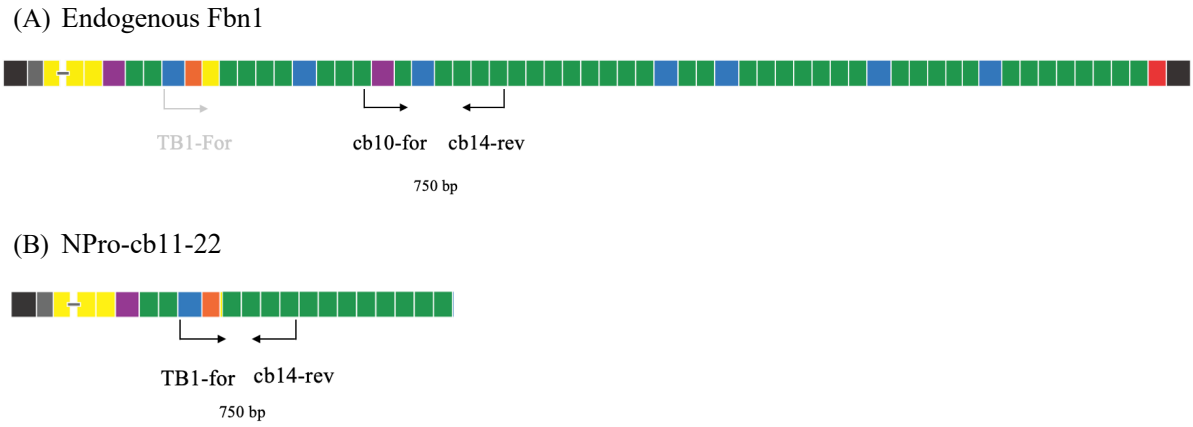


Figure 4.5 Primers used for gene expression analysis by RT-PCR. A schematic diagram of endogenous recombinant proteins. Total RNA was extracted from pools of MSU clones grown to ~80-90% confluent in a T25 flask. Reverse transcription was carried out using a reverse primer that binds to a part of the sequence encoding cbEGF14 (cb14_rev). (A) PCR amplification of the endogenous RNA was carried out using the same reverse primer in combination with a forward primer that binds a part of the sequence encoding cbEGF 10 (cb10_For) yielding a 750 bp product. (B) A forward primer that binds to a part of the sequence encoding TB1 (TB1_for) was used for amplification of the recombinant RNA yielding a 750 bp product.

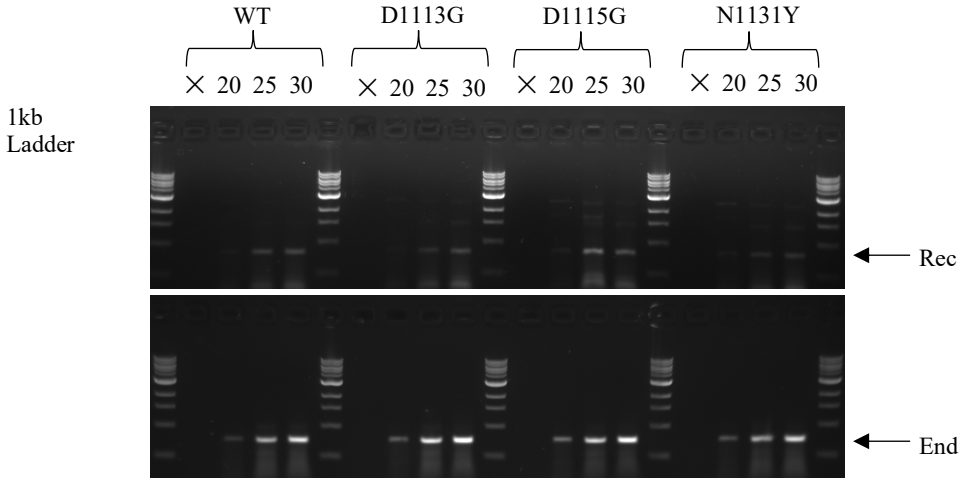


Figure 4.6 Sem-quantitative Gene Expression Analysis using RT-PCR. Analysis of gene expression of of pools of MSU1.1 fibroblasts stably expressing the Npro-cb11-22 recombinant construct. Different primer pairs were used for selective amplification of the recombinant (Rec; top) and endogenous (End; bottom) RNA. Gradual increase in cycle number was used to assess variation in expression levels of the recombinant gene. Endogenous Fbn1 was used as an internal control to compare amount of starting material used in all the reactions. A no-RT sample (×) was used to test for the presence of any contaminant DNA. Results indicate similar expression levels of all mutant mini-genes to the WT cb11-22 construct.

4.5.2 Classical and neonatal MFS calcium binding variants in NPro-cbEGF11-22 are retained in cells

SDS-PAGE of conditioned media of pools of clones followed by western blot analysis is shown (Figure 4.7). The WT NPro-cb11-22 fragment was detected in conditioned media at a position in the gel corresponding to a molecular weight of ~125 kDa, higher than its expected approximate molecular mass of ~103 kDa, due to glycosylation. The NPro-cb11-22 mutant fragments however were not detected in the media, confirming the previously published result that stated MFS associated substitutions involved in calcium binding (N1131Y, D1113G, and D1115G) are retained within the cell when examined in the context

of cbEGF11-22. Detection of the recombinant band in the cell samples ensures that lack of variant detection in the media is not a result of lack of protein production.

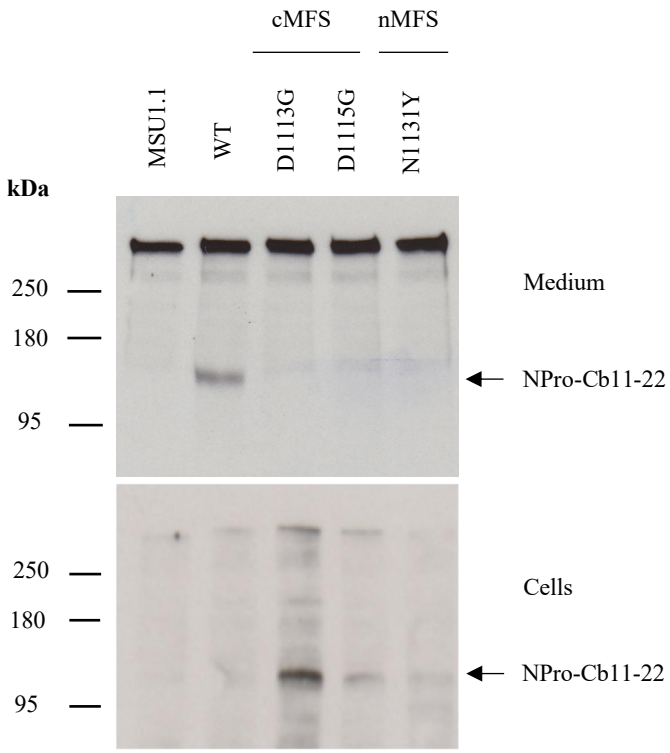


Figure 4.7 MSU secretion profile of cb11-22 mutant constructs associated with cMFS and nMFS. Cell lysate and conditioned media samples of pools of MSU clones were analyzed on 6% reducing SDS-PAGE followed by western blotting using the anti-pro antibody. Endogenous fibrillin-1 (~350 kDa) was used as an internal loading control. The lower molecular weight of recombinant proteins (~125) allowed for their identification on the blot. The wild-type (WT) recombinant construct and untransfected MSUs (MSU1.1) were used as positive and negative controls. Results confirm data previously shown by Whiteman *et al.,* (2007).

4.6 Recombinant protein (NPro-TB3-cb19) secretion from HEK293T cells

To ensure that secretion results of the mutant variants from HEK293T cells were not distorted by the high efficiency cytomegalovirus (CMV) promoter present in the GFP fibrillin expression vector (Appendix 1), the NPro-TB3-cb19 fragment was expressed transiently, using the pKG52polyA expression vector, under the control of the HSVTK promoter, in HEK293T cells. Testing the secretion profile of the recombinant proteins in

HEK239T cells provided a direct comparison to the full-length GFP-Fbn assay, as both recombinant proteins were expressed transiently in HEK293T cells. It also directly compares to the fibroblast secretion data, as both systems use the same recombinant constructs and are expressed under the same promoter.

4.6.1 Classical and neonatal MFS recombinant constructs are secreted from HEK293T cells

Results were consistent with the MSU1.1 secretion data, showing that both cMFS and nMFS recombinant proteins are secreted into conditioned media of HEK293T cells at levels similar to WT (Figure 4.8). All variants were detected in the cell lysate samples at reasonable levels. Consistent with the fibroblast secretion results, the molecular weight of the recombinant constructs (~130 kDa) was marginally higher than the predicted molecular weight (~100 kDa) due to the presence of *N*-glycan chains. Similarly, the decrease in migration rate of the I1048T construct is due to the addition of an extra *N*-glycan chain, while the increase in migration rate of the ΔcbEGF16 fragment is associated with the loss of domain cbEGF16. Noticeable absence of the full length fibrillin band at 350 kDa in both cells and media samples confirms the known low level of endogenous Fibrillin-1 expression by HEK293T cells.

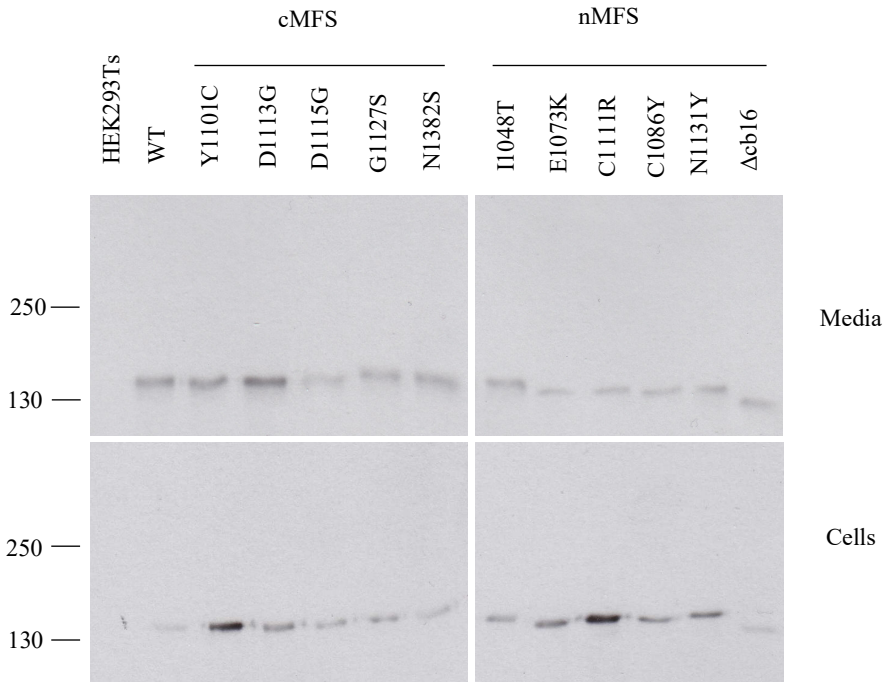


Figure 4.8 Secretion of TB3-cbEGF19 WT and mutant constructs from HEK293T cells. Cell lysate and conditioned media samples of transiently transfected HEK293T cells were separated on 6% reducing SDS-PAGE followed by western blotting using the anti-pro antibody. The wild-type (WT) recombinant construct and un-transfected HEK293T cells were used as positive and negative controls. Molecular masses (kDa) of marker proteins are indicated.

4.6.2 Fibrillin-1 domain cbEGF11 neonatal MFS variant (I1048T) introduces an extra *N*-linked glycosylation site

It has previously been reported that the I1048T mutation introduces an extra *N*-glycan chain to the Asp residue 1046 in domain cbEGF11 (Lonnqvist *et al.,* 1996). To confirm this as the cause of decreased migration rate of the I1048T variant within our recombinant construct (Figure 4.8), WT and I1048T variants, expressed transiently in HEK293T cells, were treated with the endoglycosidase enzymes PNGase F and Endo H. PNGase F hydrolysis removes both simple and complex glycan chains by cleaving the bond between the innermost GlcNAc and asparagine (Asn) residues of higher mannose, hybrid and complex oligosaccharides. Endo H hydrolyses more simple sugars such as the chitobiose core of higher mannose and some oligosaccharides. Addition of the complex glycan chains takes places in the Golgi-apparatus, after the protein leaves the ER, therefore, secreted fragments have a different glycosylation profile to those retained in the ER (Whiteman and Handford, 2003).

Treatment of the I1048T fragment with the amidase PNGase F resulted in reduction in molecular weight of the protein and its migration to the same band position as the untreated fragment, both inside the cell and in the medium (Figure 4.9). The increase in migration rate was more pronounced in for the secreted fragment, consistent with simple sugar addition taking place in ER and more complex carbohydrate addition occurring in the golgi-apparatus. Furthermore, the I1048T fragment in the cell fractions, but not media, was

susceptible to hydrolysis by Endo H, confirming the presence of a complex carbohydrate chain on the secreted protein.

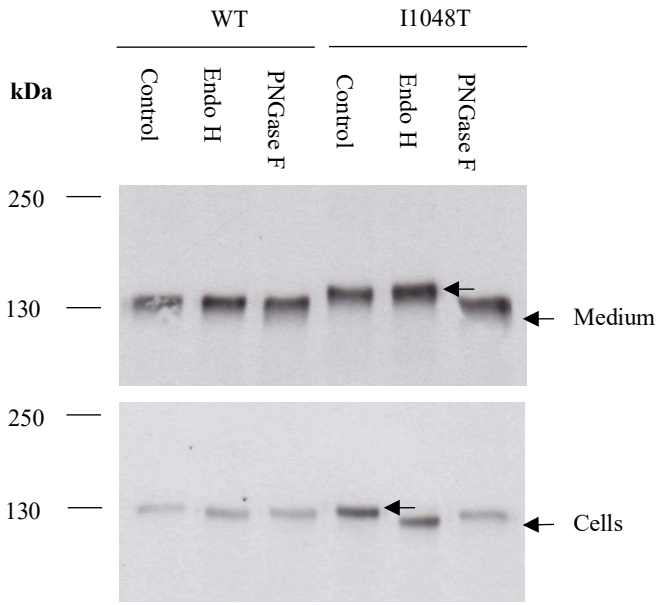


Figure 4.9 Deglycosylation of the I1048T recombinant construct produced from transiently transfected HEK293T cells. Cell lysate and conditioned media samples of the WT and I1048T nMFS variant were deglycosylated using endoglycosidase enzymes PNGase F and Endo H followed by analysis on 6% reducing SDS-PAGE and western blotting using the anti-Pro antibody. An un-treated (control) sample was used as a negative control to confirm that decrease in molecular weight resulted from of glycan cleavage. The IT variant detected in conditioned media showed sensitivity to PNGase but not EndoH, while the construct within the cells was sensitive to both. Results confirm the addition of an extra *N*-glycan chain as a result of the I→T substitution, as previously shown by Lonnqvist *et al.,*1996.

4.7 Discussion

In this chapter, a well-established recombinant protein expression system was used to compare the cell trafficking profile of cMFS and nMFS variants in the neonatal region. Using this system provided a number of advantages. As aforementioned, the recombinant protein is expressed using a natural leader sequence of fibrillin-1. Secondly, expression of the recombinant protein could be compared to the endogenously produced fibrillin-1 that is used as an internal control. It also tells us if expression or production of mutant recombinant protein influences the trafficking of endogenous fibrillin-1. Furthermore, the significant size

difference allows for clear identification of the recombinant protein and for the differences in migration rates of the I1048T and ΔcbEGF16 fragments, associated with the changes introduced by their respective mutations, to be detected by western blotting. These size differences were indistinguishable when using the full-length recombinant construct, because of the low resolving capacity of SDS-PAGE of proteins with very large molecular masses (Results section 3.3.1). Additionally, detection of the recombinant protein by western blotting did not require a prior concentration or precipitation step, which could result in loss of the protein.

The recombinant gene expression level was tested in the MSU1.1 fibroblast line using semi-quantitative RT-PCR. Similar RNA levels were observed for all mutant and WT transgene products, except the G1127S and Δcb16 constructs, providing evidence of equal transfection efficiency and comparable gene expression levels between mutant and WT clones. This also confirms that fibrillin mini genes containing the chosen cMFS and nMFS mutations are transcribed stably. Furthermore, the variants were tested for their effect on the secretion of the recombinant protein NPro-TB3-cbEGF19 from pools of clones of stably transfected MSU1.1 fibroblasts, and transiently transfected HEK293T cells. All the cMFS and nMFS recombinant proteins, except the ones expressed at lower concentrations (G1127S and Δcb16), were detected in the media at levels comparable to WT. These results indicate that cMFS and nMFS associated substitutions within domains TB3-cbEGF19 do not substantially affect the trafficking of fibrillin-1. Furthermore, normal secretion of endogenous fibrillin-1 from MSU1.1 fibroblasts confirms that the production of the mutant recombinant construct does not interfere with secretion of WT fibrillin from cells. Using the two different expression systems (stable expression in MSU1.1 fibroblasts and transient expression in HEK293T cells), our results exclude any influences of different promoter

efficiencies or how readily transfectable a cell line is on the secretion profiles observed. Furthermore, the deglycosylation assay performed for the WT and I1048T fragments verified the presence of an extra-glycosylation site associated with the I → T substitution but showed that it had no effect on fibrillin secretion either from HEK293T cells or MSU1.1 fibroblasts.

A limitation remains that although the fibrillin domains included in the fusion construct contain a long stretch of cbEGF domains, which provides a native-like context for the substitution, recombinant fragments could be processed differently from the corresponding full-length fibrillin-1 proteins. This was seen in the case of the nMFS associated C1086Y and C1111R variants that demonstrated partial retention in the full-length GFP-Fbn form, but normal secretion in the recombinant construct form. However, the rest of the NPro-TB3-cbEGF18 secretion results from MSU1.1 fibroblasts were consistent with the full-length GFP-Fbn secretion results. Secretion from HEK293 cells was previously seen for the I1048T and E1073K nMFS associated variants, in the form of a recombinant fragment spanning domains EGF4-cbEGF22 (Kirschner *et al.,* 2011) and N1382S and G1127S associated with cMFS and isolated aortic aneurysm were previously shown to secrete from MSU1.1 fibroblasts in the form of NPro-cb11-22 constructs (Whiteman and Handford 2003; by Whiteman *et al.,* 2007).

Our secretion data from HEK293T cells and fibroblasts show normal secretion of cbEGF13 calcium binding variants (D1113G, D1115G, N1131Y) while the previous study by Whiteman *et al.,* (2007), using the same fibroblast secretion system, reported intracellular retention of these mutations, owing to major structural perturbation of the domain fold. The only difference between the respective assays was the use of a fusion construct spanning

domains cbEGF11-22 rather than TB3-cbEGF19. In this study, the assay outlined by Whiteman *et al.,* (2007) was reproduced and confirmed that recombinant fragments NPro-cb11-22 containing D1113G, D1115G, N1131Y mutations are retained in cells. When creating the fusion construct for this study, domain TB3 was included to place adjacent domain cbEGF11 in a native context. Unexpectedly, the presence of this domain had a differentiating effect on the ability of cbEGF13 mutant fibrillin fragments to be secreted from fibroblasts. The previous study described a post-translational rather than a co-translational model of folding within this region, with domain cbEGF13 adopting its native fold before cbEGF12. It demonstrated that due to the cooperative folding of cbEGF12-13, calcium binding substitutions in cbEGF13 also cause loss of calcium binding in cbEGF12 resulting in a protein folding defect. Loss of calcium binding in cbEGF13 also exhibited long-range effects, causing loss of calcium protection from proteolysis in cbEGF11. This highlights the importance of interdomain interactions and calcium dependent folding within this region of fibrillin-1. Consistent with this model of folding, our results raise the possibility that domain TB3 plays a crucial role in the folding of domains cbEGF11-13, and that only when TB3 is absent is the folding of cbEGF12 fully dependent on that of cbEGF13. Hydrophobic interactions between TB3 and cbEGF11, involving the aromatic residue of the G-F/Y motif in TB domains, could indirectly stabilize the calcium dependent folding of cbEGF12-13. This finding highlights the importance of domain context within limited fragments, and the need for assessing the functional consequences of substitutions in the context of full-length fibrillin-1.

Chapter 5

Discussion

5. Discussion

Currently, we do not understand the mechanisms involved in determining the severity of neonatal MFS compared to classical MFS, and there is no way of predicting whether a given mutation will cause a milder or more severe form of the disease. Therefore, in an effort to determine any differences in their molecular and cellular behaviour, our study compared the secretion and microfibril assembly of fibrillin-1 variants associated with classical and neonatal MFS, with a particular focus on domains TB3-cbEGF18. Using full-length GFP-Fbn expressed transiently in HEK293T cells and recombinant fibrillin constructs expressed stably in MSU1.1 fibroblasts, we demonstrate that cMFS and nMFS substitutions in the TB3-cbEGF18 neonatal region do not abrogate fibrillin-1 secretion from cells. Furthermore, microfibril assembly results provided a clear distinction between the ability of cMFS and nMFS variants to incorporate into microfibrils. GFP-Fbn variants containing cMFS mutations were detected in the fibrillin-1 matrix surrounding cultured cells, while no GFP-Fbn variants harboring nMFS mutations were detected in such assemblies, despite their secretion from cells, in most cases, at similar concentrations to WT. Together, these results (Figure 5.1) suggest that the differing effects of cMFS- and nMFS-associated substitutions are asserted at the point of microfibril assembly. Since nMFS substitutions fail to incorporate although they retain the N- and C termini required for early stages of assembly (Introduction section 1.4.3), these data suggest an importance of the neonatal region for the lateral assembly of fibrillin monomers during microfibril assembly.

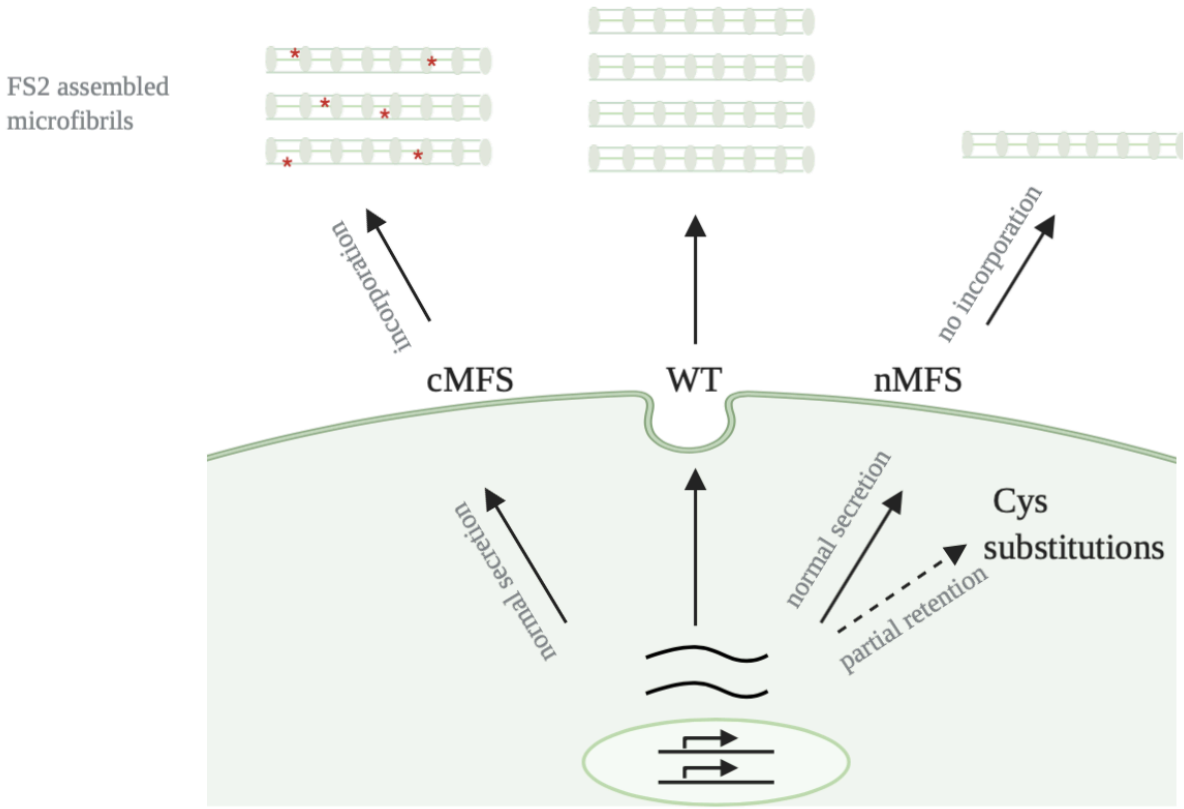


Figure 5.1 Schematic representation summarizing key findings of this study. Both cMFS and nMFS variants in domains TB3-cbEGF19 are secreted normally from cells, apart from two cysteine substitutions that showed partial retention. cMFS variants were able to assemble into FS2 derived microfibrils, while nMFS variants showed no microfibril incorporation.

5.1 Correlating molecular defects of cMFS and nMFS mutations to the trafficking of fibrillin-1

Microfibril formation is dependent on the amount of effectively synthesized fibrillin-1, the efficiency of intracellular processing, and the stability of the secreted monomers. Detailed analysis of the consequences of fibrillin-1 mutations on these aforementioned steps is fundamental to understanding the molecular pathogenesis of individual *FBN1* mutations. Prior to this study there was no clear explanation as to why some variants should be more severe than others, but for the first time, a microfibril assembly assay has been able to distinguish two different cellular phenotypes based on incorporation of the disease-causing

variant into the microfibril network assembled by fibroblasts. Most of the cMFS and nMFS mutations investigated in this study are predicted to impart structural changes to fibrillin-1 (Results Table 3.1). On closer inspection are there any additional features that might explain the different effects of such mutations?

5.1.1 Calcium binding residues in domains TB3-cbEGF19

Calcium binding can act as a marker for the correct, native fold of cbEGF domains. Mutations that affect residues of the calcium binding consensus sequence introduce conformational changes to cbEGF domains, as a result of reduced calcium affinity. We assessed the effect of calcium binding substitutions in cbEGF12 (E1073K), cbEGF13 (D1113G, D1115G, N1131Y) and cbEGF19 (N1382S) on the secretion and assembly of fibrillin-1. A set of the chosen calcium binding substitutions result in nMFS (E1073K and N1131Y) while others result in the milder form, cMFS (D1113G, D1115G, N1382S). Our data shows secretion of all the indicated variants from both HEK293T cells and MSU1.1 fibroblasts. Nonetheless, the D1113G, D1115G and N1382S (cMFS) variants were able to incorporate into microfibrils, while the E1073K and N1131Y (nMFS) variants severely impaired microfibril incorporation. The incorporation of fibrillin molecules harboring calcium binding substitutions in the neonatal region has not been shown previously, as calcium binding substitutions were thought to result in major folding defects that precluded the secretion of mutant fibrillin-1 (Whiteman *et al.,* 2007). However, the opposing secretion results of recombinant constructs Npro-TB3-cb19 and NPro-cb11-22 harboring the same substitutions have shown that previous results were due to expressing recombinant variants in a non-native context. (Results section 4.7)

Interestingly, the N1131Y (nMFS) variant severely impaired microfibril incorporation, while the D1113G and D1115G (cMFS) variants that affect the same calcium binding site, had little effect on microfibril incorporation. This suggests that even in the same cbEGF domain, calcium binding substitutions have different levels of importance. The more disruptive effect of the N1131Y substitution could be because it resides on the central ß-hairpin where it may contribute to a protein-protein interaction (Whiteman *et al.,* 2013). Furthermore, the N1382S (cMFS) variant in cbEGF19, which affects the same calcium binding ligand as N1131Y, showed normal microfibril incorporation, highlighting the importance of this binding interface in cbEGF13, within the neonatal region of fibrillin-1. This information implies that the degree of disruption is also associated with the context of the substitution within the extended monomer.

The only other study that discriminated between cMFS and nMFS associated substitutions was based on proteolytic susceptibility as a measure of calcium-dependent protection from proteolysis and overall recombinant fragment stability (Kirschner *et al.,* 2011). They demonstrated increased proteolytic susceptibility of nMFS variants in comparison to the cMFS forms, which can be indicative of a more significant structural change as a consequence of the loss of calcium binding. This is consistent with the prediction that disease severity is correlated with the extent of structural perturbation caused by a given mutation.

5.1.2 Cysteine residues in domains TB3-cbEGF19

Disulfide bonding between conserved cysteine residues in cbEGF domains contributes to the stability of their fold. Disease-causing mutations that cause disruption of native disulfide bond formation, have been shown to perturb the native fold of cbEGF domains. Such

mutations have been implicated in a large number of diseases associated with transmembrane and extracellular proteins (Suk *et al.,* 2004). The full-length GFP-Fbn studies show reduced secretion of two variants with nMFS associated cysteine substitutions in cbEGF12 (C1086Y, C1111R), but they were still detectable in conditioned media. This suggests partial intracellular retention of these variants, consistent with that cysteine substitutions change a key element of the cbEGF domain fold.

Intracellular retention was previously seen in the case of MFS substitutions in domains TB4 (C1564Y) TB5 (C1917Y and C1720Y; Jensen *et al.,* 2015). ER retention of these variants was attributed to misfolding of the more globular TB domain due to loss of a conserved disulfide bond. These results were in contrast to cysteine substitutions associated with GD in TB5 (C1719W) and SSS in TB4 (C1564S), that showed normal mutant secretion into the media. Normal secretion of these variants was predicted to result from less disruptive effects of tryptophan and serine residues in the position of the cysteine, in comparison to the tyrosine (Jensen *et al.,* 2015). It is possible that the different secretion results of functionally similar substitutions in cbEGF and TB domains arise due to the structural differences between TB and cbEGF domains. In TB domains, the small hydrophobic core formed by a conserved aromatic residue could be more sensitive to structural changes associated with loss of disulfide bonds than the more open structure of cbEGF domains. The two cysteine substitutions investigated were defective in their ability to assemble into microfibrils. It is not clear, whether this is due to the lower concentration of mutant monomers being produced, and/or because the mutations result in radical disruption of fibrillin stability and its ability to form the appropriate specific interactions required for assembly.

Cysteine substitutions in the neonatal region can result in cMFS or nMFS, and some cysteines when substituted to two different residues give rise to two distinct severities of

MFS (ex: C1153S(nMFS) C1153F/Y(cMFS), C1055G/W(nMFS) C1055Y(cMFS)). Therefore, similar to in TB domains, the degree of disruption associated with the amino acid change itself could contribute to the outcome of severity. Determining the secretion profile of one example of such would be necessary to experimentally verify this prediction.

5.1.3 Interdomain packing and cbEGF fold residues in domains TB3-cbEGF19

Interdomain interactions with N-terminally adjacent domains significantly modulates calcium binding affinity of cbEGF domains. Interdomain packing residues investigated in this study were those that affect domains TB3-cbEGF11 (I1048T), and cbEGF12-13 (Y1101C).

Our analysis of the I1048T substitution in cbEGF11 reiterated that the additional *N*-linked glycosylation site created is utilized during intracellular processing of fibrillin-1. Our result showing normal secretion indicates that the substitution and addition of an *N*-linked glycan does not completely perturb the domain fold, as previously predicted by computer-based analysis showing no changes to the secondary structure or isoelectric point of the mutant domain (Lonnqvist *et al.,* 1996). The inability of the mutant variant to incorporate into microfibrils suggests that the introduced glycan disrupts an interaction surface required for assembly. Altered glycosylation of secretory proteins has only been implicated in a few diseases. The presence of an additional bulky oligosaccharide in fibrinogen was thought to significantly hinder its polymerization in dysfibrinogenemia patients (Yamazumi *et al.,* 1989). A similar effect, in which the bulky oligosaccharide chain sterically blocks fibrillin interactions or alters the surface charge distribution in the region to make a particular intermolecular interaction less favorable, is possible. The Ile 1048 residue is part of the 'XG' motif in cbEGF11, which is involved in interdomain packing of domains TB3 and

cbEGF11. Therefore, disruption of this site potentially results in further structural alterations which, as postulated by Jensen *et al.,* (2005) could influence flexibility in this region, alter biomechanical properties and intermolecular interactions of the protein. This result highlights the importance of a native TB3-cbEGF11 interface and correct *N*-linked glycosylation of fibrillin-1 for its assembly into microfibrils.

Y1101C mutation, associated with cMFS, substitutes the conserved aromatic residue, Tyr1101. This residue is involved in interdomain packing, it is located at the open end of the minor ß-sheet of cbEGF12 and packs against the top of the major ß-sheet of cbEGF13. Furthermore, substitution of a tyrosine residue to a cysteine could result in the formation of non-native disulfide bonds within cbEGF12 and/or form intermolecular cross-links with different domains in fibrillin-1 (Rommel *et al.,* 2002). Nonetheless, in contrast to the other cysteine substitutions, the Y1101C variant was seen to secrete normally from both HEK293T cells and MSU1.1 fibroblasts and readily incorporate into microfibrils. This suggests that the creation of an additional cysteine residue did not result in radical disruption of the domain fold or stability of the protein in this case.

In addition to calcium binding and disulfide bonding, the cbEGF domain fold also depends on residues that contribute to the formation of the EGF secondary structure. The effect of substituting one such residue in cbEGF13 (G1127S) was investigated. The G1127S mutation has been identified in patients affected with aortic root aneurysm and/or dissection but lacking skeletal or ocular phenotypes of MFS (Franke *et al.* 1995). The mutation substitutes a glycine to a less flexible serine residue at one end the antiparallel ß-sheet structure and was shown to have small, subtle changes on the fold and proteolytic susceptibility of cbEGF13 (Whiteman *et al.,* 2001). Previously, a similar glycine to serine substitution in an

EGF domain in the Factor IX protein was shown to reduce its biological activity to 10% of normal (Denton *et al.,* 1988). This shows that residues at the turn, adjacent to the antiparallel ß-sheet structure in EGF/cbEGF domains are critical for their ability to adopt a native fold. Nonetheless, secretion of this variant in the context of full-length and recombinant proteins, indicates that the change to the fold of the domain introduced by this substitution did not result in its retention in the ER. This is consistent with results from the initial clinical case report that showed normal mutant fibrillin secretion from cultured fibroblasts of a G1127S carrier, using pulse-chase analysis (Franke *et al.* 1995). Nonetheless, our assembly assay results demonstrating normal microfibril assembly of GFP-Fbn containing this substitution, contrasts their finding of reduced fibrillin deposition into the ECM of cultured patient fibroblasts. This could result from the metabolic state of the patients' fibroblasts having an effect on fibrillin-1 deposition examined using pulse-chase analysis, and/or that minor quantitative effects on assembly could evade detection by our microfibril assembly assay performed.

5.1.4 cbEGF deletions in domains TB3-cbEGF19

The splice site mutation associated with nMFS that causes loss of domain cbEGF16 by in frame exon skipping, was shown to be secreted normally but failed to incorporate into FS2 assembled microfibrils. Detection of the ΔcbEGF16 full-length and recombinant constructs in the media indicates that removing cbEGF16 does not prevent secretion of the mutant molecule being produced. This is consistent with a study that investigated the effects of mutations that cause loss of cbEGF domains, using pulse-chase analysis of patient fibroblasts, which reported normal fibrillin secretion but significantly reduced matrix deposition. These domain deletion mutations were postulated to disrupt microfibril formation as a result of interrupting the contiguous stretch of cbEGF domains that might be

critical for phasing of individual monomers during fibrillin polymerization (Liu *et al.,* 1996). Inability of the ΔcbEGF16 variant to assemble strongly suggests that length of the neonatal region is of importance for fibrillin-1 assembly, as despite the presence of an intact TB3-cbEGF13 region in this variant, no microfibril incorporation was seen. However, genomic deletion mutations have been reported in both cMFS and nMFS cases (Liu *et al.,* 2001; Li *et al.,* 2017), indicating that altering register does not always result in drastic disruption of microfibril assembly but is context dependent.

5.2 Molecular pathogenesis of Marfan syndrome

Collectively, the secretion and assembly results presented suggest that disease severity within the TB3-cbEGF18 region is likely correlated with the degree of disruption caused by a given mutation and how it influences fibrillin assembly into microfibrils. As previously discussed, Marfan syndrome results from loss of tissue integrity, associated with deficiencies in the biogenesis of the microfibril system and perturbed TGF-ß signaling (Introduction section 1.6.4). However, the precise mechanisms through which fibrillin mutations cause a reduction in fibrillin microfibrils remains obscure. Haploinsufficiency, which indicates that reduced dosage of fibrillin-1 accounts for decreased fibrillin deposition in the ECM, has been the established pathogenic mechanism underlying MFS (Figure 5.2B). This model is supported by studies showing nonsense-mediated decay of the mutant transcript (Hewett *et al.,* 1994) and data reporting intracellular retention of mutant recombinant fragments from cultured fibroblasts, resulting from a folding defect (Whiteman and Handford 2003, Whiteman *et al.,* 2007, Jensen *et al.,* 2015). Furthermore, studies showing that introduction of a wild type human *FBN1* transgene could rescue the aortic phenotype in $Fbn1^{C1039G/+}$ mouse models, emphasizes the importance of haploinsufficiency in MFS pathogenesis (Judge *et al.,* 2004). Haploinsufficiency provides a plausible

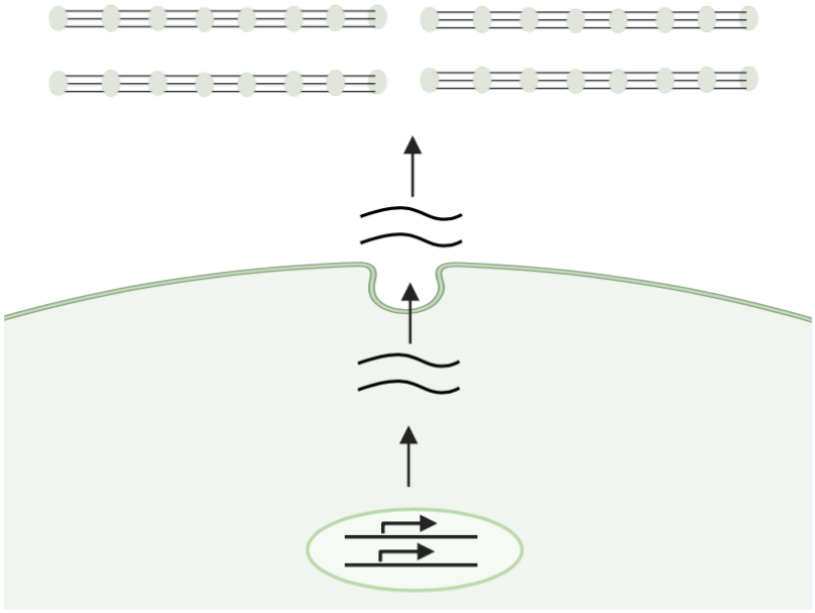
mechanism of pathogenesis for MFS, however, it does not explain the dramatic paucity of fibrillin microfibrils to levels ≤50% of wild type in heterozygous patient samples or provide an explanation for the spectrum of severity in MFS phenotypes observed in different cases (Milewicz *et al.,* 1992; Kielty *et al.,* 1995). Although there are reports of allelic variation in the expression of the WT allele which could contribute to expression of a more severe phenotype in haploinsufficiency patients (Hutchinson *et al.,* 2003), this does not explain the clustering and overrepresentation of missense mutations associated with nMFS in the TB3-cbEGF18 region.

The work presented here adds further insight into dominant negative mechanisms operating in microfibril biogenesis associated with cMFS and nMFS substitutions in domain TB3-cbEGF18. Our data suggest two different dominant negative mechanisms. In the case of cMFS variants where we see minor differences in incorporation efficiency, we postulate that the mutant proteins exert their dominant negative effect by mildly affecting lateral assembly and being mis-incorporated into the microfibril (Figure 5.2C). This dominant negative model of pathogenesis is supported by observations in the literature. Although there are difficulties in quantitating deposited fibrillin-1 in extracted microfibrils, a study by Aoyama *et al.,* (1994) divided patients into four groups depending on the quantitative differences in fibrillin-1 biosynthesis and matrix deposition studied using pulse-chase analysis of [35S]cysteine-labeled fibrillin. Two groups showed normal fibrillin secretion and mildly impaired or normal deposition into microfibrils. Normal microfibril incorporation was also previously seen for heterozygous (mgΔ/+) mice with an in-frame deletion of exons 19-24 that were histologically and morphologically indistinguishable from the WT mice (Pereira *et al.,* 1997), and for the MFS associated substitution (C1663R) in a transgenic mouse model (Judge *et al.,* 2004), consistent with the dominant negative model proposed for cMFS. These results indicate that a different pathogenic mechanism involving microfibril incorporation

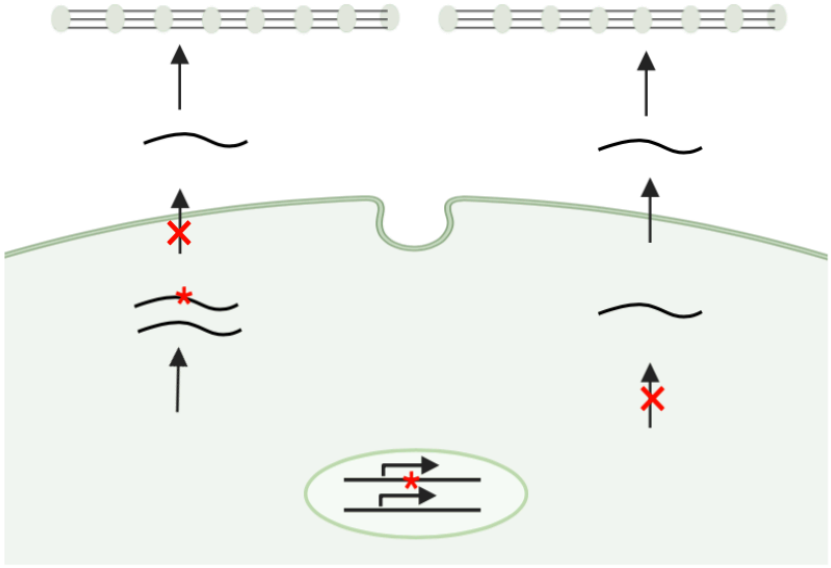
could give rise to MFS phenotypes. In these cases, incorporation of mutant monomers is likely to destabilize the microfibrils, leading to a progressive loss of their biomechanical properties. A normal microfibril network was observed in other type-1 fibrillinopathies, including WMS, GD and SSS, which are likely to result from altered cell-matrix interactions (Jensen *et al.,* 2015).

In the case of nMFS variants, where there was no evidence of microfibril incorporation, despite secretion of most variants at comparable levels to WT, we propose that the mutant fibrillin interacts with WT fibrillin, hindering their assembly into microfibrils. This would lead to the threshold loss of fibrillin microfibrils below the 50% level expected from simple loss of the mutant allele and would lead to the more severe form of the disease (Figure 5.2C). In electron microscopy after rotary shadowing (Lonnqvist *et al.,* 1996) and immunohistochemical studies of patient cell cultures (Superti-Fruga *et al.,* 1992; Raghunath *et al.,* 1993; Lonnqvist *et al.,* 1996) nMFS cultures showed complete absence of microfibrils. Additionally, extensive quantitative pulse-chase analysis was carried out on MFS patients harboring different missense mutations that affect the conformation of cbEGF domains. For ~80% of these substitutions, the deposition of fibrillin microfibrils was reduced to less than 30% (Schrijver *et al.,* 1999). Normal secretion of the nMFS variants with intact N- and C-terminal domains, which would allow for the association of mutant and WT fibrillin during early stages of assembly, suggests that they form non-productive complexes that hinder further assembly steps involving the neonatal region. In EM studies 8 fibrillin monomers are estimated to contribute to the microfibril structure (Baldock *et al.,* 2001), incorporation of mutant, nonlinear monomers into C-terminal multimers, shown to be a key step in early assembly, would greatly affect avidity-driven lateral assembly, if this depended on the native conformation of the TB3-cbEGF18 region.

(A) Normal



(B) Haploinsufficiency



(C) Dominant Negative

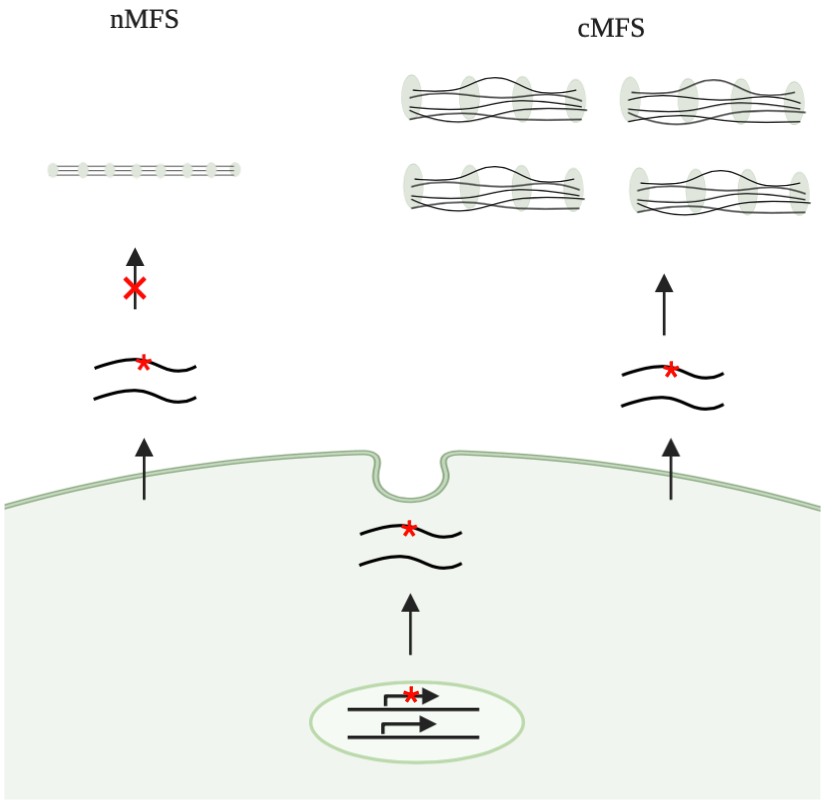


Figure 5.2 Models of Marfan Syndrome Pathogenesis. (A) Normal fibrillin secretion and assembly into microfibrils. (B) Possible fates of mutant fibrillin molecules that lead to haploinsufficiency, including intracellular retention (right), non-sense mediated decay of mutant RNA (middle) or defective microfibril incorporation (left). (C) Possible pathways by which mutant fibrillin results in a dominant negative effect, where it either hinders normal fibrillin assembly into microfibrils (right) or is itself misincorporated into microfibrils (left).

5.3 The neonatal region

The observation that similar mutations result in different severities of MFS depending on their domain context, indicates that the type of amino-acid substitution alone is not sufficient to predict genotype-phenotype correlations in MFS. Thus, additional factors including the influence of the mutation on effective microfibril assembly and/or protein-protein interactions must also play a role in determining the severity of MFS phenotypes. The clustering of mutations associated with a severe form of MFS in the neonatal region suggests that it contains functionally critical domains. Interestingly all the substitutions associated

with congenital contractural arachnodactyly are also localized to domains TB3-cbEGF18 in fibrillin-2, suggesting a conserved function of this region. The neonatal region is located within the longest contiguous stretch of cbEGF domains in fibrillin-1. Notably, Smallridge *et al.,* (1999) have shown that cbEGF13, in the cbEGF12-13 pair, possesses the highest calcium affinity of any investigated cbEGF pair of fibrillin-1, and that cbEGF13 and 14 have significantly higher calcium binding affinities than other cbEGF domains within tandem repeats along the protein. Consistently, another study demonstrated that nMFS mutations in domains cbEGF11-13 resulted in increased proteolytic susceptibility of fibrillin fragments by plasmin, thrombin, trypsin, and chymotrypsin, verifying that loss of calcium-dependent protection occurs, compromising the stability of the protein (Kirschner *et al.,* 2011) Therefore, in addition to its clinical relevance, the particular role of these domains in maintaining the central stability of the monomer highlights its importance at the biochemical level. The conformation imposed by high affinity calcium binding in this region could be essential for later stages of fibrillin assembly into microfibrils. Furthermore, the precise organization of fibrillin domains has been evolutionarily conserved from Cnidarians to humans, this underlines its importance for microfibril assembly and function. Consistent with the staggered model of microfibril assembly, our data suggest the presence of a previously undefined assembly site within domains TB3-cbEGF18 that is crucial for lateral association of fibrillin monomers beyond the C-terminal multimerization step. These lateral homotypic interactions of fibrillin monomers are also likely to be essential for the stabilization of multimers during microfibril formation (Marson *et al.,* 2005). Furthermore, bioinformatics analysis of fibrillin (Results section 3.7) was used to identify residues in cbEGF11-14 that are potential candites for protein interactions, it would be interesting to

target the identified residues in GFP-fibrillin and determine if they affect assembly in our co-culture system.

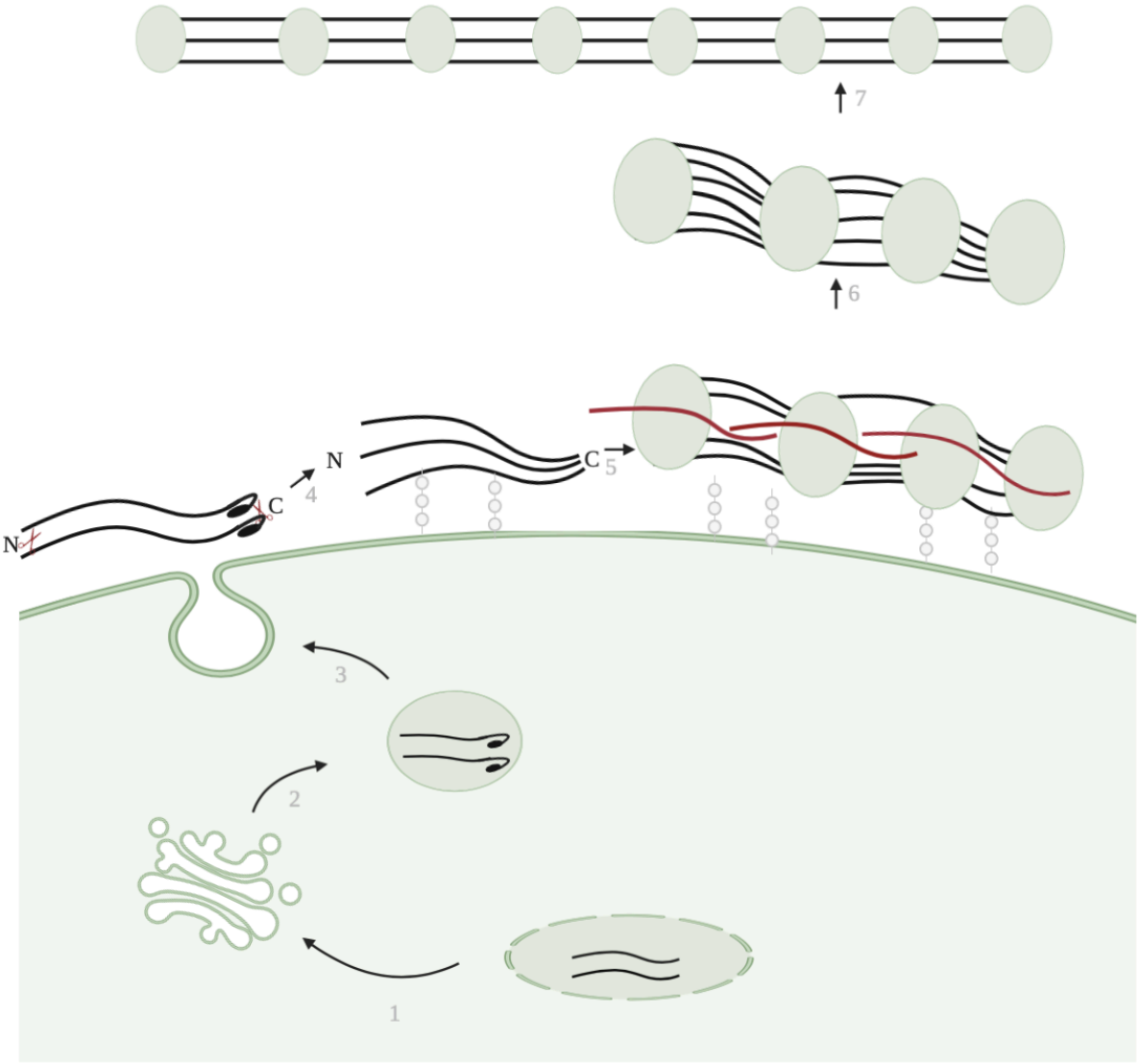


Figure 5.2 Lateral Interactions of fibrillin-1. Diagram demonstrating steps of fibrillin assembly into microfibrils as per figure 1.4 particularly highlighting the interaction of the N- and C- terminal ends with the central region containing domains TB3-cbEGF18 of fibrillin molecules (red).

The critical events that govern fibrillin assembly into microfibrils are still poorly understood, however, the role of domains TB3-cbEGF18 in interacting with other matrix components provides insight into the diverse functional roles of this region. Studies have demonstrated that heparin/heparan sulfate proteoglycans are involved in early coordination of assembly, through sequestering fibrillin at the cell surface (Cain *et al.,* 2008). The observation that nMFS mutations showed a significant reduction in heparin binding of fibrillin-1 (Kirschner *et al.,* 2011), raises the possibility that the pathogenic mechanism associated with these mutations involves a defect in heparin mediated assembly. There are seven heparin binding sites across fibrillin-1, and previous studies have identified the role of one site within domains TB5-cbEGF25 in cell-matrix interaction and signaling. The slightly weaker heparin binding site in domains cbEGF12-14 may be involved in microfibril assembly. However, further studies, showing the effect of disrupting this heparin binding site on microfibril assembly would be need demonstrated at the biochemical level to confirm this hypothesis. Furthermore, the TB3-cbEG18 region was also identified as a major tropoelastin binding site (Rock *et al.,* 2004). It is also possible that the pathogenic mechanism of mutations in this region also involves weakened interaction with elastin, which exacerbates the loss of ECM strength and integrity.

5.4 Concluding remarks

Analysis of the consequences of fibrillin-1 mutations has increased our understanding of the normal functions of fibrillin-1 and revealed steps that are critical to the microfibril assembly process. Our results identified different assembly mechanisms associated with *FBN1* mutations in the neonatal region and provided insight into the additional factors that could influence the severity of a given mutation. A dominant negative effect is invoked as the major mechanism of pathogenesis associated with missense mutations in domains TB3-

cbEGF19. We show that the production of the mutant protein and its incorporation into microfibrils is associated with the less severe 'classical' form of MFS, while the lack of mutant fibrillin incorporation into microfibrils is associated with the more severe neonatal form of MFS. The mechanisms leading to TGF-ß dysregulation in MFS remain unclear (Introduction section 1.6.2.1). For cMFS variants in domains TB3-cbEGF18 it is likely that altered biomechanical properties of microfibrils affect TGF-ß regulation in the matrix, although we cant rule out some quantitative changes in microfibrils, while for nMFS it is a lack of microfibrils in the matrix that result in TGF-ß dysregulation.

The mechanism behind the severe morbidity associated with a dysfunctional neonatal fibrillin-1 locus remains elusive, however, the potential role of the contiguous stretch of cbEGF domains in microfibril assembly could partially explain the severity associated with mutations in this region. Although widely supported by observations in the literature, direct interactions of the neonatal region would need to be investigated biochemically to verify the hypothesis suggesting the presence of a critical assembly site within domains TB3-cbEGF18.

References

1. Albert, B., 2008. Molecular biology of the cell.
2. Aoyama, T., Francke, U., Dietz, H.C. and Furthmayr, H., 1994. Quantitative differences in biosynthesis and extracellular deposition of fibrillin in cultured fibroblasts distinguish five groups of Marfan syndrome patients and suggest distinct pathogenetic mechanisms. *The Journal of clinical investigation*, *94*(1), pp.130-137.
3. Aoyama, T., Tynan, K., Dietz, H.C., Francke, U. and Furthmayr, H., 1993. Missense mutations impair intracellular processing of fibrillin and microfibril assembly in Marfan syndrome. *Human molecular genetics*, *2*(12), pp.2135-2140.
4. Ashworth, J.L., Kelly, V., Wilson, R., Shuttleworth, C.A. and Kielty, C.M., 1999. Fibrillin assembly: dimer formation mediated by amino-terminal sequences. *Journal of cell science*, *112*(20), pp.3549-3558.
5. Baldock, C., Koster, A.J., Ziese, U., Rock, M.J., Sherratt, M.J., Kadler, K.E., Shuttleworth, C.A. and Kielty, C.M., 2001. The supramolecular organization of fibrillin-rich microfibrils. *The Journal of cell biology*, *152*(5), pp.1045-1056.
6. Baldock, C., Siegler, V., Bax, D.V., Cain, S.A., Mellody, K.T., Marson, A., Haston, J.L., Berry, R., Wang, M.C., Grossmann, J.G. and Roessle, M., 2006. Nanostructure of fibrillin-1 reveals compact conformation of EGF arrays and mechanism for extensibility. *Proceedings of the National Academy of Sciences*, *103*(32), pp.11922-11927.
7. Barnett, C.P., Wilson, G.J., Chiasson, D.A., Gross, G.J., Hinek, A., Hawkins, C. and Chitayat, D., 2010. Central nervous system abnormalities in two cases with neonatal Marfan syndrome with novel mutations in the fibrillin-1 gene. *American Journal of Medical Genetics Part A*, *152*(9), pp.2409-2412.
8. Bax, D.V., Bernard, S.E., Lomas, A., Morgan, A., Humphries, J., Shuttleworth, C.A., Humphries, M.J. and Kielty, C.M., 2003. Cell adhesion to fibrillin-1 molecules and microfibrils is mediated by α5β1 and αvβ3 integrins. *Journal of Biological Chemistry*, *278*(36), pp.34605-34616.
9. Biery, N., Eldadah, Z., Moore, C., Stetten, G., Spencer, F. and Dietz, H., 1999. Revised Genomic Organization ofFBN1and Significance for Regulated Gene Expression. *Genomics*, 56(1), pp.70-77
10. Biggin, A., Holman, K., Brett, M., Bennetts, B. and Adès, L., 2004. Detection of thirty novel FBN1 mutations in patients with Marfan syndrome or a related fibrillinopathy. *Human mutation*, *23*(1), pp.99-99.
11. Birk, D.E. and Brückner, P., 2011. Collagens, suprastructures, and collagen fibril assembly. In *The extracellular matrix: an overview* (pp. 77-115). Springer, Berlin, Heidelberg.
12. Bona, C.A., Murai, C., Casares, S., Kasturi, K., Nishimura, H., Honjo, T. and Matsuda, F., 1997. Structure of the mutant fibrillin-1 gene in the tight skin (TSK) mouse. *DNA Research*, *4*(4), pp.267-271.
13. Booms, P., Withers, A.P., Boxer, M., Kaufmann, U.C., Hagemeier, C., Vetter, U. and Robinson, P.N., 1997. A novel de novo mutation in exon 14 of the fibrillin-1 gene associated with delayed secretion of fibrillin in a patient with a mild Marfan phenotype. *Human genetics*, *100*(2), pp.195-200.
14. Brenn, T., Aoyama, T., Francke, U. and Furthmayr, H., 1996. Dermal fibroblast culture as a model system for studies of fibrillin assembly and pathogenetic mechanisms: defects in distinct groups of individuals with Marfan's syndrome. *Laboratory investigation; a journal of technical methods and pathology*, *75*(3), pp.389-402.

15. Bresters, D., Nikkels, P.G.J., Meijboom, E.J.M., Hoorntje, T.M., Pals, G. and Beemer, F.A., 1999. Clinical, pathological and molecular genetic findings in a case of neonatal Marfan syndrome. *Acta Pædiatrica*, *88*(1), pp.98-101.
16. Caffrey, D.R., Somaroo, S., Hughes, J.D., Mintseris, J. and Huang, E.S., 2004. Are protein–protein interfaces more conserved in sequence than the rest of the protein surface?. *Protein Science*, *13*(1), pp.190-202.
17. Cain, S.A., Baldock, C., Gallagher, J., Morgan, A., Bax, D.V., Weiss, A.S., Shuttleworth, C.A. and Kielty, C.M., 2005. Fibrillin-1 interactions with heparin Implications for microfibril and elastic fiber assembly. *Journal of Biological Chemistry*, *280*(34), pp.30526-30537.
18. Cain, S.A., Baldwin, A.K., Mahalingam, Y., Raynal, B., Jowitt, T.A., Shuttleworth, C.A., Couchman, J.R. and Kielty, C.M., 2008. Heparan sulfate regulates fibrillin-1 N-and C-terminal interactions. *Journal of Biological Chemistry*, *283*(40), pp.27017-27027.
19. Cardy, C.M. and Handford, P.A., 1998. Metal ion dependency of microfibrils supports a rod-like conformation for fibrillin-1 calcium-binding epidermal growth factor-like domains. *Journal of molecular biology*, *276*(5), pp.855-860.
20. Carta, L., Pereira, L., Arteaga-Solis, E., Lee-Arteaga, S.Y., Lenart, B., Starcher, B., Merkel, C.A., Sukoyan, M., Kerkis, A., Hazeki, N. and Keene, D.R., 2006. Fibrillins 1 and 2 perform partially overlapping functions during aortic development. *Journal of biological chemistry*, *281*(12), pp.8016-8023.
21. Chandra, A., Aragon-Martin, J.A., Hughes, K., Gati, S., Reddy, M.A., Deshpande, C., Cormack, G., Child, A.H., Charteris, D.G. and Arno, G., 2012. A genotype-phenotype comparison of ADAMTSL4 and FBN1 in isolated ectopia lentis. *Investigative ophthalmology & visual science*, *53*(8), pp.4889-4896.
22. Chen, Y., Ali, T., Todorovic, V., O'Leary, J.M., Downing, A.K. and Rifkin, D.B., 2005. Amino acid requirements for formation of the TGF-β-latent TGF-β binding protein complexes. *Journal of molecular biology*, *345*(1), pp.175-186.
23. Comeglio, P., Johnson, P., Arno, G., Brice, G., Evans, A., Aragon-Martin, J., Silva, F.P.D., Kiotsekoglou, A. and Child, A., 2007. The importance of mutation detection in Marfan syndrome and Marfan-related disorders: report of 193 FBN1 mutations. *Human mutation*, *28*(9), pp.928-928.
24. Cordle, J., Johnson, S., Tay, J.Z.Y., Roversi, P., Wilkin, M.B., De Madrid, B.H., Shimizu, H., Jensen, S., Whiteman, P., Jin, B. and Redfield, C., 2008. A conserved face of the Jagged/Serrate DSL domain is involved in Notch trans-activation and cis-inhibition. *Nature structural & molecular biology*, *15*(8), p.849.
25. Corson, G., Chalberg, S., Dietz, H., Charbonneau, N. and Sakai, L., 1993. Fibrillin Binds Calcium and Is Coded by cDNAs That Reveal a Multidomain Structure and Alternatively Spliced Exons at the 5′ End. *Genomics*, 17(2), pp.476-484.
26. Corson, G., Charbonneau, N., Keene, D. and Sakai, L., 2004. Differential expression of fibrillin-3 adds to microfibril variety in human and avian, but not rodent, connective tissues. *Genomics*, 83(3), pp.461-472.
27. Corson, G.M., Chalberg, S.C., Dietz, H.C., Charbonneau, N.L. and Sakai, L.Y., 1993. Fibrillin binds calcium and is coded by cDNAs that reveal a multidomain structure and alternatively spliced exons at the 5′ end. *Genomics*, *17*(2), pp.476-484.
28. Davison, I.G., Wright, G.M. and DeMont, M.E., 1995. The structure and physical properties of invertebrate and primitive vertebrate arteries. *Journal of Experimental Biology*, *198*(10), pp.2185-2196.
29. De Backer, J., Loeys, B., Leroy, B., Coucke, P., Dietz, H. and De Paepe, A., 2007. Utility of molecular analyses in the exploration of extreme intrafamilial variability in the Marfan syndrome. *Clinical genetics*, *72*(3), pp.188-198.

30. Del Cid, J.S., Reed, N.I., Molnar, K., Liu, S., Dang, B., Jensen, S.A., DeGrado, W., Handford, P.A., Sheppard, D. and Sundaram, A.B., 2019. A disease-associated mutation in fibrillin-1 differentially regulates integrin-mediated cell adhesion. *Journal of Biological Chemistry*, *294*(48), pp.18232-18243.
31. Denton, P.H., Fowlkes, D.M., Lord, S.T. and Reisner, H.M., 1988. Hemophilia B Durham: a mutation in the first EGF-like domain of factor IX that is characterized by polymerase chain reaction.
32. Dietz, H., Cutting, C., Pyeritz, R., Maslen, C., Sakai, L., Corson, G., Puffenberger, E., Hamosh, A., Nanthakumar, E., Curristin, S., Stetten, G., Meyers, D. and Francomano, C., 1991. Marfan syndrome caused by a recurrent de novo missense mutation in the fibrillin gene. *Nature*, 352(6333), pp.337-339.
33. Dietz, H.C. and Pyeritz, R.E., 1995. Mutations in the human gene for fibrillin-1 (FBN1) in the Marfan syndrome and related disorders. *Human molecular genetics*, *4*(suppl_1), pp.1799-1809.
34. Dietz, H.C., McIntosh, I., Sakai, L.Y., Corson, G.M., Chalberg, S.C., Pyeritz, R.E. and Francomano, C.A., 1993. Four novel FBN1 mutations: significance for mutant transcript level and EGF-like domain calcium binding in the pathogenesis of Marfan syndrome. *Genomics*, *17*(2), pp.468-475.
35. Dietz, H.C., Valle, D., Francomano, C.A., Kendzior, R.J., Pyeritz, R.E. and Cutting, G.R., 1993. The skipping of constitutive exons in vivo induced by nonsense mutations. *Science*, *259*(5095), pp.680-683.
36. Downing, A.K., Knott, V., Werner, J.M., Cardy, C.M., Campbell, I.D. and Handford, P.A., 1996. Solution structure of a pair of calcium-binding epidermal growth factor-like domains: implications for the Marfan syndrome and other genetic disorders. *Cell*, *85*(4), pp.597-605
37. Doyle, J.J., Gerber, E.E. and Dietz, H.C., 2012. Matrix-dependent perturbation of TGFβ signaling and disease. *FEBS letters*, *586*(14), pp.2003-2015.
38. Eldadah, Z.A., Brenn, T., Furthmayr, H. and Dietz, H.C., 1995. Expression of a mutant human fibrillin allele upon a normal human or murine genetic background recapitulates a Marfan cellular phenotype. *The Journal of clinical investigation*, *95*(2), pp.874-880.
39. Engel, J. and Chiquet, M., 2011. An overview of extracellular matrix structure and function. In *The extracellular matrix: an overview* (pp. 1-39). Springer, Berlin, Heidelberg.
40. Francke, U., Berg, M.A., Tynan, K., Brenn, T., Liu, W., Aoyama, T., Gasner, C., Miller, D.C. and Furthmayr, H., 1995. A Gly1127Ser mutation in an EGF-like domain of the fibrillin-1 gene is a risk factor for ascending aortic aneurysm and dissection. *American journal of human genetics*, *56*(6), p.1287.
41. Frantz, C., Stewart, K.M. and Weaver, V.M., 2010. The extracellular matrix at a glance. *Journal of cell science*, *123*(24), pp.4195-4200.
42. Frischmeyer, P.A. and Dietz, H.C., 1999. Nonsense-mediated mRNA decay in health and disease. *Human molecular genetics*, *8*(10), pp.1893-1900.
43. Glanville, R.W., Qian, R.Q., McClure, D.W. and Maslen, C.L., 1994. Calcium binding, hydroxylation, and glycosylation of the precursor epidermal growth factor-like domains of fibrillin-1, the Marfan gene protein. *Journal of Biological Chemistry*, *269*(43), pp.26630-26634.
44. Godfrey, M., Raghunath, M., Cisler, J., Bevins, C.L., DePaepe, A., Di Rocco, M., Gregoritch, J., Imaizumi, K., Kaplan, P., Kuroki, Y. and Silberbach, M., 1995. Abnormal morphology of fibrillin microfibrils in fibroblast cultures from patients with neonatal Marfan syndrome. *The American journal of pathology*, *146*(6), p.1414.

45. Gregory, K.E., Ono, R.N., Charbonneau, N.L., Kuo, C.L., Keene, D.R., Bächinger, H.P. and Sakai, L.Y., 2005. The prodomain of BMP-7 targets the BMP-7 complex to the extracellular matrix. *Journal of Biological chemistry*, *280*(30), pp.27970-27980.
46. Habashi, J.P., Judge, D.P., Holm, T.M., Cohn, R.D., Loeys, B.L., Cooper, T.K., Myers, L., Klein, E.C., Liu, G., Calvi, C. and Podowski, M., 2006. Losartan, an AT1 antagonist, prevents aortic aneurysm in a mouse model of Marfan syndrome. *Science*, *312*(5770), pp.117-121.
47. Halliday, D., Hutchinson, S., Kettle, S., Firth, H., Wordsworth, P. and Handford, P.A., 1999. Molecular analysis of eight mutations in FBN1. *Human genetics*, *105*(6), pp.587-597.
48. Handford, P.A., 2000. Fibrillin-1, a calcium binding protein of extracellular matrix. *Biochimica et Biophysica Acta (BBA)-Molecular Cell Research*, *1498*(2-3), pp.84-90.
49. Handford, P.A., Downing, A.K., Reinhardt, D.P. and Sakai, L.Y., 2000. Fibrillin: from domain structure to supramolecular assembly. *Matrix Biology*, *19*(6), pp.457-470.
50. Handford, P.A., Mayhew, M., Baron, M., Winship, P.R., Campbell, I.D. and Brownlee, G.G., 1991. Key residues involved in calcium-binding motifs in EGF-like domains. *Nature*, *351*(6322), pp.164-167.
51. Hanssen, E., Hew, F.H., Moore, E. and Gibson, M.A., 2004. MAGP-2 has multiple binding regions on fibrillins and has covalent periodic association with fibrillin-containing microfibrils. *Journal of Biological Chemistry*, *279*(28), pp.29185-29194.
52. Hewett, D., Lynch, J., Child, A., Firth, H. and Sykes, B., 1994. Differential allelic expression of a fibrillin gene (FBN1) in patients with Marfan syndrome. *American journal of human genetics*, *55*(3), p.447.
53. Hewett, D.R., Lynch, J.R., Smith, R. and Sykes, B.C., 1993. A novel fibrillin mutation in the Marfan syndrome which could disrupt calcium binding of the epidermal growth factor-like module. *Human molecular genetics*, *2*(4), pp.475-477.
54. Hirani, R., Hanssen, E. and Gibson, M.A., 2007. LTBP-2 specifically interacts with the amino-terminal region of fibrillin-1 and competes with LTBP-1 for binding to this microfibrillar protein. *Matrix Biology*, *26*(4), pp.213-223.
55. Hoda, S.A. and Ginter, P.S., 2015. Robbins and cotran pathologic basis of disease. *American Journal of Clinical Pathology*, *144*(1), p.172.
56. Holm, T.M., Habashi, J.P., Doyle, J.J., Bedja, D., Chen, Y., Van Erp, C., Lindsay, M.E., Kim, D., Schoenhoff, F., Cohn, R.D. and Loeys, B.L., 2011. Noncanonical TGFβ signaling contributes to aortic aneurysm progression in Marfan syndrome mice. *Science*, *332*(6027), pp.358-361.
57. Hubmacher, D., Bergeron, E., Fagotto-Kaufmann, C., Sakai, L.Y. and Reinhardt, D.P., 2014. Early fibrillin-1 assembly monitored through a modifiable recombinant cell approach. *Biomacromolecules*, *15*(4), pp.1456-1468.
58. Hubmacher, D., El-Hallous, E.I., Nelea, V., Kaartinen, M.T., Lee, E.R. and Reinhardt, D.P., 2008. Biogenesis of extracellular microfibrils: Multimerization of the fibrillin-1 C terminus into bead-like structures enables self-assembly. *Proceedings of the National Academy of Sciences*, *105*(18), pp.6548-6553.
59. Hubmacher, D., Tiedemann, K., Bartels, R., Brinckmann, J., Vollbrandt, T., Bätge, B., Notbohm, H. and Reinhardt, D.P., 2005. Modification of the structure and function of fibrillin-1 by homocysteine suggests a potential pathogenetic mechanism in homocystinuria. *Journal of Biological Chemistry*, *280*(41), pp.34946-34955.
60. Hutchinson, S., Furger, A., Halliday, D., Judge, D.P., Jefferson, A., Dietz, H.C., Firth, H. and Handford, P.A., 2003. Allelic variation in normal human FBN1 expression in a

family with Marfan syndrome: a potential modifier of phenotype?. *Human molecular genetics*, *12*(18), pp.2269-2276.
61. Isogai, Z., Aspberg, A., Keene, D.R., Ono, R.N., Reinhardt, D.P. and Sakai, L.Y., 2002. Versican interacts with fibrillin-1 and links extracellular microfibrils to other connective tissue networks. *Journal of Biological Chemistry*, *277*(6), pp.4565-4572.
62. Isogai, Z., Ono, R.N., Ushiro, S., Keene, D.R., Chen, Y., Mazzieri, R., Charbonneau, N.L., Reinhardt, D.P., Rifkin, D.B. and Sakai, L.Y., 2003. Latent transforming growth factor β-binding protein 1 interacts with fibrillin and is a microfibril-associated protein. *Journal of Biological Chemistry*, *278*(4), pp.2750-2757.
63. Jacobs, A.M., Toudjarska, I., Racine, A., Tsipouras, P., Kilpatrick, M.W. and Shanske, A., 2002. A recurring FBN1 gene mutation in neonatal Marfan syndrome. *Archives of pediatrics & adolescent medicine*, *156*(11), pp.1081-1085.
64. Jensen, S.A. and Handford, P.A., 2016. New insights into the structure, assembly and biological roles of 10–12 nm connective tissue microfibrils from fibrillin-1 studies. *Biochemical Journal*, *473*(7), pp.827-838.
65. Jensen, S.A., Aspinall, G. and Handford, P.A., 2014. C-terminal propeptide is required for fibrillin-1 secretion and blocks premature assembly through linkage to domains cbEGF41-43. *Proceedings of the National Academy of Sciences*, *111*(28), pp.10155-10160.
66. Jensen, S.A., Corbett, A.R., Knott, V., Redfield, C. and Handford, P.A., 2005. Ca2+-dependent interface formation in fibrillin-1. *Journal of Biological Chemistry*, *280*(14), pp.14076-14084.
67. Jensen, S.A., Iqbal, S., Bulsiewicz, A. and Handford, P.A., 2015. A microfibril assembly assay identifies different mechanisms of dominance underlying Marfan syndrome, stiff skin syndrome and acromelic dysplasias. *Human molecular genetics*, *24*(15), pp.4454-4463.
68. Jensen, S.A., Iqbal, S., Lowe, E.D., Redfield, C. and Handford, P.A., 2009. Structure and interdomain interactions of a hybrid domain: a disulphide-rich module of the fibrillin/LTBP superfamily of matrix proteins. *Structure*, *17*(5), pp.759-768.
69. Jensen, S.A., Reinhardt, D.P., Gibson, M.A. and Weiss, A.S., 2001. Protein interaction studies of MAGP-1 with tropoelastin and fibrillin-1. *Journal of Biological Chemistry*, *276*(43), pp.39661-39666.
70. Jensen, S.A., Robertson, I.B. and Handford, P.A., 2012. Dissecting the fibrillin microfibril: structural insights into organization and function. *Structure*, *20*(2), pp.215-225.
71. Jovanović, J., Takagi, J., Choulier, L., Abrescia, N.G., Stuart, D.I., Van Der Merwe, P.A., Mardon, H.J. and Handford, P.A., 2007. αVβ6 Is a novel receptor for human fibrillin-1 comparative studies of molecular determinants underlying integrin-Rgd affinity and specificity. *Journal of Biological Chemistry*, *282*(9), pp.6743-6751.
72. Judge, D.P. and Dietz, H.C., 2005. Marfan's syndrome. *The Lancet*, *366*(9501), pp.1965-1976.
73. Judge, D.P., Biery, N.J., Keene, D.R., Geubtner, J., Myers, L., Huso, D.L., Sakai, L.Y. and Dietz, H.C., 2004. Evidence for a critical contribution of haploinsufficiency in the complex pathogenesis of Marfan syndrome. *The Journal of clinical investigation*, *114*(2), pp.172-181.
74. Keene, D.R., Maddox, B.K., Kuo, H.J., Sakai, L.Y. and Glanville, R.W., 1991. Extraction of extendable beaded structures and their identification as fibrillin-containing extracellular matrix microfibrils. *Journal of Histochemistry & Cytochemistry*, *39*(4), pp.441-449.

75. Kettle, S., Cardy, C., Hutchinson, S., Sykes, B. and Handford, P., 2000. Characterisation of fibrillin-1 cDNA clones in a human fibroblast cell line that assembles microfibrils. *The International Journal of Biochemistry & Cell Biology*, 32(2), pp.201-214.
76. Kielty, C.M. and Shuttleworth, C.A., 1995. Fibrillin-containing microfibrils: structure and function in health and disease. *The international journal of biochemistry & cell biology*, *27*(8), pp.747-760.
77. Kielty, C.M., Rantamaki, T., Child, A.H., Shuttleworth, C.A. and Peltonen, L., 1995. Cysteine-to-arginine point mutation in a 'hybrid'eight-cysteine domain of FBN1: consequences for fibrillin aggregation and microfibril assembly. *Journal of cell science*, *108*(3), pp.1317-1323.
78. Kinsey, R., Williamson, M.R., Chaudhry, S., Mellody, K.T., McGovern, A., Takahashi, S., Shuttleworth, C.A. and Kielty, C.M., 2008. Fibrillin-1 microfibril deposition is dependent on fibronectin assembly. *Journal of cell science*, *121*(16), pp.2696-2704.
79. Kirschner, R., Hubmacher, D., Iyengar, G., Kaur, J., Fagotto-Kaufmann, C., Brömme, D., Bartels, R. and Reinhardt, D.P., 2011. Classical and neonatal Marfan syndrome mutations in fibrillin-1 cause differential protease susceptibilities and protein function. *Journal of Biological Chemistry*, *286*(37), pp.32810-32823.
80. Knott, V., Downing, K.A., Cardy, C.M. and Handford, P., 1996. Calcium binding properties of an epidermal growth factor-like domain pair from human fibrillin-1.
81. Kozak, M., 1991. An analysis of vertebrate mRNA sequences: intimations of translational control. *The Journal of Cell Biology*, 115(4), pp.887-903.
82. Kuo, C.L., Isogai, Z., Keene, D.R., Hazeki, N., Ono, R.N., Sengle, G., Bächinger, H.P. and Sakai, L.Y., 2007. Effects of fibrillin-1 degradation on microfibril ultrastructure. *Journal of Biological Chemistry*, *282*(6), pp.4007-4020.
83. Le Goff, C., Mahaut, C., Wang, L.W., Allali, S., Abhyankar, A., Jensen, S., Zylberberg, L., Collod-Beroud, G., Bonnet, D., Alanay, Y. and Brady, A.F., 2011. Mutations in the TGFβ binding-protein-like domain 5 of FBN1 are responsible for acromicric and geleophysic dysplasias. *The American Journal of Human Genetics*, *89*(1), pp.7-14.
84. Lee, B., Godfrey, M., Vitale, E., Hori, H., Mattei, M., Sarfarazi, M., Tsipouras, P., Ramirez, F. and Hollister, D., 1991s. Linkage of Marfan syndrome and a phenotypically related disorder to two different fibrillin genes. *Nature*, 352(6333), pp.330-334.
85. Lee, S.S., Knott, V., Jovanović, J., Harlos, K., Grimes, J.M., Choulier, L., Mardon, H.J., Stuart, D.I. and Handford, P.A., 2004. Structure of the integrin binding fragment from fibrillin-1 gives new insights into microfibril organization. *Structure*, *12*(4), pp.717-729.
86. Lee, T., Takeshima, Y., Okizuka, Y., Hamahira, K., Kusunoki, N., Awano, H., Yagi, M., Sakai, N., Matsuo, M. and Iijima, K., 2013. A Japanese child with geleophysic dysplasia caused by a novel mutation of FBN1. *Gene*, *512*(2), pp.456-459.
87. Li, J., Wu, W., Lu, C., Liu, Y., Wang, R., Si, N., Liu, F., Zhou, J., Zhang, S. and Zhang, X., 2017. Gross deletions in FBN1 results in variable phenotypes of Marfan syndrome. *Clinica Chimica Acta*, *474*, pp.54-59.
88. Lin, G., Tiedemann, K., Vollbrandt, T., Peters, H., Bätge, B., Brinckmann, J. and Reinhardt, D.P., 2002. Homo-and heterotypic fibrillin-1 and-2 interactions constitute the basis for the assembly of microfibrils. *Journal of Biological Chemistry*, *277*(52), pp.50795-50804.
89. Liu, W., Qian, C., Comeau, K., Brenn, T., Furthmayr, H. and Francke, U., 1996. Mutant fibrillin-1 monomers lacking EGF-like domains disrupt microfibril assembly and cause severe Marfan syndrome. *Human molecular genetics*, *5*(10), pp.1581-1587.
90. Liu, W., Schrijver, I., Brenn, T., Furthmayr, H. and Francke, U., 2001. Multi-exon deletions of the FBN1 gene in Marfan syndrome. *BMC medical genetics*, *2*(1), p.11.

91. Loeys, B., Nuytinck, L., Delvaux, I., De Bie, S. and De Paepe, A., 2001. Genotype and phenotype analysis of 171 patients referred for molecular study of the fibrillin-1 gene FBN1 because of suspected Marfan syndrome. *Archives of Internal Medicine*, *161*(20), pp.2447-2454.
92. Loeys, B.L., Chen, J., Neptune, E.R., Judge, D.P., Podowski, M., Holm, T., Meyers, J., Leitch, C.C., Katsanis, N., Sharifi, N. and Xu, F.L., 2005. A syndrome of altered cardiovascular, craniofacial, neurocognitive and skeletal development caused by mutations in TGFBR1 or TGFBR2. *Nature genetics*, *37*(3), pp.275-281.
93. Loeys, B.L., Gerber, E.E., Riegert-Johnson, D., Iqbal, S., Whiteman, P., McConnell, V., Chillakuri, C.R., Macaya, D., Coucke, P.J., De Paepe, A. and Judge, D.P., 2010. Mutations in fibrillin-1 cause congenital scleroderma: stiff skin syndrome. *Science translational medicine*, *2*(23), pp.23ra20-23ra20.
94. Lönnqvist, L., Karttunen, L., Rantamäki, T., Kielty, C., Raghunath, M. and Peltonen, L., 1996. A Point Mutation Creating an ExtraN-Glycosylation Site in Fibrillin-1 Results in Neonatal Marfan Syndrome. *Genomics*, *36*(3), pp.468-475.
95. Lönnqvist, L., Reinhardt, D., Sakai, L. and Peltonen, L., 1998. Evidence for furin-type activity-mediated C-terminal processing of profibrillin-1 and interference in the processing by certain mutations. *Human molecular genetics*, *7*(13), pp.2039-2044.
96. Magenis, R., Maslen, C., Smith, L., Allen, L. and Sakai, L., 1991. Localization of the fibrillin (FBN) gene to chromosome 15, band q21.1. *Genomics*, 11(2), pp.346-351.
97. Marson, A., Rock, M.J., Cain, S.A., Freeman, L.J., Morgan, A., Mellody, K., Shuttleworth, C.A., Baldock, C. and Kielty, C.M., 2005. Homotypic fibrillin-1 interactions in microfibril assembly. *Journal of Biological Chemistry*, *280*(6), pp.5013-5021.
98. Maslen, C., Corson, G., Maddox, B., Glanville, R. and Sakai, L., 1991. Partial sequence of a candidate gene for the Marfan syndrome. *Nature*, 352(6333), pp.334-337.
99. McGettrick, A.J., Knott, V., Willis, A. and Handford, P.A., 2000. Molecular effects of calcium binding mutations in Marfan syndrome depend on domain context. *Human molecular genetics*, *9*(13), pp.1987-1994.
100. Milewicz, D.M., Grossfield, J., Cao, S.N., Kielty, C., Covitz, W. and Jewett, T., 1995. A mutation in FBN1 disrupts profibrillin processing and results in isolated skeletal features of the Marfan syndrome. *The Journal of clinical investigation*, *95*(5), pp.2373-2378.
101. Milewicz, D.M., Michael, K., Fisher, N., Coselli, J.S., Markello, T. and Biddinger, A., 1996. Fibrillin-1 (FBN1) mutations in patients with thoracic aortic aneurysms. *Circulation*, *94*(11), pp.2708-2711.
102. Milewicz, D.M., Pyeritz, R.E., Crawford, E.S. and Byers, P.H., 1992. Marfan syndrome: defective synthesis, secretion, and extracellular matrix formation of fibrillin by cultured dermal fibroblasts. *The Journal of clinical investigation*, *89*(1), pp.79-86.
103. Miyazono, K., Hellman, U., Wernstedt, C. and Heldin, C.H., 1988. Latent high molecular weight complex of transforming growth factor beta 1. Purification from human platelets and structural characterization. *Journal of Biological Chemistry*, *263*(13), pp.6407-6415.
104. Miyazono, K., Olofsson, A., Colosetti, P. and Heldin, C.H., 1991. A role of the latent TGF-beta 1-binding protein in the assembly and secretion of TGF-beta 1. *The EMBO journal*, *10*(5), pp.1091-1101.
105. Molloy, S.S., Thomas, L., VanSlyke, J.K., Stenberg, P.E. and Thomas, G., 1994. Intracellular trafficking and activation of the furin proprotein convertase: localization to the TGN and recycling from the cell surface. *The EMBO journal*, *13*(1), pp.18-33.

106. Neptune, E.R., Frischmeyer, P.A., Arking, D.E., Myers, L., Bunton, T.E., Gayraud, B., Ramirez, F., Sakai, L.Y. and Dietz, H.C., 2003. Dysregulation of TGF-β activation contributes to pathogenesis in Marfan syndrome. *Nature genetics*, *33*(3), pp.407-411.
107. Ng, C.M., Cheng, A., Myers, L.A., Martinez-Murillo, F., Jie, C., Bedja, D., Gabrielson, K.L., Hausladen, J.M., Mecham, R.P., Judge, D.P. and Dietz, H.C., 2004. TGF-β–dependent pathogenesis of mitral valve prolapse in a mouse model of Marfan syndrome. *The Journal of clinical investigation*, *114*(11), pp.1586-1592.
108. Nijbroek, G., Sood, S., McIntosh, I., Francomano, C.A., Bull, E., Pereira, L., Ramirez, F., Pyeritz, R.E. and Dietz, H.C., 1995. Fifteen novel FBN1 mutations causing Marfan syndrome detected by heteroduplex analysis of genomic amplicons. *American journal of human genetics*, *57*(1), p.8.
109. Ono, R.N., Sengle, G., Charbonneau, N.L., Carlberg, V., Bächinger, H.P., Sasaki, T., Lee-Arteaga, S., Zilberberg, L., Rifkin, D.B., Ramirez, F. and Chu, M.L., 2009. Latent transforming growth factor β-binding proteins and fibulins compete for fibrillin-1 and exhibit exquisite specificities in binding sites. *Journal of Biological Chemistry*, *284*(25), pp.16872-16881.
110. Peng, Q., Deng, Y., Yang, Y. and Liu, H., 2016. A novel fibrillin-1 gene missense mutation associated with neonatal Marfan syndrome: a case report and review of the mutation spectrum. *BMC pediatrics*, *16*(1), p.60.
111. Pereira, L., Andrikopoulos, K., Tian, J., Lee, S.Y., Keene, D.R., Ono, R., Reinhardt, D.P., Sakai, L.Y., Biery, N.J., Bunton, T. and Dietz, H.C., 1997. Targetting of the gene encoding fibrillin–1 recapitulates the vascular aspect of Marfan syndrome. *Nature genetics*, *17*(2), pp.218-222.
112. Pereira, L., D'Alessio, M., Ramirez, F., Lynch, J., Sykes, B., Pangilinan, T. and Bonadio, J., 1993. Genomic organization of the sequence coding for fibrillin, the defective gene product in Marfan syndrome. *Human Molecular Genetics*, 2(10), pp.1762-1762.
113. Pereira, L., Lee, S.Y., Gayraud, B., Andrikopoulos, K., Shapiro, S.D., Bunton, T., Biery, N.J., Dietz, H.C., Sakai, L.Y. and Ramirez, F., 1999. Pathogenetic sequence for aneurysm revealed in mice underexpressing fibrillin-1. *Proceedings of the National Academy of Sciences*, *96*(7), pp.3819-3823.
114. Pfaff, M., Reinhardt, D.P., Sakai, L.Y. and Timpl, R., 1996. Cell adhesion and integrin binding to recombinant human fibrillin-1. *FEBS letters*, *384*(3), pp.247-250.
115. Piha-Gossack, A., Sossin, W. and Reinhardt, D.P., 2012. The evolution of extracellular fibrillins and their functional domains. *PloS one*, *7*(3).
116. Putnam, E.A., Cho, M., Zinn, A.B., Towbin, J.A., Byers, P.H. and Milewicz, D.M., 1996. Delineation of the Marfan phenotype associated with mutations in exons 23–32 of the FBN1 gene. *American journal of medical genetics*, *62*(3), pp.233-242.
117. Putnam, E.A., Zhang, H., Ramirez, F. and Milewicz, D.M., 1995. Fibrillin–2 (FBN2) mutations result in the Marfan–like disorder, congenital contractural arachnodactyly. *Nature genetics*, *11*(4), pp.456-458.
118. Raghunath, M., Kielty, C.M. and Steinmann, B., 1995. Truncated profibrillin of a Marfan patient is of apparent similar size as fibrillin: intracellular retention leads to over-N-glycosylation. *Journal of molecular biology*, *248*(5), pp.901-909.
119. Raghunath, M., Putnam, E.A., Ritty, T., Hamstra, D., Park, E.S., Tschodrich-Rotter, M., Peters, R., Rehemtulla, A. and Milewicz, D.M., 1999. Carboxy-terminal conversion of profibrillin to fibrillin at a basic site by PACE/furin-like activity required for incorporation in the matrix. *Journal of Cell Science*, *112*(7), pp.1093-1100.

120. Raghunath, M., Superti-Furga, A., Godfrey, M. and Steinmann, B., 1993. Decreased extracellular deposition of fibrillin and decorin in neonatal Marfan syndrome fibroblasts. *Human genetics*, *90*(5), pp.511-515.
121. Rao, Z., Handford, P., Mayhew, M., Knott, V., Brownlee, G.G. and StuartZ, D., 1995. The structure of a Ca2+-binding epidermal growth factor-like domain: its role in protein-protein interactions. *Cell*, *82*(1), pp.131-141.
122. Reber-Müller, S., Spissinger, T., Schuchert, P., Spring, J. and Schmid, V., 1995. An extracellular matrix protein of jellyfish homologous to mammalian fibrillins forms different fibrils depending on the life stage of the animal. *Developmental biology*, *169*(2), pp.662-672.
123. Rees, D.J., Jones, I.M., Handford, P.A., Walter, S.J., Esnouf, M.P., Smith, K.J. and Brownlee, G.G., 1988. The role of beta-hydroxyaspartate and adjacent carboxylate residues in the first EGF domain of human factor IX. *The EMBO Journal*, *7*(7), pp.2053-2061.
124. Reinhard, D.P., Gambee, J.E., Ono, R.N., Bächinger, H.P. and Sakai, L., 2000. Initial steps in assembly of microfibrils: Formation of disulfide-cross-linked multimers containing fibrillin-1. *Journal of Biological Chemistry*, *275*(3), pp.2205-2210.
125. Reinhardt, D.P., Keene, D.R., Corson, G.M., Pöschl, E., Bächinger, H.P., Gambee, J.E. and Sakai, L.Y., 1996. Fibrillin-1: organization in microfibrils and structural properties. *Journal of molecular biology*, *258*(1), pp.104-116.
126. Reinhardt, D.P., Mechling, D.E., Boswell, B.A., Keene, D.R., Sakai, L.Y. and Bächinger, H.P., 1997. Calcium determines the shape of fibrillin. *Journal of Biological Chemistry*, *272*(11), pp.7368-7373.
127. Reinhardt, D.P., Ono, R.N. and Sakai, L.Y., 1997. Calcium stabilizes fibrillin-1 against proteolytic degradation. *Journal of Biological Chemistry*, *272*(2), pp.1231-1236.
128. Reinhardt, D.P., Ono, R.N., Notbohm, H., Müller, P.K., Bächinger, H.P. and Sakai, L.Y., 2000. Mutations in Calcium-binding Epidermal Growth Factor Modules Render Fibrillin-1 Susceptible to Proteolysis A POTENTIAL DISEASE-CAUSING MECHANISM IN MARFAN SYNDROME. *Journal of Biological Chemistry*, *275*(16), pp.12339-12345.
129. Reinhardt, D.P., Sasaki, T., Dzamba, B.J., Keene, D.R., Chu, M.L., Göhring, W., Timpl, R. and Sakai, L.Y., 1996. Fibrillin-1 and fibulin-2 interact and are colocalized in some tissues. *Journal of Biological Chemistry*, *271*(32), pp.19489-19496.
130. Robertson, I., Jensen, S. and Handford, P., 2011. TB domain proteins: evolutionary insights into the multifaceted roles of fibrillins and LTBPs. *Biochemical Journal*, *433*(2), pp.263-276.
131. Robertson, I.B., Dias, H.F., Osuch, I.H., Lowe, E.D., Jensen, S.A., Redfield, C. and Handford, P.A., 2017. The N-terminal region of fibrillin-1 mediates a bipartite interaction with LTBP1. *Structure*, *25*(8), pp.1208-1221.
132. Robinson, P., 2000. The molecular genetics of Marfan syndrome and related microfibrillopathies. *Journal of Medical Genetics*, 37(1), pp.9-25.
133. Rock, M.J., Cain, S.A., Freeman, L.J., Morgan, A., Mellody, K., Marson, A., Shuttleworth, C.A., Weiss, A.S. and Kielty, C.M., 2004. Molecular Basis of Elastic Fiber Formation Critical Interactions and a Tropoelastin-Fibrillin-1 Cross-Link. *Journal of Biological Chemistry*, *279*(22), pp.23748-23758.
134. Rommel, K., Karck, M., Haverich, A., Schmidtke, J. and Arslan-Kirchner, M., 2002. Mutation screening of the fibrillin-1 (FBN1) gene in 76 unrelated patients with Marfan syndrome or Marfanoid features leads to the identification of 11 novel and three previously reported mutations. *Human mutation*, *20*(5), pp.406-407.

135. Sabatier, L., Chen, D., Fagotto-Kaufmann, C., Hubmacher, D., McKee, M.D., Annis, D.S., Mosher, D.F. and Reinhardt, D.P., 2009. Fibrillin assembly requires fibronectin. *Molecular biology of the cell*, *20*(3), pp.846-858.
136. Sabatier, L., Djokic, J., Fagotto-Kaufmann, C., Chen, M., Annis, D.S., Mosher, D.F. and Reinhardt, D.P., 2013. Complex contributions of fibronectin to initiation and maturation of microfibrils. *Biochemical Journal*, *456*(2), pp.283-295.
137. Saharinen, J. and Keski-Oja, J., 2000. Specific sequence motif of 8-Cys repeats of TGF-β binding proteins, LTBPs, creates a hydrophobic interaction surface for binding of small latent TGF-β. *Molecular biology of the cell*, *11*(8), pp.2691-2704.
138. Sakai, L.Y., Keene, D.R., Glanville, R.W. and Bächinger, H.P., 1991. Purification and partial characterization of fibrillin, a cysteine-rich structural component of connective tissue microfibrils. *Journal of Biological Chemistry*, *266*(22), pp.14763-14770.
139. Sakai, L.Y., Keene, D.R., Renard, M. and De Backer, J., 2016. FBN1: The disease-causing gene for Marfan syndrome and other genetic disorders. *Gene*, *591*(1), pp.279-291.
140. Sakai, LY. Keene DR, Engvall E., 1986. Fibrillin, a new 350-kD glycoprotein, is a component of extracellular microfibrils. *The Journal of Cell Biology*, 103(6), pp.2499-2509.
141. Sakamoto, H., Broekelmann, T., Cheresh, D.A., Ramirez, F., Rosenbloom, J. and Mecham, R.P., 1996. Cell-type specific recognition of RGD-and non-RGD-containing cell binding domains in fibrillin-1. *Journal of Biological Chemistry*, *271*(9), pp.4916-4922.
142. Schrijver, I., Liu, W., Brenn, T., Furthmayr, H. and Francke, U., 1999. Cysteine substitutions in epidermal growth factor–like domains of fibrillin-1: distinct effects on biochemical and clinical phenotypes. *The American Journal of Human Genetics*, *65*(4), pp.1007-1020.
143. Segars, J. and DeCherney, A., 2010. Is There a Genetic Basis for Polycystic Ovary Syndrome?. *The Journal of Clinical Endocrinology & Metabolism*, 95(5), pp.2058-2060.
144. Sengle, G., Charbonneau, N.L., Ono, R.N., Sasaki, T., Alvarez, J., Keene, D.R., Bächinger, H.P. and Sakai, L.Y., 2008. Targeting of bone morphogenetic protein growth factor complexes to fibrillin. *Journal of Biological Chemistry*, *283*(20), pp.13874-13888.
145. Siracusa, L.D., McGrath, R., Ma, Q., Moskow, J.J., Manne, J., Christner, P.J., Buchberg, A.M. and Jimenez, S.A., 1996. A tandem duplication within the fibrillin 1 gene is associated with the mouse tight skin mutation. *Genome Research*, *6*(4), pp.300-313.
146. Smallridge, R.S., Whiteman, P., Doering, K., Handford, P.A. and Downing, A.K., 1999. EGF-like domain calcium affinity modulated by N-terminal domain linkage in human fibrillin-1. *Journal of molecular biology*, *286*(3), pp.661-668.
147. Smallridge, R.S., Whiteman, P., Werner, J.M., Campbell, I.D., Handford, P.A. and Downing, A.K., 2003. Solution structure and dynamics of a calcium binding epidermal growth factor-like domain pair from the neonatal region of human fibrillin-1. *Journal of Biological Chemistry*, *278*(14), pp.12199-12206.
148. Stheneur, C., Collod-Béroud, G., Faivre, L., Buyck, J.F., Gouya, L., Le Parc, J.M., Moura, B., Muti, C., Grandchamp, B., Sultan, G. and Claustres, M., 2009. Identification of the minimal combination of clinical features in probands for efficient mutation detection in the FBN1 gene. *European Journal of Human Genetics*, *17*(9), pp.1121-1128.

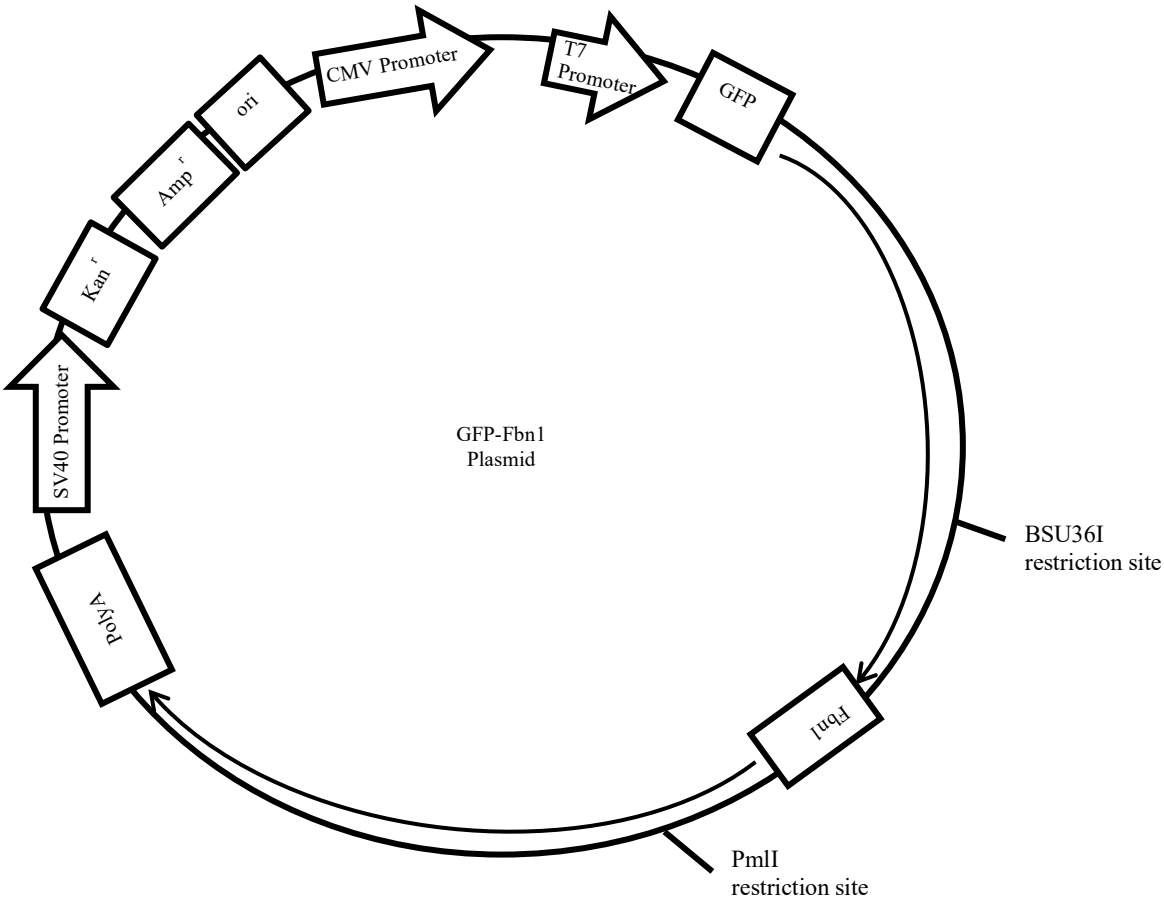
149. Superti-Furga, A., Raghunath, M. and Willems, P.J., 1992. Deficiencies of fibrillin and decorin in fibroblast cultures of a patient with neonatal Marfan syndrome. *Journal of medical genetics*, *29*(12), pp.875-878.
150. Tekin, M., Cengiz, F.B., Ayberkin, E., Kendirli, T., Fitoz, S., Tutar, E., Çiftçi, E. and Conba, A., 2007. Familial neonatal Marfan syndrome due to parental mosaicism of a missense mutation in the FBN1 gene. *American Journal of Medical Genetics Part A*, *143*(8), pp.875-880.
151. Thomson, J., Singh, M., Eckersley, A., Cain, S.A., Sherratt, M.J. and Baldock, C., 2019, May. Fibrillin microfibrils and elastic fibre proteins: Functional interactions and extracellular regulation of growth factors. In *Seminars in cell & developmental biology* (Vol. 89, pp. 109-117). Academic Press.
152. Thurmond, F. and Trotter, J., 1996. Morphology and biomechanics of the microfibrillar network of sea cucumber dermis. *Journal of Experimental Biology*, *199*(8), pp.1817-1828.
153. Tiecke, F., Katzke, S., Booms, P., Robinson, P.N., Neumann, L., Godfrey, M., Mathews, K.R., Scheuner, M., Hinkel, G.K., Brenner, R.E. and Hövels-Gürich, H.H., 2001. Classic, atypically severe and neonatal Marfan syndrome: twelve mutations and genotype–phenotype correlations in FBN1 exons 24–40. *European Journal of Human Genetics*, *9*(1), pp.13-21.
154. Tiedemann, K., Bätge, B., Müller, P.K. and Reinhardt, D.P., 2001. Interactions of fibrillin-1 with heparin/heparan sulfate, implications for microfibrillar assembly. *Journal of Biological Chemistry*, *276*(38), pp.36035-36042.
155. Tjeldhorn, L., Rand-Hendriksen, S., Gervin, K., Brandal, K., Inderhaug, E., Geiran, O. and Paus, B., 2006. Rapid and efficient FBN1 mutation detection using automated sample preparation and direct sequencing as the primary strategy. *Genetic testing*, *10*(4), pp.258-264.
156. Wallis, D.D., Putnam, E.A., Cretoiu, J.S., Carmical, S.G., Cao, S.N., Thomas, G. and Milewicz, D.M., 2003. Profibrillin-1 maturation by human dermal fibroblasts: Proteolytic processing and molecular chaperones. *Journal of cellular biochemistry*, *90*(3), pp.641-652.
157. Wang, M., Ji-Yi, W., Cisler, J., Imaizumi, K., Burton, B.K., Jones, M.C., Lamberti, J.J. and Godfrey, M., 1997. Three novel fibrillin mutations in exons 25 and 27: classic versus neonatal Marfan syndrome. *Human mutation*, *9*(4), p.359.
158. Wang, M.C., Lu, Y. and Baldock, C., 2009. Fibrillin microfibrils: a key role for the interbead region in elasticity. *Journal of molecular biology*, *388*(1), pp.168-179.
159. Wess, T.J., Purslow, P.P., Sherratt, M.J., Ashworth, J., Shuttleworth, C.A. and Kielty, C.M., 1998. Calcium determines the supramolecular organization of fibrillin-rich microfibrils. *The Journal of cell biology*, *141*(3), pp.829-837.
160. Whiteman, P. and Handford, P.A., 2003. Defective secretion of recombinant fragments of fibrillin-1: implications of protein misfolding for the pathogenesis of Marfan syndrome and related disorders. *Human molecular genetics*, *12*(7), pp.727-737.
161. Whiteman, P., De Madrid, B.H., Taylor, P., Li, D., Heslop, R., Viticheep, N., Tan, J.Z., Shimizu, H., Callaghan, J., Masiero, M. and Li, J.L., 2013. Molecular basis for Jagged-1/Serrate ligand recognition by the Notch receptor. *Journal of Biological Chemistry*, *288*(10), pp.7305-7312.
162. Whiteman, P., Willis, A.C., Warner, A., Brown, J., Redfield, C. and Handford, P.A., 2007. Cellular and molecular studies of Marfan syndrome mutations identify co-operative protein folding in the cbEGF12–13 region of fibrillin-1. *Human molecular genetics*, *16*(8), pp.907-918.

163. Yadin, D.A., Robertson, I.B., McNaught-Davis, J., Evans, P., Stoddart, D., Handford, P.A., Jensen, S.A. and Redfield, C., 2013. Structure of the fibrillin-1 N-terminal domains suggests that heparan sulfate regulates the early stages of microfibril assembly. *Structure*, *21*(10), pp.1743-1756.
164. Yamazumi, K., Shimura, K., Terukina, S., Takahashi, N. and Matsuda, M., 1989. A gamma methionine-310 to threonine substitution and consequent N-glycosylation at gamma asparagine-308 identified in a congenital dysfibrinogenemia associated with posttraumatic bleeding, fibrinogen Asahi. *The Journal of clinical investigation*, *83*(5), pp.1590-1597.
165. Yanagisawa, H. and Davis, E.C., 2010. Unraveling the mechanism of elastic fiber assembly: the roles of short fibulins. *The international journal of biochemistry & cell biology*, *42*(7), pp.1084-1093.
166. Yuan, X., Downing, A.K., Knott, V. and Handford, P.A., 1997. Solution structure of the transforming growth factor β-binding protein-like module, a domain associated with matrix fibrils. *The EMBO journal*, *16*(22), pp.6659-6666.
167. Yuan, X., Werner, J.M., Lack, J., Knott, V., Handford, P.A., Campbell, I.D. and Downing, A.K., 2002. Effects of the N2144S mutation on backbone dynamics of a TB-cbEGF domain pair from human fibrillin-1. *Journal of molecular biology*, *316*(1), pp.113-125.
168. Zeyer, K.A. and Reinhardt, D.P., 2015. Engineered mutations in fibrillin-1 leading to Marfan syndrome act at the protein, cellular and organismal levels. *Mutation Research/Reviews in Mutation Research*, *765*, pp.7-18.
169. Zhang, H., Apfelroth, S.D., Hu, W., Davis, E.C., Sanguineti, C., Bonadio, J., Mecham, R.P. and Ramirez, F., 1994. Structure and expression of fibrillin-2, a novel microfibrillar component preferentially located in elastic matrices. *The Journal of cell biology*, *124*(5), pp.855-863.

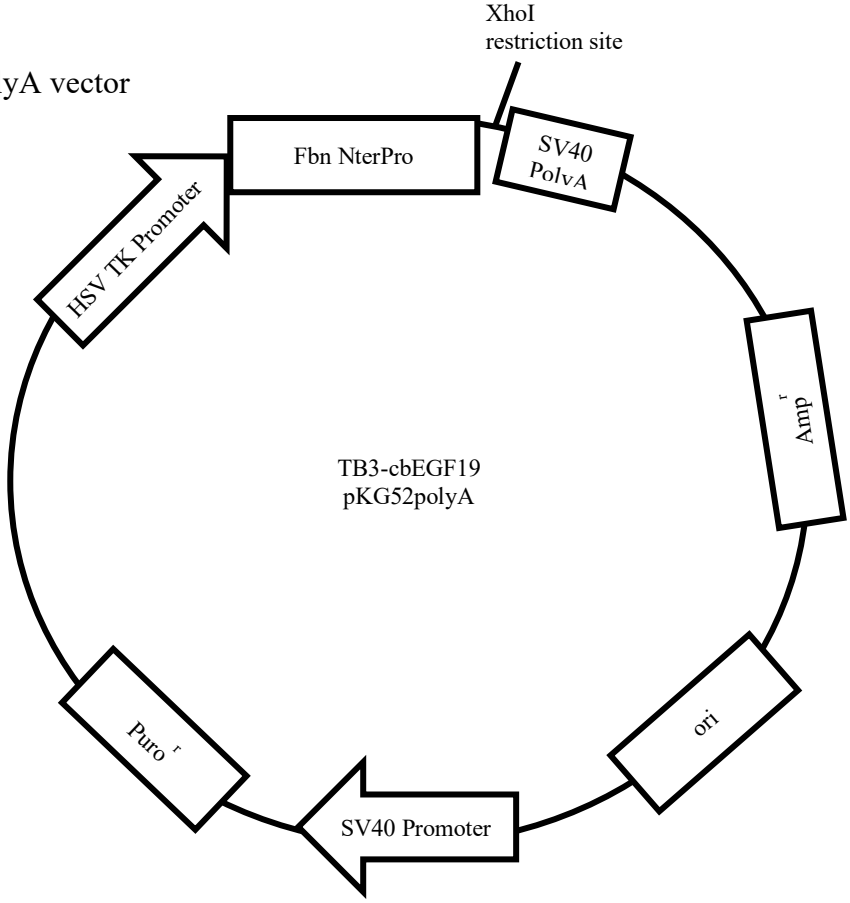
Appendix

Appendix 1

GFP Fibrillin vector



pKG52polyA vector



Appendix 2

Table 1 Primers for amplification of domains TB3-cbEGF19 for insertion into pKGpolyA vector.

Primer Name	Primer Sequence 5'→ 3'
TB3_pKG_Sal1_for	TAGTAGGTCGACAATCAGCAGATATCCGCCTGGAAACCTG
cb19_pKG_Sal1rev	TAGTAGGTCGACTTATGTACAAGTGAAGCCATCACC

Table 2 PCR Based colony screen primers.

Primer Name	Primer Sequence 5'→ 3'
Forward	GCTGTCCCCCAACATCTCC
pKG_rev	CAGGGTCAAGGAAGGCACG

Table 3 Reverse transcription primer and cDNA amplification primers.

Primer Name	Primer Sequence 5'→ 3'
cb14_rev	ATCGGGAGTTGAATGGTAGCC
cb10_for	GCCACAGGAAGGATCTGTC
TB1_for	CTCTAACCAGCTGCCACAG

Appendix 3

Protein Gels:

5× resolving buffer
46 g Tris
1 g SDS
200 ml H_2O pH to 8.8 with HCl

5× stacking buffer
30.25 g Tris
1 g SDS
200ml H_2O pH to 6.8 with HCl

6% polyacrylamide resolving gel
1.5 ml 40% acrylamide
2 ml 5× resolving buffer
6.5 ml milliQ-H_2O/
150 µl APS/
15 µl TEMED (before use)

6% polyacrylamide stacking gel
1 ml 40% acrylamide
2 ml 5× stacking buffer
7 ml milliQ-H_2O/
200 µl APS/
20 µl TEMED (before use)

Western blots

4× SDS-loading dye
200 mM Tris-Cl (pH 6.8)
8% SDS
40% glycerol
Trace bromophenol blue
Reducing: 5% ß-mercaptoethanol (before use)

5× running buffer
90 g glycine
18.75 g Tris
5 g SDS
1 L H_2O no need to adjust pH(~8.3)

1× transfer buffer
3.03 g Tris
14.4 g glycine
200 ml methanol
1L H_2O cool well before use

Bacterial growth

ampicillin
50mg/ml stock, store -20,
100ug/ml in medium or agar

ampicillin plates
agar plates with 100 µg/ml ampicillin

DNA techniques

10× TBE
108.8g Tris-HCl
55.4g Boric acid
9.3g EDTA 1L (pH 8-8.3)

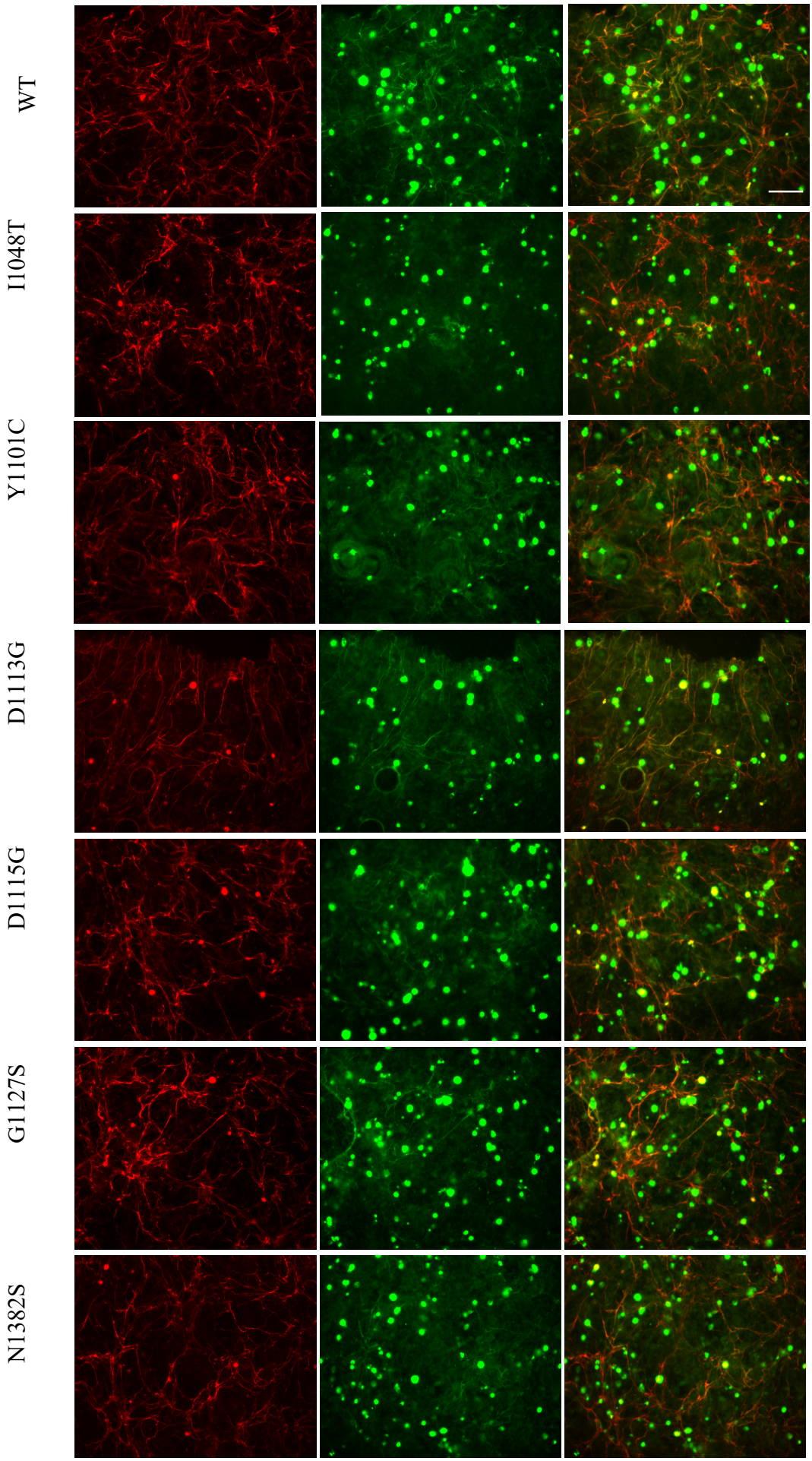
1-2% agarose
0.5-1 g agarose (Roche) in 50 ml boiled TBE buffer with 3 µl ethidium bromide.

Fluorescence microscopy techniques

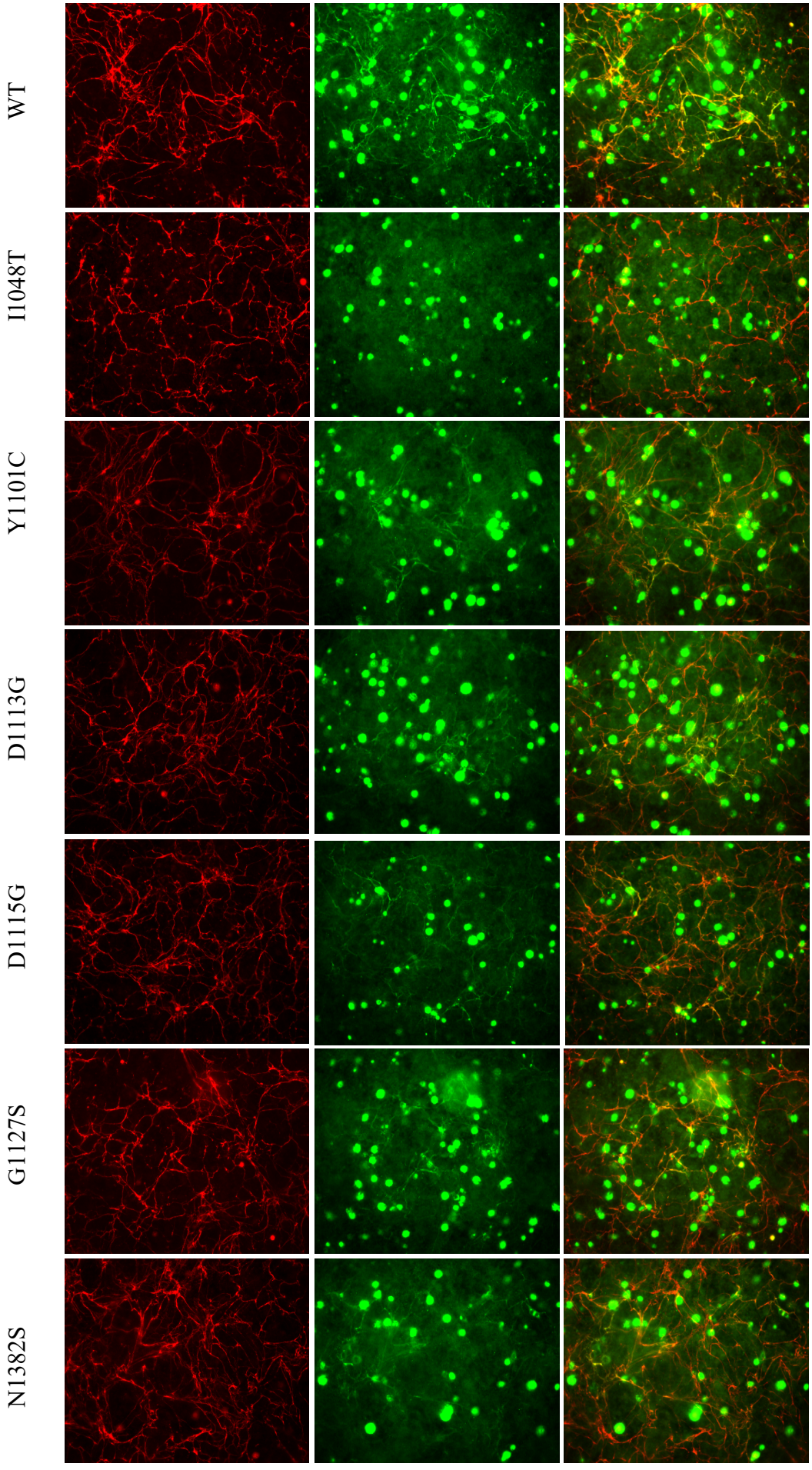
Preparation of Mowiol Coverslip Mounting Solution
1. Add 2.4 g Mowiol (Calbiochem); stir to mix.
2. While stirring, add 6 ml distilled water and leave 2 hours at room temperature.
3. Add 12 ml 0.2M Tris (pH 8.5).
4. Add a small amount of NaN_3 (Sodium Azide) such that the final concentration is 0.02% (optional).
5. Incubate the tube in hot water (50 – 60°C) for 10 minutes to dissolve the Mowiol. This can be repeated over several hours if necessary.
6. Centrifuge at 5000 g for 15 minutes to remove any undissolved solids. Store 1ml aliquots in eppendorf tubes at -20°C.
7. Warm tubes to room temperature for use. Opened tubes can be stored at 4°C for approximately 1 month. Discard if any crystalline material is seen in the tube or on the slides.
8. Leave cover slipped slides in the dark overnight to harden before oil immersion lenses are used or put at 37°C for about 10 min.

Appendix 4 GFP-Fbn assay repeats

Repeat 2

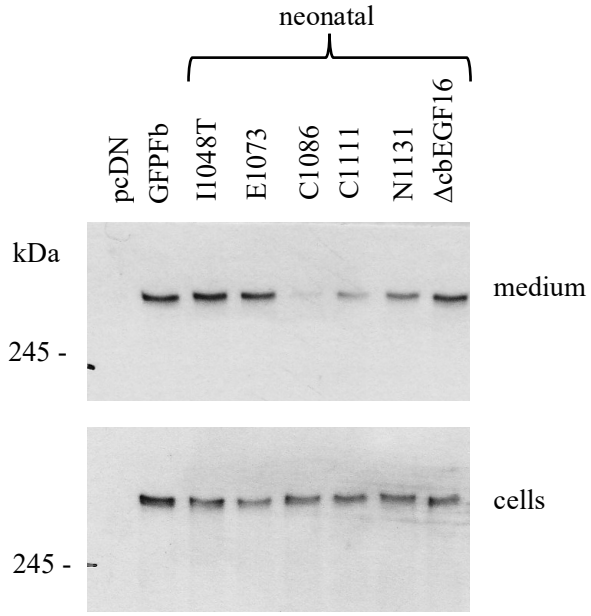


Repeat 3



Appendix 5 nMFS GFP-Fbn secretion and assembly assays performed by Dr. Sasha Jensen (unpublished data)

nMFS GFP-Fbn secretion assay results



nMFS GFP-Fbn assembly assay

